STATIC AND DYNAMICAL MODELS OF LONG-PERIOD VARIABLE STARS

Thesis by

Douglas Allan Keeley

In Partial Fulfillment of the Requirements

For the Degree of

Doctor of Philosophy

California Institute of Technology

Pasadena, California 91109

1970

Submitted September 10, 1969.

ACKNOWLEDGEMENTS

I am greatly indebted to W. D. Arnett for his help in the initial development of the main computer program, and for his interest and advice during the course of the work. By supplying an equation of state table for the early static model calculations, John Castor freed me temporarily from a non-trivial digression from the main course of the work. I also thank him for many discussions on convection, and for introducing me to some of the finer points of computing. I had many helpful conversations with R. B. Larson on the subject of implicit difference equations and convergence problems. I wish to thank T. Tsuji for supplying an essential ingredient for the calculations — the molecular opacity data. I thank Roger Ulrich for many helpful discussions on convection, for communicating results of his static model calculations, and for his interest in my work. I thank Professor Jesse L. Greenstein for a generous allowance of computing time.

I am especially grateful to Robert F. Christy for invaluable advice concerning all aspects of the calculations, and for guidance in setting a reasonable goal for this work. His interest and encouragement are greatly appreciated.

Peter Goldreich has been a constant source of encouragement, guidance, and inspiration; no words can express fully my gratitude to him for serving as my advisor.

I am grateful for the financial support given me by the California Institute of Technology, the National Research Council of Canada, and the Woodrow Wilson Foundation.

STATIC AND DYNAMICAL MODELS OF LONG-PERIOD VARIABLE STARS

by Douglas Allan Keeley

ABSTRACT

The parameters of the models were $M = 1$ and $1.3\,M_\odot$, $M_B = -3.8$ to -5, and $T_e = 2200°K$ to $3200°K$. The equation of state included a detailed calculation of ionization equilibrium and the dissociation of H_2, OH, CO, and H_2O. The opacity of CO, OH, and H_2O was included. The dynamical calculations show that large-amplitude pulsation can occur in convective models. The opacity mechanism causes strong driving of the pulsation in the region outside the hydrogen ionization zone, and the Γ-mechanism results in very low dissipation in the hydrogen zone. The phase relation between the bolometric luminosity and the radius variations is similar to that of Cepheids. The static models have large ionization and dissociation zones, which cause the pulsation parameter $Q = P_{days}(\rho/\rho_\odot)^{\frac{1}{2}}$ to become greater than 0.15 in some models. The fundamental periods range from 180 days to greater than 2000 days; the overtone periods are about $\frac{1}{3}$ as long. The positions of many observed stars in the theoretical HR diagram suggest that their periods should be associated with the overtone periods of the models.

TABLE OF CONTENTS

Table of Contents, (Cont'd.)

INTRODUCTION

The original goal of the work which led to this thesis was to investigate the possibility that an extreme red giant of about 1.3 $M_\odot$ could produce a planetary nebula by ejecting one or two tenths of a solar mass. The basis for this idea was discussed by Abell and Goldreich (1966). Goldreich suggested that the instability would prove to be in the envelope rather than the deep interior.

Very few published static model calculations available at that time included the complications of molecular dissociation, ionization zones, and superadiabatic convection. Thus it was necessary to calculate static models to provide a clear picture of the envelope structure of extreme red giants. The static model calculations suggested that there was, in fact, a good possibility that large-scale mass-loss could occur in these stars.

In Poland, B. Paczynski began a similar study of static models at about the same time, and concluded that red giants in the mass-range required should become dynamically unstable and should be able to eject their entire envelopes. His conclusion was based on the fact that the total energy of the envelope was positive for extreme models; if the ionization energy of hydrogen could be converted efficiently into kinetic energy of expansion, it would be sufficient to expel the envelope.

The condition of positive energy is related to the usual condition for dynamical instability through the virial theorem. Although a linear stability analysis may make a reliable prediction of vibrational instability, its prediction of dynamical instability must be viewed with caution. The instability is of little interest for the present application unless it

develops into a large amplitude phenomenon, and the linear stability analysis can't predict this. For this reason it was necessary to work with the full non-linear equations of the problem.

No satisfactory way was found for treating the inner boundary condition for envelope models close to dynamical instability. Although interesting results were obtained, and will be described briefly, they were not sufficiently secure to be worth pursuing until the inner boundary condition could be made more realistic. By this point in the work, numerous pulsating models had been calculated, and the boundary condition was not a problem for them. It seemed advisable at that time to set aside the original goal, and to pursue an investigation of pulsation in convective stars.

Pulsating models of Cepheids and RR Lyrae stars have provided a new method of analyzing observations; they can give information on the mass and helium content which for most stars could not be obtained in any other way. The calculations were not extended to convective stars, partly because of the difficulty in describing convection in a time-dependent situation, and partly because the people with experience in hydrodynamics problems of this type were already engaged in fruitful work on RR Lyrae stars, supernovae, etc. For the present work it was assumed that if a model were really dynamically unstable, the details of the treatment of convection would not be of great importance in determining the final result. Therefore a relatively simple treatment was used, even after the decision was made to concentrate on pulsating models.

Before the models can be used to analyze the observations, the observations must be used to refine the physics in the models. The stage

of analyzing observations has been reached for RR Lyrae models, but it is still a distant goal for the long-period variables. The more limited goal of this thesis was to make some initial contribution toward understanding the pulsation phenomenon in convective stars.

The text has been written in three distinct sections. Part 1 and Part 2 were written with the intention of submitting them for publication as two separate papers. They are therefore self-contained; each has tables and figures numbered starting from one, and each has its own appendices and references. In Part 3 there is extra material not intended for publication.

PART 1

THE STATIC STRUCTURE OF LONG-PERIOD VARIABLE STARS

ABSTRACT

Static model calculations for $1M_{\odot}$ and $1.3\ M_{\odot}$ stars of solar composition are presented. The equation of state includes a detailed calculation of ionization equilibrium and the dissociation of H_2, OH, CO, and H_2O. The opacity due to H_2O, OH, and CO is included. Preliminary dynamical calculations show fundamental and overtone instability. The fundamental periods range from 180 days to greater than 2000 days; the first overtone periods are roughly $\frac{1}{3}$ as long. The periods and positions of models in the HR diagram suggest that many observed stars may be overtone pulsators.

I. INTRODUCTION

The object of the static model calculations was two-fold: 1) To survey the part of the HR diagram occupied by the long-period variable stars. 2) To provide initial conditions for dynamical calculations. The detailed results of dynamical calculations will be reported in a separate paper, but some of the results will be used in the present discussion.

The general procedure for calculating static models is to choose values of luminosity, mass, and radius compatible with observations, and integrate inward with the luminosity independent of depth until a small fraction of the radius is reached. No core is integrated, but it is possible to determine the core mass from the envelope integration. If the core mass is in a range consistent with the requirements of the theory of stellar evolution, and if the envelope is a reasonable model for comparison with observations, it is assumed that a physically-reasonable core could be connected to the envelope.

Some models of long-period variables have been discussed previously. One of the earliest models to include the ionization zones and the dissociation of hydrogen molecules in detail was the model of Kamijo (1962). Recently Paczynski (1969) has studied models of 1 $M_{\odot}$ extreme red giants. Some results of these calculations will be mentioned briefly.

The equation of state, the opacity, and numerical procedures are discussed in the appendices. The chemical composition used was $X = 0.788$, $Y = 0.197$, $Z = 0.015$; details of the metal abundances are given in Appendix C.

II. STRUCTURE OF A TYPICAL MODEL

A red giant interior structure including a core is shown in Figure 1. The data was taken from Schwarzschild (1958). The main difference between the structure of his model and the structure of the more extreme models considered in the present work is that the flat part of the M_r vs. log P relation begins at much lower pressure in the extreme models. In Figure 1 it is clear that the core mass can be estimated reasonably well from an integration which doesn't go all the way to the centre.

The envelope structure of a $1\ M_\odot$ model of a long-period variable is shown in Figure 2. The mass and radius curves are similar to those in Figure 1 but the mass curve becomes flat at $\log P = 8.0$ instead of 12.0. An integration to $\log P = 10.0$ yields a close estimate of the core mass, which in this case is $0.54\ M_\odot$. The log T curve in Figure 2 is flat at low pressure but the molecular opacity causes a gradual rise in temperature until $\log P = 3.0$. With no molecular opacity in the model, the curve would stay relatively flat and then rise abruptly at higher pressure. The beginning of the region unstable to convection is marked by the cross near $\log P = 2.0$. Although the actual temperature gradient is low, the adiabatic gradient is lower because of the dissociation of hydrogen molecules. The convective flux is very small and the log T curve is essentially the same as if the region were radiative. The steep rise in temperature through $\log T = 3.75$ is caused by the opacity of H^-, and is a characteristic feature of the structure of cool stars. Before the temperature is up to $10^4\ ^\circ K$, convection carries almost the entire flux of energy. The temperature gradient $\nabla \equiv d\ln T / d\ln P$ drops

as the adiabatic temperature gradient drops in the ionization zone of hydrogen, but rises again where almost all the hydrogen is ionized. When ∇ becomes greater than 0.25 the radiation pressure fraction begins to increase. Radiation accounts for about 20% of the total pressure at log P = 9.45. The bottom of the convection zone is at log P = 9.0. The temperature gradient is substantially superadiabatic throughout the convection zone.

Deviations from the perfect gas law cause the variations in $\Gamma_1 \equiv (\partial \ln P / \partial \ln \rho)_s$ shown in Figure 2. At the surface, $\Gamma_1 \approx 1.06$ because of the dissociation of hydrogen molecules. The region of neutral hydrogen is a narrow peak about one pressure scale-height wide because of the steep temperature gradient. The hydrogen ionization zone contains about 10% of the mass of the star. Ionization of He I distorts the Γ_1 curve at log P = 5.3; ionization of He II at log P = 6.2 doesn't cause Γ_1 to drop below 4/3. The broad dip in Γ_1 beginning at log P = 7.0 is caused by the increasing radiation pressure near the bottom of the ionization zone.

The small kink in the density curve (Figure 2) at log P = 2.5 is caused by an abrupt change in the mean molecular weight in the hydrogen molecule dissociation zone. The initial point of the integration was in the region of partial dissociation. As the density increases with the temperature almost unchanging the equilibrium shifts very gradually toward the molecules. When the temperature finally begins to increase the mean molecular weight decreases abruptly as complete dissociation occurs. The density inversion at log P = 3.5 is caused by the steep temperature gradient. In hotter models the density inversion may be much larger in magnitude, and the region of low density may extend over two or three pressure scale-heights.

Ulrich (1968) has calculated a number of giant envelopes using his own non-local treatment of convection. His models show the same general characteristics as the models considered here, in which the usual local mixing-length theory has been used. In particular, they have large ionization zones and are appreciably superadiabatic through the entire convection zone.

III. DEPENDENCE OF THE STRUCTURE ON POSITION IN THE HR DIAGRAM

The relevant part of the HR diagram is shown in Figure 3. The filled circles are static models at 1.3 $M_\odot$; the open circle is the 1 $M_\odot$ model described in the previous section. The core mass-fraction for each model is indicated. At a fixed luminosity the mass fraction decreases rapidly with decreasing effective temperature. The boundary of the Hayashi forbidden region is roughly at the point where the core mass would be zero. The position of this boundary determines the lowest effective temperature possible for a giant star at the mass and luminosity considered. The boundary slopes toward lower temperatures as the luminosity increases but curves back toward higher temperatures above $M_{bol} \approx -5.5$. Paczynski (1969) obtained the same result although he used an unusual expression for the temperature gradient in the optically-thin region. For the present calculations the usual diffusion equation was used. Paczynski's method is discussed further in Appendix D. The slope toward higher temperature can be seen in Figure 3 for the most luminous models at $\log T_e = 3.40$ and 3.42.

The position of the Hayashi line depends strongly on the opacity,

which depends on the composition of the envelope. Several 1.3 $M_\odot$ models with composition $X = 0.973$, $Z = 0.0001$ and no molecular opacity are indicated by crosses in Figure 3. One has almost no mass in the core and is not a physically-reasonable red giant model for this reason. An increase in opacity moves the Hayashi line to lower temperatures. In the present models water vapor contributes most of the low-temperature opacity. The amount of water vapor which can be formed depends on the numerical excess of oxygen atoms over carbon atoms. In population II stars in which the abundance of both is very low, or in population I stars in which carbon outnumbers oxygen, a different opacity source will be important at low temperatures. If it is less effective than water vapor, models with a given core mass (and total mass) and luminosity will have higher T_e. The position of the Hayashi line also depends on the total mass. The 1 $M_\odot$ model denoted by the open circle in Figure 3 has a core mass of 0.54 $M_\odot$; a 1.3 $M_\odot$ model at the same position (not shown) has 13% or 0.17 $M_\odot$ in its core.

The ratio of mixing-length to pressure scale-height is not a well-determined parameter of the convection theory and has been set to unity in these calculations. A decrease of 10% in this ratio can result in a significant increase in core mass for an envelope integrated from the same surface conditions. For a model at $\log T_e = 3.42$ with a luminosity $L = 10^{37}$ ergs/sec, changing the ratio from 1.0 to 0.9 increased the core mass-fraction from 0.49 to 0.69. When the ratio is reduced, a higher temperature gradient ∇ is required for the convection to carry the same flux. This causes a decrease in the density gradient $|d\rho/dr|$ and the mass is not used up so quickly during the inward integration. Because of the larger ∇ the convection zone

is less deep and the model is more centrally-condensed. Auman and Bodenheimer (1967) investigated the relative importance of changes in the opacity and changes in convective efficiency in determining the position of the Hayashi line. They found that it is more sensitive to the efficiency of convection.

An important property of a sequence of models at a given luminosity and total mass is that the mass in the hydrogen ionization zone is largest in the model nearest the Hayashi line. For example, the four coolest models at $L = 2 \times 10^{37}$ ergs/sec in Figure 3 have, respectively, greater than 7%, 15%, 29%, and 53% of the mass above the region of full hydrogen ionization. If two models with the same core mass but different luminosity are compared, the model with higher luminosity will have more mass in the hydrogen zone. (This is true at least up to the luminosity at which the lines of constant core mass turn back toward higher T_e.) At fixed luminosity, the mass outside the hydrogen zone increases as T_e decreases. At fixed T_e, a model with higher luminosity (at least up to the turn-back point) has more mass outside the hydrogen zone. At a given T_e and luminosity, a model with lower total mass has a greater mass fraction outside the hydrogen zone. These last three results are probably related to changes in the surface gravity, but this may not be the only factor involved.

Some of the high-luminosity low-temperature envelopes were found to have positive total energy, as was first reported for models of this type by Paczynski and Ziolkowski (1968 a, b).

IV. PERIODS OF THE MODELS: THE PERIOD-MEAN DENSITY RELATION

The pulsation period is given roughly by

$$P = 2\pi\left(\frac{I}{\Omega}\ \frac{1}{3\Gamma_1 - 4}\right)^{\frac{1}{2}} \equiv \frac{\alpha_1}{\alpha_2}\left(\frac{R^3}{M}\ \frac{1}{3\Gamma_1 - 4}\right)^{\frac{1}{2}}, \qquad (1)$$

where

$I = \alpha_1^2\, MR^2$ is the moment of inertia of the star about its centre,

$\Omega = \alpha_2^2\, M^2/R$ is the gravitational energy, and

Γ_1 = is a mean of $(\partial \ln P/\partial \ln \rho)_s$ over the star (Rosseland 1949).

The pulsation constant Q is defined by

$$Q = P_{\text{days}}\left[\frac{M}{M_\odot} \Big/ \left(\frac{R}{R_\odot}\right)^3\right]^{\frac{1}{2}}, \qquad (2)$$

and so is of the form

$$Q = \text{constant times } \frac{\alpha_1}{\alpha_2}\,(3\Gamma_1 - 4)^{-\frac{1}{2}}. \qquad (3)$$

It is not strictly constant since α_1, α_2, and Γ_1 depend on the detailed structure of the star.

The time-dependent behaviour of many of the models in Figure 3 was investigated. The periods and Q values for the fundamental mode and an overtone are given in Table 1. The period for model 2.5 is not well-determined since much less than a full period was followed; it is probably longer than the time given. The fundamental periods for Sequence 1 are not accurate because the overtone mode dominated at that luminosity. It is difficult to be certain that there is only one node in an overtone model unless the model is fairly well-relaxed. In the case of Sequence 1 the

identification as the first overtone is certain. For Sequences 2 and 3 the overtone periods are not very reliable because of the strong interference from the fundamental mode. The anomalous value of Q_1 for model 2.3 is an indication of the uncertainty in the period estimates for Sequence 2.

In Sequence 2, Q increases as the temperature decreases. The same behaviour was found in the extensive calculations by Christy (1966a). It may be seen to arise from the structural changes along the sequence, which were described in the previous section.

The ratio of overtone period to fundamental period P_1/P_0 is low compared to the value $\approx \frac{3}{4}$ found for Cepheids and RR Lyrae stars, but is consistent with results quoted by Ledoux and Walraven (1958). The work of Schwarzschild (1941), as displayed by Christy (1966b), shows that a value $P_1/P_0 \approx 0.3$ is expected for $Q_0 \approx 0.1$.

Epstein (1950) showed that the pulsation frequency is very sensitive to the physical conditions near a fractional radius of 0.7 for the fundamental mode and 0.8 for the first overtone. This is just the region where ionization of hydrogen causes a low value of Γ_1 in the present models. From the Γ_1-dependence of Epstein's expression for the frequency, (modified to take into account the variations in Γ_1 [see Ledoux and Pekeris {1941}]), it is clear that a value of Γ_1 less than $4/3$ near the critical radius could result in a significant decrease in the pulsation frequency and increase in Q.

In Sequence 1 all the models pulsated preferentially in the overtone mode; the models in Sequence 2 generally had a mixture of fundamental and overtone. Model 2.3 had a mixture even after many periods of calculation. At a fixed luminosity the strength of the fundamental mode

increased as the temperature decreased. Also, at a given luminosity and effective temperature, models of lower mass showed a stronger fundamental. These effects seem to be correlated with the mass above the hydrogen ionization zone; an increase in this mass results in a stronger fundamental mode. This is because strong driving of the pulsation occurs near the outer edge of the hydrogen ionization zone; the closer this region is to the surface, the stronger is the driving in the overtone mode. It may be possible that below some critical luminosity only the overtone mode will be driven effectively. This has not been checked by calculations.

Kamijo's model of Mira (Kamijo 1962) had parameters $M = M_{\odot}$, $T_e = 2370°K$, $R = 2.85 \times 10^{13}$ cms, and its composition included 18% helium by number. Its structure was similar to that of the present models but the two helium ionization zones were much larger. From a linear stability analysis with a standing-wave boundary condition at the surface, Kamijo found a period of about 1050 days. Although this is too long for Mira it is consistent with what would be expected from the present work.

Schwarzschild and Stothers (1961) calculated the adiabatic pulsation period of an unpublished model with $M = 1.3\ M_{\odot}$, $L = 6390\ L_{\odot}$, $R = 175\ R_{\odot}$, $\log T_e \approx 3.60$, and with a composition $X = 0.90$, $Y = 0.099$. They found $Q_0 = 0.063$ and a fundamental period of 107 days, both of which are smaller than any calculated in the present work. The radius of their model is about the same as that of model 1.1 (Table 1), but the effective temperature is much higher. Their period is shorter by a factor approximately equal to the ratio of the Q's. Schwarzschild and Stothers used $\gamma = 5/3$ throughout, whereas in model 1.1, Γ_1 was less than 4/3 in the outer part of the star

due to hydrogen molecule dissociation and hydrogen ionization. The difference in γ's must be responsible for the difference in periods.

V. COMPARISON WITH OBSERVATIONS

a) Uncertainties in the Models

The comparison of static models with observations is subject to many difficulties. The uncertainty in the position of the Hayashi line (and therefore in the core mass at a given luminosity and effective temperature) has been discussed in §III. Inclusion of a full atmosphere calculation using the equation of transfer and boundary conditions appropriate for real stars may also make a difference in the position of the Hayashi line. The effective temperature can't be defined uniquely by σT_e^4 = flux if the flux is not independent of depth in the atmosphere. Two methods of eliminating the ambiguity are discussed in Appendix D.

The periods of the models, and the knowledge of which pulsation modes dominate are potentially the most valuable information for comparison with observations. If Q were a constant a reasonable estimate of the mass would give a strong hold on the radius. In Table 1 it is shown that Q changes fairly slowly along a model sequence at constant luminosity except near the Hayashi line. The changes occur faster at higher luminosity because of the generally-larger amount of mass in the hydrogen ionization zone.

A change in the position of the Hayashi line must cause a change in the Q of models near the line, but it may also change Q in models far from the line. For example, a change in the opacity below some

temperature T_c can only influence models with T_e near or below T_c; the structure of a model should not be changed if T_e is sufficiently high that the optical depth is very small in the part of the atmosphere where the change in opacity is made. However, if the Hayashi line is moved by a change in the ratio of mixing-length to scale-height, then the structure will be changed in all models in which convection is important.

Q also depends on the mass because a change in the mass of a model at given luminosity and effective temperature causes a change in the central condensation. This effect is large near the Hayashi line for the mass considered, as the example in § II showed. The $1 M_\odot$ model in Figure 3 (the open circle) had $Q = 0.11$. This is probably smaller than the Q of the $1.3 M_\odot$ model at the same position, but is not very different from the Q's of the other models at the same luminosity. At higher luminosity the ionization zone occupies a greater fraction of the envelope mass at a given core mass (cf. §III), so Q could be more sensitive to changes in the envelope mass.

The long-period variables are apparently of mixed stellar population. Plaut (1965) groups them as follows in order of increasing population II characteristics:

group 1 : period > 300 days

group 2 : period < 150 days and 200 < period < 300 days

group 3 : 150 < period < 200 days.

Possible differences in mass and composition for the three groups complicate the interpretation of the HR diagram.

b) Requirements from the Theory of Stellar Evolution

Stellar evolution theory leads to some restrictions on the models. The masses of the models are in agreement with the results of Fernie (1959), and Fernie and Brooker (1961), who found that the masses of X Oph and o Ceti could not be much more than $1\,M_{\odot}$. Stars with mass less than 0.7 or $0.8\,M_{\odot}$ must have main-sequence lifetimes greater than the age of the galaxy. Thus the long-period variables could be substantially less massive than the sun only if they have undergone considerable mass loss. They are observed to lose mass (Deutsch 1960), but the rate is not high enough to allow a loss of the order of several tenths of a solar mass. On the other hand, the long-period variables can't be too massive because they don't have a galactic distribution expected for young stars with masses of $2.5\,M_{\odot}$ or greater.

The luminosity required by observations can be produced by stars with masses about $1\,M_{\odot}$. Pre-helium-flash models by Schwarzschild and Selberg (1962), and by Schwarzschild and Harm (1962, 1964), at $1\,M_{\odot}$ and $1.3\,M_{\odot}$ reached luminosities of $10^4\,L_{\odot}$ for an interval of about 10^4 years just before the peak of the helium flash. A lifetime of 10^4 years is probably too short to account for the observed number of long-period variables. More recent calculations by Iben (1968) suggest slightly lower luminosities at the peak of the flash. Solar mass stars in the stage of helium shell-burning, or combined hydrogen and helium shell-burning may be able to reach luminosities around $10^4\,L_{\odot}$ for appreciable lengths of time.

The core masses of the Schwarzschild models were about 0.5 $M_{\odot}$. Iben (1968) found similar values for a range of chemical compositions

and for masses from 0.7 to 1.3$M_\odot$. He found that neutrino losses increase the core mass and the luminosity at the peak of the helium flash.

c) Discussion of the Observations

Some of the observational data has been plotted in Figure 3. The X's are the statistical data of Osvalds and Risley (1961). These authors estimated absolute visual magnitudes at maximum light for eight groups of M stars by means of statistical parallaxes. The absolute bolometric magnitudes for their points are given by Smak (1966a) and the effective temperatures are given by Smak (1964). The loops are the data of Pettit and Nicholson (1933) for seven stars which they observed with a thermocouple. The absolute magnitudes of R Hya, X Oph, and o Ceti have been adjusted as discussed in Appendix A, but the rest of the Pettit and Nicholson data has been used unchanged. The circles in Figure 4 are the same models as in Figure 3. The fundamental periods of the models and the observed periods for the observational points are indicated.

The loops show that the bolometric luminosity range is about one magnitude, and the full radius amplitude is about 25%. The data points of Osvalds and Risley are at the high-temperature high-luminosity ends of similar loops. Interpreted in this way, the points cover the same general range of temperature and luminosity as the models, but the periods are much shorter. The masses appropriate to the statistical points are unknown, but since the period goes roughly as $M^{-1/2}$, masses much larger than 1.3 $M_\odot$ would be required to explain the discrepancy. In many cases the periods are in much better agreement

with the overtone periods of the models. However, it is not certain that the overtone mode would always be favored over the fundamental, especially for the points with log T_e below 3.40.

Feast (1963) suggested on the basis of radial velocity data that the stars with periods less than 149 days were overtone pulsators corresponding to stars with fundamental periods around 300 days. Plaut (1965) has associated stars with periods less than 150 days with those having periods between 200 and 300 days. Only one of the Osvald and Risley points has a period less than 150 days, and its position in the HR diagram suggests it may be an overtone pulsator. It is considerably less luminous than most of the other Osvald and Risley points, and so it doesn't support Feast's hypothesis that the two groups of stars he associates consist of essentially identical stars pulsating in different modes. The possible interpretation of most of the Osvald and Risley points as overtone pulsators is also inconsistent with Feast's idea.

The Pettit and Nicholson data presents a problem. R Leo, R Aql, χ Cyg, o Ceti, and possibly R Tri are beyond the Hayashi line for 1.3 $M_\odot$. It is necessary to move the Hayashi line to lower temperatures to give them reasonable core masses. A model with mass considerably below 1 $M_\odot$ would be required to account for the low effective temperature of R Aquilae if its luminosity is really $M_B = -3.8$. For the stars at higher luminosity a smaller decrease in mass would suffice. An increase in the low-temperature opacity and/or a decrease in convective efficiency would also help, and may even be necessary to explain the temperature of R Aquilae.

The periods are so short that they pose a serious problem if the radii inferred from the temperatures are correct. If the mass of

R Aquilae is assumed to be 1 $M_\odot$, a Q of 0.046 would be required to give the correct period. This Q would require an extreme change in the structure, which is probably impossible to achieve under reasonable assumptions. A Q of 0.046 would be reasonable for a first overtone. However, it has been noted previously that the fundamental mode becomes progressively stronger as the mass and temperature are decreased at a given luminosity. The 1 $M_\odot$ model indicated in Figure 4 by the open circle showed a strong fundamental component in its pulsation. The problem with the periods is about the same or worse for the stars at higher luminosity; their radii are larger, the observed periods are about the same, and they are expected to show a stronger fundamental mode. A reasonable increase in mass would not help much to explain the periods, and would make it more difficult to explain the low temperatures.

Smak gives a calibration of T_e vs. spectral type (Smak 1964), and bolometric correction vs. spectral type (Smak 1966a), which together give a relation between B.C. and T_e. The temperature change of the Pettit and Nicholson stars during a period causes a change in the bolometric correction. If this change is added to the change in bolometric luminosity from maximum to minimum, the result should be greater than or equal to the observed visual luminosity amplitude. When this procedure is applied to R Tri the calculated visual range is too small by about 1.5 magnitudes. This test can't be applied to any of the other Pettit and Nicholson stars because they are off the cool end of Smak's calibration of T_e at minimum luminosity. Some of the hotter Osvald and Risley data points may also present the same problem as R Tri.

The main conclusion from the observations is that it is difficult to explain the periods in terms of the fundamental mode of pulsation. This is especially true for all the Pettit and Nicholson stars except R Tri. At the same time dynamical calculations suggest that the fundamental mode may be dominant at low temperature and high luminosity. Any general upward adjustment of the temperature scale may cause problems in explaining the visual luminosity amplitude if Smak's determination (Smak 1964) of the effect of TiO is correct. Perhaps the observed temperature characterizes conditions in an extended envelope around the actual star, and is not a good indicator of the radius (or effective temperature) of the pulsating star.

This entire discussion must be considered tentative until it is shown that the present treatment of the low-temperature atmosphere does not result in a serious error in the position of the Hayashi line.

I wish to thank Peter Goldreich and Robert F. Christy for their interest, advice, encouragement, and many valuable discussions. Thanks also go to T. Tsuji for making available his detailed opacity calculations, and to Roger K. Ulrich for communicating results of his calculations in advance of publication. I gratefully acknowledge the financial assistance of the California Institute of Technology, the National Research Council of Canada, and the Woodrow Wilson Foundation.

APPENDIX A

The absolute bolometric magnitudes given by Pettit and Nicholson (1928) were used to establish the zero points for the light curves (Pettit and Nicholson 1933). Changes were made in the three cases listed below:

1) o Ceti: A distance modulus of 3.0 and an absolute visual magnitude at maximum of $M_v = -1.0$ were taken from Allen (1963). The bolometric correction at maximum bolometric luminosity is -3.5 (Pettit and Nicholson 1928). The difference in bolometric correction between maximum visual light and maximum bolometric luminosity was estimated to be 0.5 magnitudes from the Pettit and Nicholson temperatures and Smak's calibration of T_e (1964) and B.C (1966a) vs. spectral type. The luminosity was normalized to give $M_B = -4.0$ at visual phase 0.0.

2) X Oph: Smak's (1964) distance modulus of 7.4 was used with the Pettit and Nicholson (1928) values of m_v and B.C. to normalize the light curve.

3) R Hya: Smak's (1964) distance modulus of 5.9 was used as in the case of X Oph.

APPENDIX B

The opacity table was generated from the following formula:

$$\kappa = P_e \left\{ \frac{5.4\times10^{-13}}{\rho T} + X\left[\frac{T^{1/2}}{2\times10^6/T^4 + 2.1T^6} + \frac{(1-2\,NH2/NHT)}{4.5T^6 + T^{-1}(4\times10^{-3}/T^4 + 2\times10^{-4}/\rho^{1/4})^{-1}}\right] \right.$$

$$+ Y\left[\frac{1}{1.4\times10^3\,T + T^6} + \frac{1.5}{10^6 + 0.1\,T^6}\right]$$

$$\left. + Z\left[\frac{T^{1/2}}{20T + 5T^4 + T^5}\right]\right\}$$

$$+ \frac{(NH + NH2)}{\rho}\left[\frac{5.55\times10^{-27}\,T^4}{1 + 10T^6 + 3.42\times10^{-5}/T^6}\right] + \frac{NCO}{\rho}(2.75\times10^{-26})$$

$$+ \frac{NOH}{\rho}\left(\frac{1.4\times10^{-21}\,T^6}{0.1 + T^6}\right) + \frac{NH2O}{\rho}\left(\frac{2.6\times10^{-27}}{4.23\times10^{-4} + T^4} + \frac{9.72\times10^{-18}\,e^{-3.2553/T}}{1 + 3.78\times10^3\,T^{10}}\right)$$

T is in units of 10^4 °K

ρ is the density

P_e is the electron pressure

X, Y, and Z are the usual mass-fractions

NHT is the total number density of protons in any form (hydrogen molecules, atoms, ions, H^- etc.)

NH, NH2, etc. are the number densities of the species indicated by the symbols following N.

The terms multiplied by P_e are the same as those described by Christy (1966a), with one exception. The term contributing the low-temperature opacity of hydrogen has been modified to account for the depletion of hydrogen atoms due to formation of molecules. The term

with coefficient (NH + NH2) takes account of Rayleigh scattering by hydrogen and hydrogen molecules. (The cross-sections are about the same and have been taken equal for simplicity.)

Data on molecular opacities was supplied by Tsuji (1967). In these calculations the smearing parameter discussed by Tsuji (1966) was taken equal to unity. This results in the highest opacity of all the cases he considered. Although Tsuji gave the Rosseland mean absorption coefficient explicitly, his monochromatic data was required for resolving the mean opacity into contributions by different species. Since the Rosseland mean of a sum of monochromatic opacities does not equal the sum of the Rosseland means, the breakdown can be made clearly only when one particular species dominates. Individual terms in the formula are not to be considered as a good representation of the opacity contributed by a particular molecule except over a limited range where that molecule dominates. Terms which never dominate were constructed essentially to fill the gaps left by dominant terms, and were attributed to the species which was considered on the basis of the monochromatic data to be responsible for the extra opacity required.

The errors in fitting a formula to Tsuji's data should not exceed 10 % for most combinations of temperature and pressure. This is acceptable in view of the uncertainties in his calculated data.

The molecular contributions have been written explicitly in terms of number densities and may be useful over some range of composition. However, the formula should be used with caution for carbon and oxygen abundances much different from those used by Tsuji (1966).

Figure 5 is a plot of $\ell n \kappa$ in the range of temperature and density where the molecules contribute. The plateau at the lowest temperatures,

and the hump next to it in the high density region are caused by water vapor.

APPENDIX C

The Equation of State

A general program was developed for calculating the ionization equilibrium for any number of elements with any number of stages of ionization contributing simultaneously. The dissociation equilibria of H^-, H_2, H_2^+, CO, OH, and H_2O were included.

The chemical composition is given in Table C1; it was taken from the work of Lambert (1967).

Six quantities were tabulated for the equation of state. They were $\ell n\, P_{gas}$, $\ell n\, \kappa$, E_{ion} (the internal energy due to ionization), $(\partial \ell nN/\partial \ell nT)_\rho$, $(\partial \ell n(N/\rho)/\partial \ell n\rho)_T$, and $(\partial E_{ion}/\partial T)_\rho$. From these, all the required thermodynamic functions may be calculated.

The tabular spacing was 0.3 in log ρ. In log T it was 0.02 for $3.0 < \log T < 4.80$, and 0.05 for $\log T > 4.80$.

The dissociation equilibria for H^-, H_2^+, and H_2 were calculated from the formulae given by Vardya (1961). The following expressions given by Tsuji (1967) were used for CO, OH, and H_2O:

$$\log_{10}\left(\frac{NcNo}{Nco}\right) = \Big(\Big(\Big(\Big(\Big(- 1.791392 \times 10^{-3}\theta + 2.835639 \times 10^{-2}\Big)\theta - .1748075\Big)\theta + .5426277\Big)\theta - 12.14802\Big)\theta + 29.74919\Big) - \log T$$

$$\log_{10}\left(\frac{N_O N_H}{N_{OH}}\right) = \Big(\Big(\Big(\Big(\Big(-3.788928\times10^{-4}\theta + 6.441536\times10^{-3}\Big)\theta - 4.547711\times10^{-2}\Big) + .1874514\Big)\theta - 5.037783\Big)\theta + 28.14544\Big) - \log T$$

$$\log_{10}\left(\frac{N_{OH} N_H}{N_{HOH}}\right) = \Big(\Big(\Big(\Big(\Big(-9.54251\times10^{-7}\theta + 665139\times10^{-5}\Big)\theta - 1.91596\times10^{-3}\Big)\theta + 3.0786\times10^{-2}\Big)\theta - 5.44421\Big)\theta + 28.90622\Big) - \log T$$

where $\theta = 5040/T$ and T is in degrees K.

The atomic ionization potentials and partition functions were taken from Allen (1963).

APPENDIX D

I. CALCULATION OF STATIC MODELS

The form for the hydrostatic equation is

$$\frac{dP_{gas}}{dr} = - \frac{G M_r \rho}{r^2} + \frac{\kappa \rho L_{rad}}{4\pi r^2 c} \qquad (D\,1)$$

The last term is the exact expression for the radiation force if κ is the flux-mean opacity or if it is independent of wavelength. In the actual calculation the Rosseland mean is used. When the diffusion equation

$$\frac{d}{dr}\left(\tfrac{1}{3} a T^4\right) = -\frac{\kappa \rho L_{rad}}{4\pi r^2 c} \qquad (D\,2)$$

is used to calculate the temperature gradient driving the radiative flux, the hydrostatic equation can be written in the form

$$\frac{dP}{dr} = - \frac{G M_r \rho}{r^2} \qquad (D\,3)$$

where $P = P_{gas} + \frac{1}{3} aT^4$. In the optically-thick part of the star P is the ordinary isotropic pressure because $\frac{1}{3}aT^4$ is the correct expression for the isotropic pressure of radiation. In the optically-thin region $\frac{1}{3}aT^4$ does not have this interpretation. However, the gradient of $\frac{1}{3}aT^4$ still gives the radiation force correctly, if the diffusion equation is used to calculate the temperature gradient.

The diffusion equation was used in the present models. In a

recent paper Paczynski (1969) modified the equation for the temperature gradient in the optically-thin region. There is some justification for imposing an r^{-2} dependence on T^4 to maintain consistency with a radiation energy-density temperature when further interaction with the atmosphere is negligible. However, this condition will not be applicable close to a star where the effects of a stellar wind, or possibly a chromosphere, etc., can cause a much different temperature distribution. Because of these problems it is not clear that the modified equation is any more satisfactory than the diffusion equation.

The convective flux for the static models was calculated using the usual mixing-length equations (Mihalas 1965; Bohm-Vitense 1958).

II. THE DEFINITION OF EFFECTIVE TEMPERATURE

In a plane parallel atmosphere in radiative equilibrium the effective temperature is defined by $\sigma T_e^4 = F$, where the flux F is constant with depth. In a gray atmosphere in local thermodynamic equilibrium, the theory of radiative transfer gives the relation

$$T^4(\tau) = \tfrac{3}{4} T_e \ (\tau + q(\tau)) = \tfrac{3}{4} \frac{F}{\sigma} (\tau + q(\tau)) \qquad \text{(D4)}$$

If τ_e is defined by $\tau_e + q(\tau_e) = 4/3$, then $T(\tau_e) = T_e$. This provides an alternative definition of the effective temperature when the appropriate value of τ_e is known. In a real star, if F is sufficiently constant over the entire range of optical depth of interest, the plane-parallel approximation is valid. In a situation where F is not sufficiently constant, not only is the plane-parallel approximation

unjustified, but the definition of T_e in terms of the flux is no longer useful. It is still possible to define $T_e = T(\tau_e)$, but it is not certain what the value of τ_e should be.

Initial values of M, L, P, T, and R are required to start the inward integration. A combination of P, T, and R is chosen such that the optical depth of a scale-height of atmosphere at that point is very small. If the integration is carried in to some pre-assigned value of τ_e it is generally found that $4\pi R^2 \sigma T^4 \neq L$ at that point. If T_e and τ_e are specified ahead of time, it is possible to choose the initial P, T, and R such that the starting point is at low optical depth, $T(\tau_e)=T_e$, and $4\pi R^2 \sigma T^4 = L$ at $\tau = \tau_e$. When this is done, the model is uniquely determined in the sense that there is no other model with the same M, L, T_e, τ_e for which all these conditions are satisfied but the pressure, for example, is different at τ_e.

Another approach was used by Paczynski (1969). The differential form of the diffusion equation is not the source of the difficulty he points out regarding starting values of T and R; the problem is in the constant of integration in the integrated form which he discusses. By putting $R(\tau = 0) = \infty$ he could have eliminated the problem, but then would have had to impose a further condition to define the model uniquely. Instead, he specifies a T(r) relation to hold at small optical depth, and uses the derivative of it to get a steeper temperature gradient than that given by the diffusion equation in the optically-thin region. Then, by defining $T_e \equiv T(\tau_e)$ he defines a unique model at each (L, T_e) point. In general the relation $4\pi R^2 \sigma T^4 = L$ will not be satisfied at $\tau = \tau_e$.

At a given M, L, T_e a whole sequence of models could be calculated, for different choices of physically reasonable τ_e's; each

would have a different core mass. A pair of models with $L = 10^{37}$ ergs/sec, $M = 1.3\, M_\odot$, $\log T_e = 3.42$ were calculated satisfying $4\pi R^2 \sigma T^4 = L$ at $\tau = \tau_e$, with $\tau_e = \frac{2}{3}$ in one model and $\tau_e = 1$ in the other. For $\tau_e = \frac{2}{3}$ the core mass-fraction was 0.491, while for $\tau_e = 1$ it was 0.386. At a given τ_e, Paczynski's method of imposing uniqueness will give a different core mass.

For most of the models calculated here an effective temperature was estimated ahead of time and the starting temperature was calculated from $T^4 = \frac{1}{2} T_e^4$. The initial radius and pressure were chosen to make the starting point at very small τ. The quantity $4\pi r^2 \sigma T^4$ decreases inward initially due to the decrease in r, but T^4 increases rapidly as τ becomes of order unity. The equation $4\pi r^2 \sigma T^4 = L$ is satisfied at a $\tau \approx 1$. The value of T at which this occurred was taken to be the effective temperature. The optical depth was not forced to have any particular value at this point so the definition of T_e was not unique. The value of τ where the condition on the luminosity was satisfied was checked in a sequence of six models at $L = 2 \times 10^{37}$ ergs/sec, with $\log T_e$ ranging from 3.477 to 3.347. The value of τ was generally in the range $0.65 < \tau < 0.75$. This uniformity was due partly to the way the starting temperature and pressure were chosen, and partly to experience in choosing the initial R. The spread in the effective temperature vs. core mass relation due to the spread in τ_e is of the order of a few per cent except very near the Hayashi line where it may be higher. For calculations where strict internal consistency was required, an iterative procedure was used to fix τ_e at a pre-determined value.

TABLE 1

THE PERIOD - MEAN DENSITY RELATION

	Model	M_c/M	R (10^{13} cms)	P_0 (days)	Q_0	P_1 (days)	Q_1
Sequence 1	1.1	0.94	1.15	180	0.098	70	0.038
$L = 10^{37}$ ergs/sec	1.2	0.88	1.31	220	0.098	81	0.036
	1.3	0.57	1.65	310	0.098	125	0.039
Sequence 2	2.1	0.93	1.86	434	0.114	---	- ---
$L = 2 \times 10^{37}$ ergs/sec	2.2	0.85	2.22	640	0.129	175	0.035
	2.3	0.64	2.65	865	0.160	250	0.046
	2.4	0.40	3.07	1600	0.198	330	0.041
	2.5	0.20	3.37	>2500	>0.27	---	- ---
Sequence 3	3.1	0.73	3.26	1190	0.135	290	0.033
$L = 3 \times 10^{37}$ ergs/sec							

TABLE C1

THE CHEMICAL COMPOSITION

Element	Relative Abundance by Number
H	1.00
K	1.12×10^{-7}
Na	1.51×10^{-6}
Al	2.51×10^{-6}
Ca	2.14×10^{-6}
Mg	3.02×10^{-5}
Fe	3.24×10^{-6}
Si	3.55×10^{-5}
S	1.62×10^{-5}
C	3.55×10^{-4}
O	5.89×10^{-4}
N	8.51×10^{-5}
Ne	7.58×10^{-5}
He	6.30×10^{-2}

FIGURE CAPTIONS

Fig. 1. Curves showing the dependence of the mass and radius on the pressure in the interior of a red giant.

Fig. 2. Curves showing the envelope structure of a $1 M_{\odot}$ extreme red giant. $L = 10^{37}$ ergs/sec. $\log T_e = 3.39$.

Fig. 3. The grid of models in the HR diagram. The closed circles are 1.3 $M_{\odot}$ models; the open circle is a $1 M_{\odot}$ model. The crosses are 1.3 $M_{\odot}$ models with low helium and metal abundance. The numbers are the core mass-fractions.

Fig. 4. Comparison of models (circles) with observational data. The crosses are the statistical points of Osvalds and Risley. The loops show the luminosity and temperature variations observed by Pettit and Nicholson.

Fig. 5. Dependence of the total opacity (calculated from the formula in Appendix B) on temperature and specific volume in the region where molecular opacity is important.

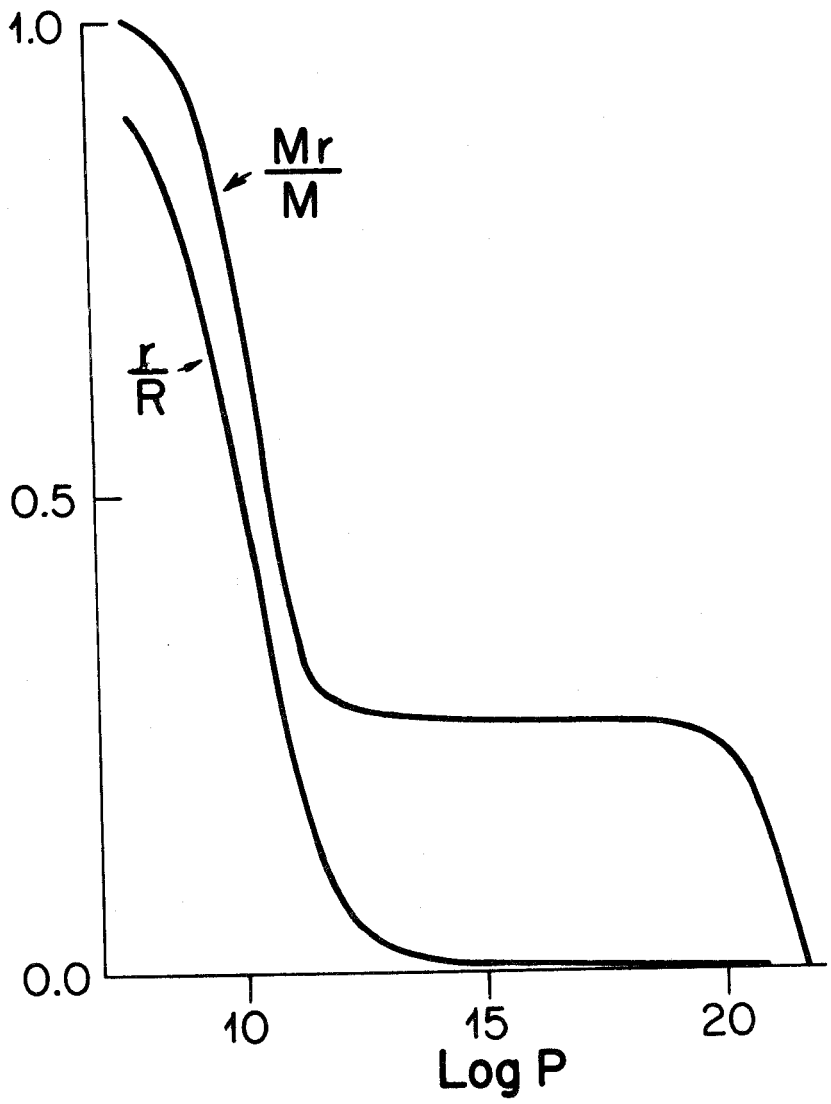

Figure 1

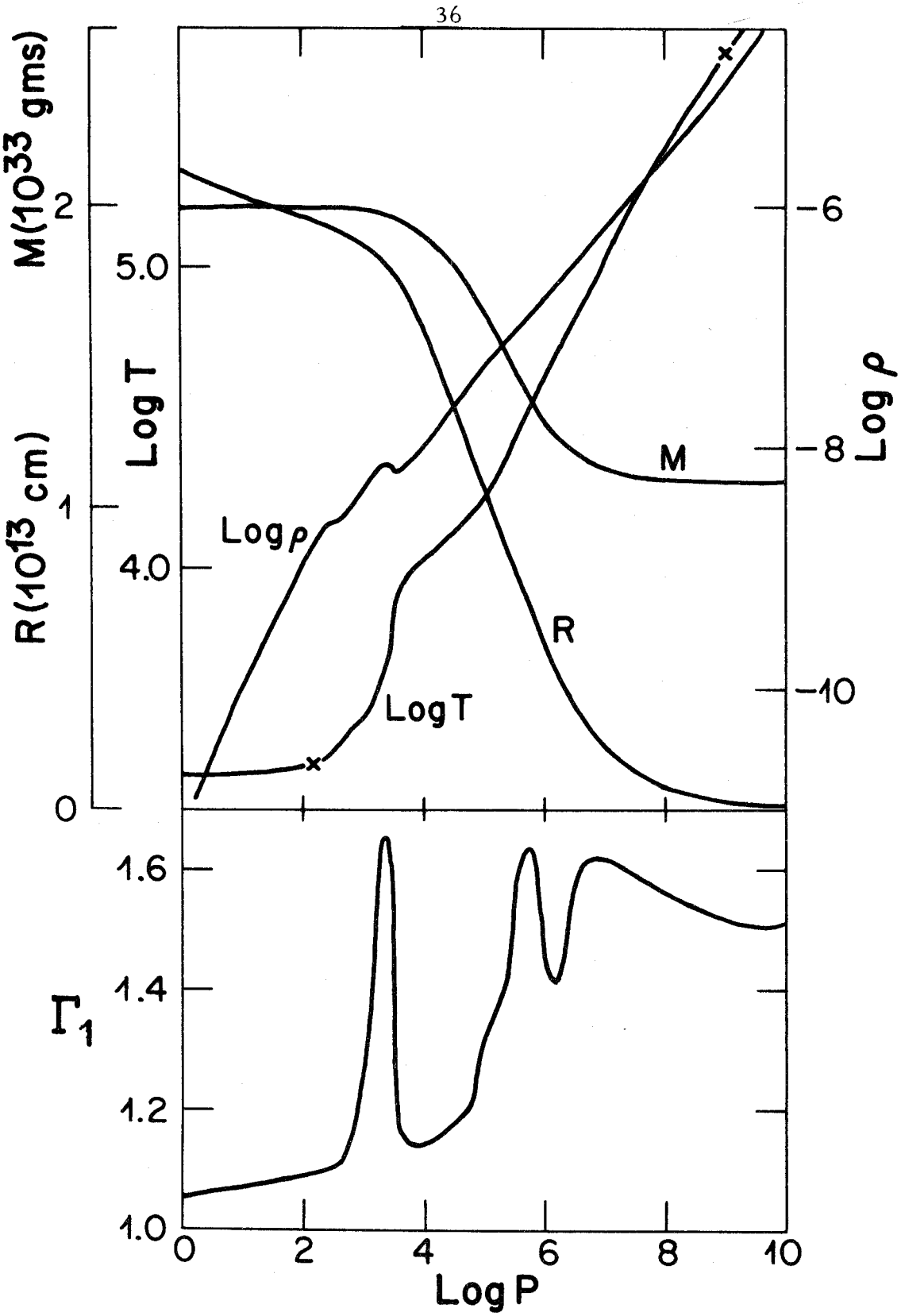
M(10^33 gms)
R(10^13 cm)
Log T
Log ρ
M
R
Log ρ
Log T
Γ1
Log P
2
1
0
5.0
4.0
-6
-8
-10
1.6
1.4
1.2
1.0
0
2
4
6
8
10

Figure 2

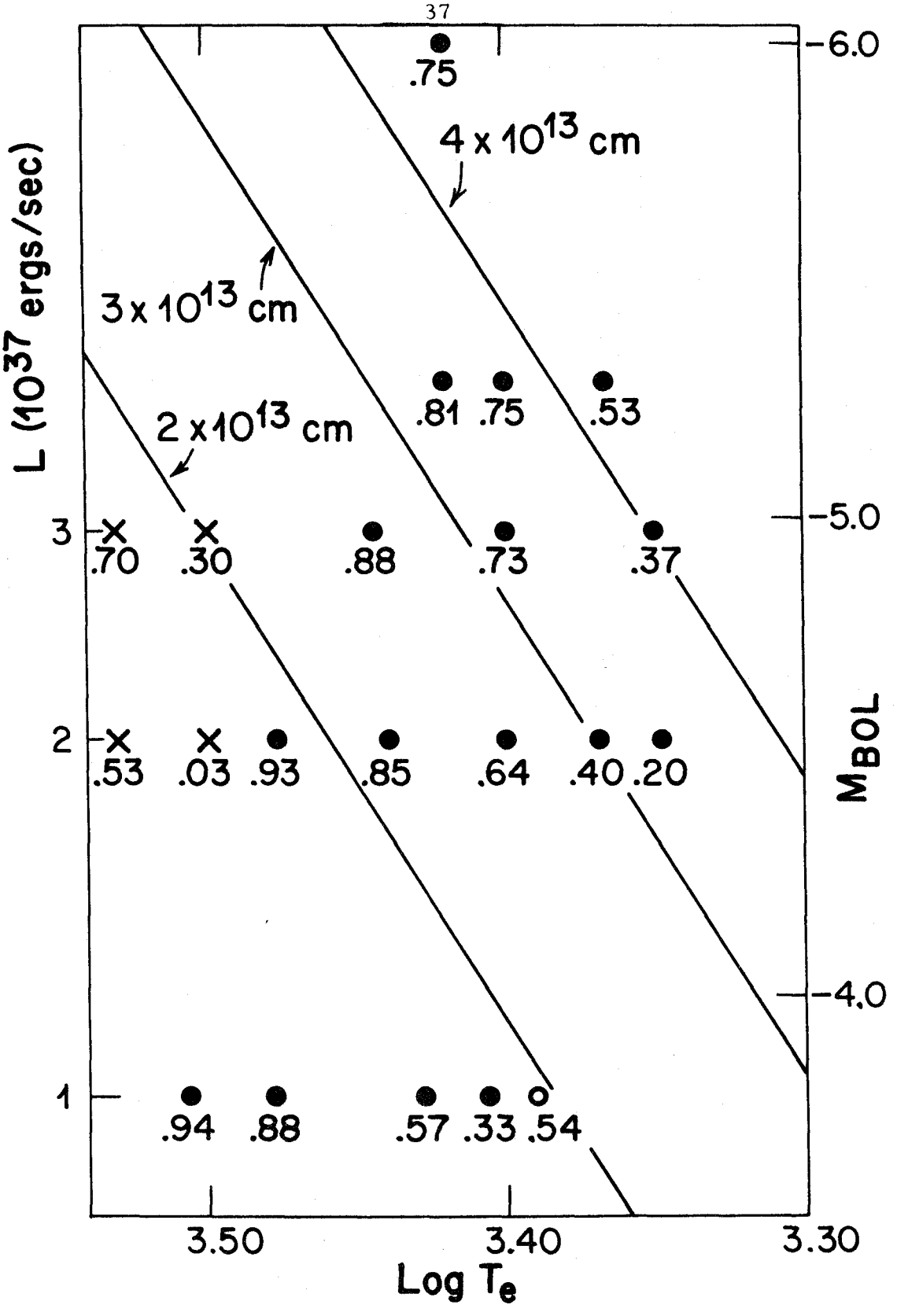
L (10^37 ergs/sec)
3
2
1
4 x 10^13 cm
3 x 10^13 cm
2 x 10^13 cm
.75
.81 .75 .53
X .70 X .30 .88 .73 .37
X .53 X .03 .93 .85 .64 .40 .20
.94 .88 .57 .33 o .54
-6.0
-5.0
-4.0
M_BOL
3.50
3.40
3.30
Log T_e

Figure 3

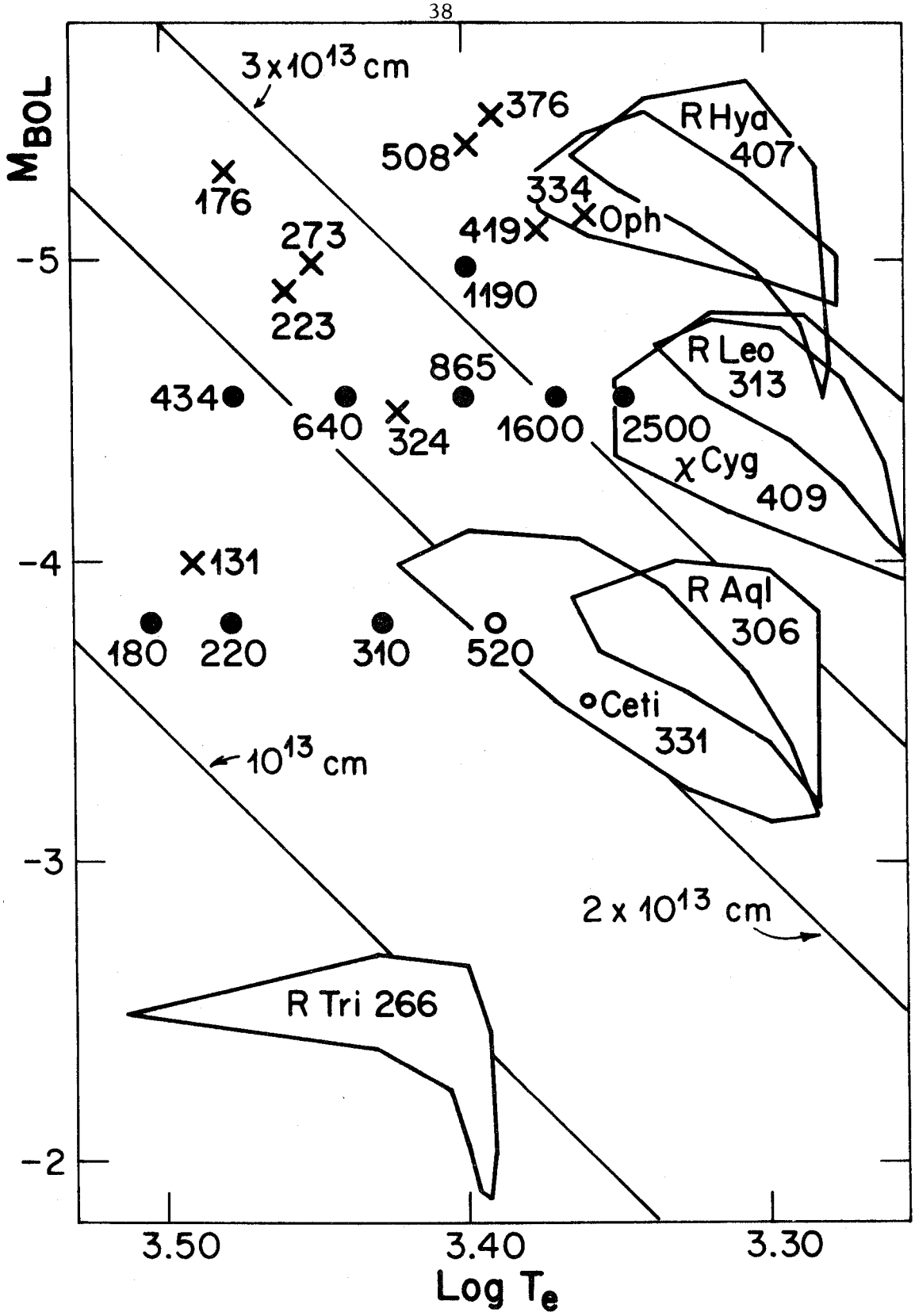
3x10^13 cm
376
508
176
334
419
Oph
273
223
1190
865
434
640
324
1600
2500
χ Cyg
409
131
180
220
310
520
10^13 cm
2 x 10^13 cm
R Hya
407
R Leo
313
R Aql
306
o Ceti
331
R Tri 266
M_BOL
-5
-4
-3
-2
3.50
3.40
3.30
Log T_e

Figure 4

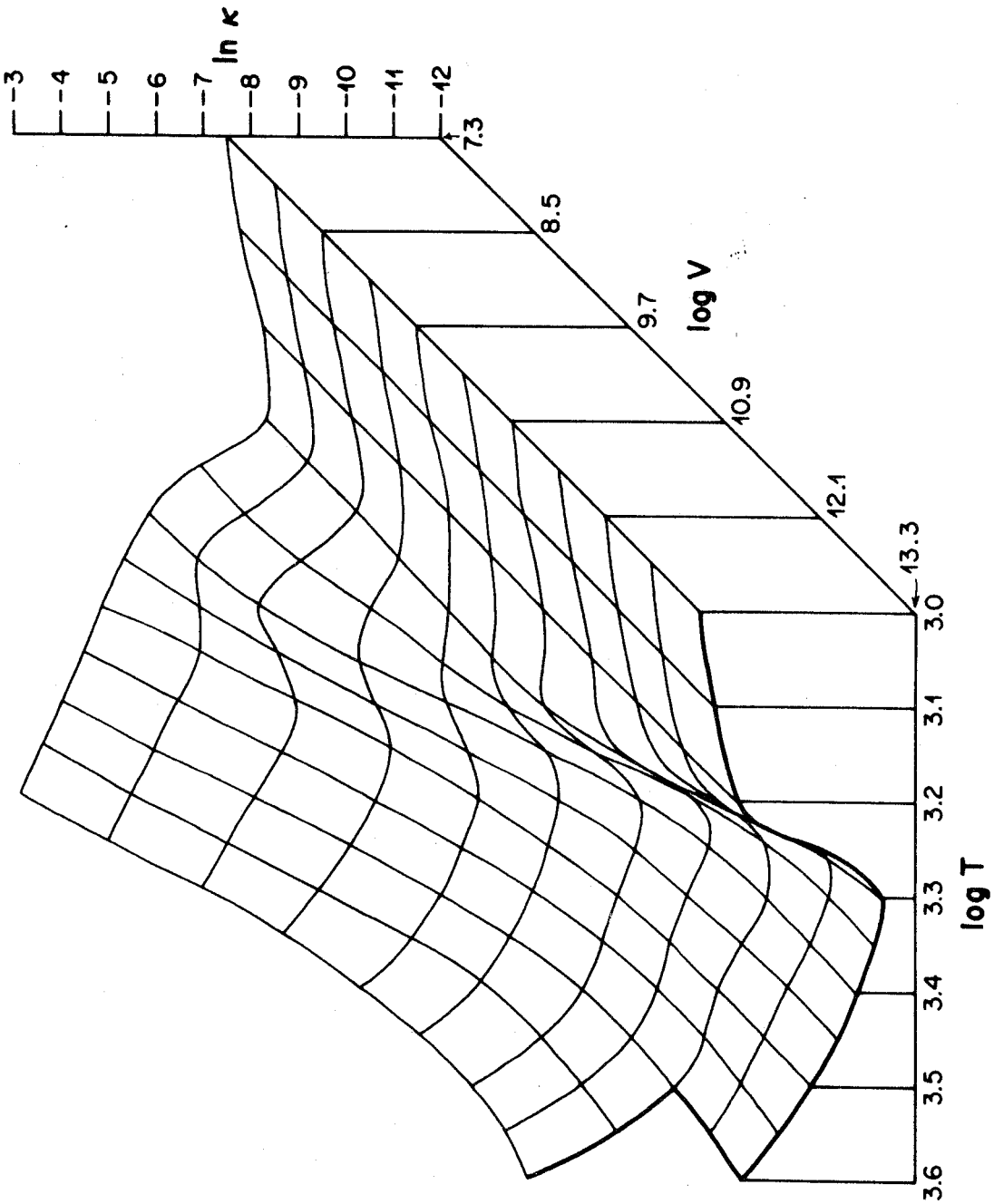
ln κ
-3
-4
-5
-6
-7
-8
-9
-10
-11
-12
7.3
8.5
9.7
10.9
12.1
13.3
log V
3.0
3.1
3.2
3.3
3.4
3.5
3.6
log T

Figure 5

REFERENCES

Allen, C. W. 1963, Astrophysical Quantities (2d ed.; London: The Athlone Press).

Auman, J., and Bodenheimer, P. 1967, Ap. J., 149, 641.

Bohm-Vitense, E. 1958, Zs. f. Ap., 46, 108.

Christy, R. F. 1966a, Ap. J., 144, 108.

_____ 1966a, Ann. Rev. Astr. and Ap., 4, 353.

Deutsch, A. J. 1960, Stellar Atmospheres, ed. J. L. Greenstein (Chicago: University of Chicago Press), Chap. XV.

Epstein, I. 1950, Ap. J., 112, 6.

Feast, M. W. 1963, M. N. R. A. S., 125, 367.

Fernie, J. D. 1959, Ap. J., 130, 611.

Fernie, J. D., and Brooker, A. A. 1961, Ap. J., 133, 1088.

Iben, I., Jr. 1968, Ap. J., 154, 581.

Kamijo, F. 1962, Pub. A. S. Japan, 14, 271.

Lambert D. L. 1967, (private communication).

Ledoux, P., and Pekeris, C. L. 1941, Ap. J., 94, 124.

Ledoux, P., and Walraven, Th. 1958, Hdb. d. Phys., 51, 353.

Mihalas, D. 1965, Ap. J., 141, 564.

Nicholson, S. B., and Pettit, E. 1928, Ap. J., 68, 279.

_____ 1933, Ap. J., 78, 320.

Osvalds, V., and Risley, A. M. 1961, Pub. Leander McCormick Obs., 11, part 21, 147.

Paczynski, B. 1969, Acta Astron., 19, 1.

Paczynski, B., and Ziolkowski, J. 1968a, I. A. U. Symposium No. 34: Planetary Nebulae.

REFERENCES, (Cont'd.)

_____ 1968 b, Acta Astron., 18, 255.

Plaut, L. 1965, Galactic Structure, ed. A. Blaauw and M. Schmidt (Chicago: University of Chicago Press). Chap. XIII.

Rosseland, S. 1949, The Pulsation Theory of Variable Stars, (Oxford: Clarendon Press).

Schwarzschild, M. 1941, Ap. J., 94, 245.

Schwarzschild, M. 1958, Structure and Evolution of the Stars, (Princeton: Princeton University Press).

Schwarzschild, M., and Selberg, H. 1962, Ap. J., 136, 150.

Schwarzschild, M., and Harm, H. 1962, Ap. J., 136, 158.

_____ 1964, Ap. J., 139, 594.

Schwarzschild, M., and Stothers, R. 1961, Ap. J., 133, 343.

Smak, J. 1964, Ap. J. Suppl. 9, 141.

_____ 1966 a, Acta Astron., 16, 1.

_____ 1966 b, Ann. Rev. Astr. and Ap., 4, 19.

Tsuji, T. 1966, Pub. A. S. Japan, 18, 127.

Tsuji, T. 1967, (private communication).

Ulrich, R. K. 1968, (private communication).

Vardya, M. S. 1961, Ap. J., 133, 107.

PART 2

DYNAMICAL MODELS OF LONG-PERIOD VARIABLE STARS

ABSTRACT

It is shown that large-amplitude pulsation can occur in stars which are convective through most of the envelope. The opacity mechanism causes strong driving of the pulsation in the region outside the hydrogen ionization zone, and the Γ-mechanism results in very low dissipation in the hydrogen zone. The phase relation between the bolometric luminosity and the radius variations is similar to that of Cepheids. A relaxed fundamental pulsator is discussed in detail, and some overtone pulsators and two models close to dynamical instability are described briefly.

I. INTRODUCTION

The text which follows is divided into six main parts. In §II-§V the detailed results for one model are described. This model has $M = M_{\odot}$, $L = 10^{37}$ ergs/sec, ($M_{bol} = -3.8$), $\log T_e = 3.39$, and a core mass-fraction of 0.54. The approach to steady pulsation is described in §II, and the influence of the treatment of convection on the model behaviour is discussed in §III. The relaxed model is discussed in §IV, and some comparisons with observations are made in §V. In §VI a brief description is given of two overtone models, a model with a strong mixture of fundamental and overtone, and two models close to dynamical instability. In §VII some of the results are reviewed and discussed.

No attempt was made to develop a detailed physical treatment of convection in a time-dependent situation because that would have been a major problem in itself, and it was apart from the main interest in the calculations. It was expected that some important results concerning the dynamical behaviour of convective stars could be obtained without such a treatment. The results which are presented below confirm that expectation. They also show clearly which aspects of the treatment of convection are most in need of improvement, and suggest what further calculations may be useful even without an improvement.

A full description of the treatment of convection is given in Appendix C. Time-dependence was included by the method used by Cox, Brownlee, and Eilers (1966), but some modifications were made. In the conventional mixing-length treatment of convection the flux is

calculated locally; it depends only on the conditions and the gradients at the point where the flux is required. One result of this is that there is no overshoot region. A simple procedure was developed which makes the convective flux depend on conditions over a region about a scale-height in thickness. The convective flux will be called non-local, or coupled, if it was calculated in this way.

In Appendix B the calculation of initial models is described briefly. Static models integrated with the usual differential equations were not used directly as initial conditions for dynamical calculations. The initial models were calculated from a system of difference equations obtained from the dynamical equations by suppressing the time derivatives. Thus the initial values for all variables were determined on the mass grid that was to be used in the dynamical calculations. In spite of this there was in some cases a suggestion of some incompatibility between the solution for the static model and the equations in the dynamical program. This problem is discussed in Appendix B.

The dynamical program is described briefly in Appendix D. It uses an implicit system of difference equations for the dynamics as well as for the heat transfer. The program has two modes of operation. In the hydrodynamic (HD) mode the equation of motion is used. In the hydrostatic (HS) mode the heat transfer is calculated in the usual way but the model is constrained to remain close to hydrostatic equilibrium at all times. A damping term (which could be set to zero) was included in the equation of motion. This made it possible to damp the pulsational motion on an arbitrary time-scale. Only the envelope was included in the dynamical calculation; the conditions applied at the inner boundary

were that the velocity be identically zero, and the luminosity be a constant in time (the core luminosity).

In Appendix A the secular stability of convective envelopes is examined by means of a simple linear analysis.

A previous paper on static models ([Keeley 1969], hereafter called Paper I) referred to some of the general results described in the present paper. In Appendix E there is a brief discussion of the models described in Paper I.

The equation of state and the opacity were discussed in the appendices of Paper I.

II. THE APPROACH TO STEADY PULSATION

The parameters for the initial model were $M = M_{\odot}$, $L = 10^{37}$ ergs/sec, $\log T_e = 3.39$, and the core mass-fraction was 0.54. This model was identical to the one solar mass model which was described in detail in Paper I.

The initial model was calculated using the local treatment of convection. When it was plugged into the dynamical program using the non-local treatment, the luminosity was not independent of depth and the model began to readjust itself to reach this condition. The model was followed for about 7×10^7 seconds in the HD mode with damping. This was enough time for the initial disturbance caused by the change in energy transfer to settle down, but was not enough for the full readjustment to occur.

The model was then given a fundamental-mode velocity perturbation and was followed in the HD mode. The kinetic energy of the initial perturbation was 1.5×10^{42} ergs. The light curve starting from the time of the initial perturbation is shown in Figure 1. The rapid initial growth in amplitude occurred in all models which were excited

in the most unstable mode. The kinetic energy reached a peak of 7.5×10^{43} ergs at $t=35.5$ [1], and then gradually decreased to 3.4×10^{43} ergs by $t=120$. The mean luminosity per period had a time-average value greater than the core luminosity until about $t=110$. By $t=110$, an excess of 1.8×10^{45} ergs had been radiated. At this time the total internal energy of the envelope was 1.75×10^{46}ergs, and the potential energy was -1.55×10^{46} ergs. Gravitational contraction provided the excess luminosity and simultaneously increased the internal energy. The effect of the contraction is clear from the period of the light curve.

The change in structure described above was not entirely the result of the change in the energy transfer. Three different contributions were identified. Table 1 contains the radius of each mass-shell for four different hydrostatic models which are described below. Model 1 is the original static model integrated with the local description of convection. Model 2 was obtained from model 1 by perturbing it slightly and then calculating in the HS mode using local convection, until it had returned to the condition of luminosity-constancy. The difference between model 2 and model 1 is a source of some concern, and is discussed in Appendix B. Model 3 was obtained from model 1 by using the non-local convection equations and integrating forward in time with the HS mode until luminosity-constancy was reached. The difference between model 2 and model 3 is caused entirely by the change to non-local convection. The overshoot from the convection zone helps transfer energy near the inner edge of the surface radiative region where the opacity is high.

---

[1] The unit of time in expressions of the form $t=\cdots$ will be 10^7 seconds unless it is explicitly given otherwise.

This causes a net energy loss from the non-local model which is stopped by the adjustment it makes. Model 3 is the static model which the pulsating model would have approached if it had been stable; in this sense, model 3 is really the initial model of the calculation.

Model 4 in Table 1 was obtained from the steadily-pulsating model by damping out the kinetic energy on a timescale of about one pulsation period. The difference between model 3 and model 4 is entirely due to the non-linearity of the pulsation. Model 4 is very close to hydrostatic equilibrium, but is far from luminosity constancy. Except near the boundary of the core the luminosity was about 0.8×10^{37} ergs/sec, which is less than the core luminosity of 10^{37} ergs/sec. The difference in radius between corresponding mass shells in models 3 and 4 is more than sufficient to account for the lower luminosity. The damping procedure was repeated with a longer timescale over which there was a slow decay of the amplitude. The result is shown in Figure 2. The luminosity and radius curves for the heavily-damped model are shown for comparison. The radius and luminosity amplitudes of the undamped model are also indicated. The heavily-damped model was followed for a long time, partly in the HS mode. It gradually expanded out past a radius of 1.65×10^{13} cms, and would certainly have returned to the structure of model 3 (Table 1) after a sufficiently long time. At least 10^{9} seconds would have passed before the luminosity difference between the core and the surface could have supplied the necessary gravitational energy.

All models, not just the one described above, developed a luminosity excess and then gradually reduced it by making a change in structure. The local treatment of convection was used in most

calculations, so the non-local treatment was not responsible for this behaviour. Models given an inward initial velocity perturbation also developed the luminosity excess. The overtone models were usually slower to show a structural change, possibly because of their generally lower amplitudes, but again the luminosity excess was clear. Some of the early models were calculated using an explicit system of difference equations for the dynamics, and using a different surface boundary condition, but they also showed the same general behaviour. The reason for this behaviour is discussed in the next section.

III. INFLUENCE OF THE TREATMENT OF CONVECTION ON THE DYNAMICAL BEHAVIOUR OF THE MODELS

The convective flux at time $t + \Delta t$ is calculated from the flux at time t by

$$\frac{F(t + \Delta t) - F(t)}{\Delta t} = \frac{F' - F(t)}{\tau} \quad , \tag{1}$$

where F' is the flux calculated from the instantaneous conditions at time $t + \Delta t$, and τ is a time-scale which will be discussed later. Thus the actual flux F is changed at a rate such that it would reach the instantaneous value F' after a time τ. At almost all times during the calculation $\Delta t/\tau < 0.2$. The differential equation corresponding to equation (1) is

$$\frac{dF}{dt} = \frac{F' - F}{\tau} \quad . \tag{2}$$

If τ is a constant, and if the driving term F' has the form

$$F' = F_0 + \sum_k F_k e^{i\omega_k t} , \tag{3}$$

the solution of (2) is

$$F(t) = F(0)\, e^{-t/\tau} + F_0 (1-e^{-t/\tau}) + \sum_k \frac{F_k}{1+i\omega_k \tau} (e^{i\omega_k t} - e^{-t/\tau}) . \tag{4}$$

Even if $F(0) = F_0$ the relaxed solution,

$$F(t) = F_0 + \sum_k \frac{F_k}{1+i\omega_k \tau}\ e^{-i\omega_k t} , \tag{5}$$

is not reached until $t/\tau >> 1$. If F' is a pure sine wave, or if $\omega_k \tau << 1$ for all k, the function $F(t)$ will look the same as F'. Terms in F' with frequencies such that $\omega_k \tau > 1$ have lower amplitude in $F(t)$; thus F' is smoothed over a time τ. The most important result is that the time-average of $F(t)$ is equal to F_0, the time average of F' in the relaxed solution. If F_0 is <u>not equal</u> to the flux in the equilibrium model, then the time-average of $F(t)$ will be different from the equilibrium flux. The solution of the difference equation (1) after n steps of equal length Δt is

$$F(n+1) = F_0 + \frac{(\Delta t/\tau) F_1\ e^{in\omega t}}{1-(1-\Delta t/\tau) e^{-i\omega \Delta t}} \tag{6}$$

if $(1-\Delta t/\tau)^n << 1$. (The driving function F' has been assumed to have only one frequency component.) If $\omega \Delta t << 1$, equation (6) reduces to

exactly the same form as the solution of the differential equation.

The time-scale τ is <u>not</u> a constant during the calculation. It is written in the form $\tau = \ell/v$, where ℓ is the mixing-length and v is the convective velocity. This choice of τ implies that the energy transferred by a convecting element builds up to the full value only after the element has moved a distance the order of a mixing-length, i.e., only after it has existed for an appreciable fraction of its lifetime. As a decay time-scale, τ is in agreement with experiments (Batchelor 1953), which give

$$\frac{1}{v^2}\,\frac{d}{dt}\,(v^2) \;=\; -A\,\frac{v}{\ell} \qquad (7)$$

where A is of order unity. Thus τ is a reasonable time-scale for the decay of turbulent kinetic energy in the absence of forces to drive the turbulence. In equation (7) the length ℓ is roughly the size of the eddies responsible for most of the energy transfer, and is usually taken to be about a pressure scale-height in stellar convection calculations. Both ℓ and v may vary considerably during a dynamical calculation. The mixing-length ℓ depends on the physical structure while the velocity v is related to the convective flux.

In almost all the calculations reported here, the instantaneous convective velocity, corresponding to the instantaneous flux F', was used for v in the calculation of τ. Using the instantaneous velocity favors a fast rise and a slow decay in $F(t)$. This is shown in Figure 3. The instantaneous velocity varies from 1.36 to 2.30 km/sec. During the decay of F' the instantaneous velocity drops quickly; the low

velocity causes a large τ and results in a slow decay of $F(t)$.

In some early model calculations the sound-speed was used in the expression for the timescale τ. It exceeds the convective velocity by a factor of four or more through the region where convection is important, and doesn't vary as much as the instantaneous velocity. Thus the time-scale is shorter, especially deep in the interior, and is not coupled to the instantaneous flux F'. In spite of these differences, a similar excess luminosity and structural change developed in the early models.

An estimate of the actual convective velocity can be obtained by assuming it is related to the actual flux $F(t)$ in the same way as in the time-independent situation. The velocity calculated in this way from the non-local flux at time t is used in the timescale τ to calculate the local flux at time $t + \Delta t$ from equation (1). The local flux is then spatially smoothed as described in Appendix C to give the non-local flux.

The instantaneous velocity was used in the calculations described in §II. Some parts of the calculation were repeated with the velocity calculated from the actual flux as described above. When the calculation of the steadily-pulsating model was continued with the new velocity, the time-average surface luminosity was immediately reduced below the core luminosity, and remained below it for the four periods in which the calculation was continued. The radius amplitude and the peak kinetic energy increased slightly. If the calculation had been continued the mean radius would have increased until a steady pulsation was reached. A new calculation was begun starting from the non-local static model 3 in Table 4. During the nine periods it was followed the

energy loss in luminosity amounted to about half the amount lost in the calculation using the instantaneous velocity, and the loss rate was still fairly large. These two calculations showed that changing the calculation of the velocity made a difference, but didn't change the order of magnitude of the energy loss. A plot of luminosity vs. time similar to Figure 3 revealed that the asymmetry between the rise and the decay of the convective luminosity had been reduced but not eliminated.

The variations in the mixing-length ℓ make an important contribution to the changes in the time-scale τ in the outer part of the convection zone where the pulsation amplitude is large. The mixing-length at a given mass shell is proportional to PVr^2, where P is the pressure, V is the specific volume, and r is the radius. The variations in r dominate in the outer regions of the model, so ℓ is largest at the time of maximum expansion. The expansion is not in phase with the convective flux (see Fig. 4); ℓ is generally small when the flux is increasing, and large when it is decreasing. This also contributes to the fast rise and slow decay of the luminosity. Near the inner edge of the hydrogen ionization zone ℓ changes by only about 10%; near the outer edge it varies by a factor of 1.7. The variation in ℓ in the outer part of the star is comparable to the variation in the convective velocity; thus the definition of ℓ is important to the dynamical behaviour, and it must be chosen carefully. For example, the mixing length would vary much more if it were defined to be the thickness of a mass layer which is one scale-height in thickness in the equilibrium model; in this case, $\ell \propto$ specific volume, and it could vary by an order of magnitude in the outer part of a large-amplitude model. The

resulting modulation of τ would be a dominant factor in the dynamical behaviour.

The behaviour of some of the quantities related to the luminosity is shown in Figure 3 for the steadily-pulsating model in which the instantantous velocity was used to calculate the time-scale. The curves are plotted for boundary 13, near the bottom of the hydrogen ionization zone. The peak in the instantaneous flux F' is off scale; F' reaches a maximum of 2.59×10^{10} ergs $cm^{-2}sec^{-1}$ at $t = 118.50$, just about the time of maximum compression in zones 13 and 14. The instantaneous flux has the form

$$F' \propto C_P \rho T v(\nabla-\nabla_E) \frac{\ell}{H} \tag{8}$$

in the standard notation. (See Appendix C.) The ratio $F'_{max}/F'_{min} \approx 8$ is made up as follows:

$$v_{max}/v_{min} = 1.71$$

$$(C_P\rho T)_{max}/(C_P\rho T)_{min} = 1.76$$

$$(\nabla-\nabla_E)_{max}/(\nabla-\nabla_E)_{min} = 2.46$$

$$(\ell/H)_{max}/(\ell/H)_{min} = 1.06$$

Thus all parts of the expression for F' contribute to its variation. The variation in C_P at the bottom of the ionization zone opposes the variation in the factor ρT, which alone gives a ratio of 2.73. At the outer edge of the ionization zone C_P and ρT work together. The

phase shift between the flux F(t) and the radius R (Fig. 3) causes the maximum luminosity to occur later than the maximum flux F, and also causes the luminosity amplitude to be smaller than the flux amplitude. The flux at boundary 13 in model 4 (Table 1) is 0.735×10^{10} erg cm^{-2} sec^{-1}, and is equal to F' since the oscillations have been damped out. The time-average value of F' in Figure 3 is larger than this. The luminosity at boundary 13 in the pulsating model gets as low as the luminosity in the damped model 4 only at the minimum luminosity in the pulsating model; the mean luminosity in the pulsating model is close to the core luminosity of 10^{37} ergs/sec. Thus the model transfers energy much more efficiently when it is pulsating.

From the above discussion it is clear that the excessive luminosity which develops in pulsating models is caused by the non-linear behaviour of the convective flux. The discussion in §IV d will show that the dynamical behaviour is also very non-linear, and should also contribute to non-linearity in the energy transfer. It is possible that the convection calculation used here gave unrealistic results for the time-average flux. Several variations of the same basic method gave similar results. A completely different approach to convection in a time-dependent situation, such as that developed by Castor (1968), should be tried, to help determine how much the result obtained here depends on the method used.

One consequence of the structural change is that the time-average temperature and specific volume near the inside rigid boundary of the steadily-pulsating model are different from the values in the original model. In other words, the pulsating model will not connect to exactly

the same core as the initial model. Thus the general behaviour of the model during the approach to steady pulsation is not associated with either the initial static model or the final pulsating model consisting of an envelope plus a core. If the non-linearity of the pulsation really does change the energy transfer as much as was found here, then it will be important to determine what would have happened if a core had been connected. Probably only a very small adjustment of the core would result, but if the energy generation rate were sensitive to the change, then the occurrence of pulsational instability could have some effect on the evolutionary timescale.

The change in structure makes the calculations more difficult. Usually, the model approaches its limiting amplitude from above rather than below, so that strong shocks and irregularities which slow the calculation are more likely to be present. It is almost impossible to study the driving mechanism at low amplitude because of the secular changes which are always occurring until the model reaches a steady pulsation. The model relaxes to a steady pulsation only after many periods.

IV. STEADY PULSATION

a) Driving of the Pulsation

Non-adiabatic effects determine whether a mechanical disturbance will damp out or grow to a finite amplitude. For growth, the star must function as a heat engine, converting heat into kinetic energy faster than the kinetic energy is dissipated. For a mass zone to produce net mechanical energy during a cyclic process it must absorb heat at a high temperature and expel it at a low temperature as it goes around the cycle.

The conversion of energy from the luminosity into mechanical energy is an alternate means of transferring energy to the outside. If the energy finally escaping from the star is entirely in the form of radiation, then the exterior luminosity averaged over a period is equal to the core luminosity. The mean luminosity across the inner boundary of a mass zone which produces kinetic energy will be greater than the mean luminosity across its outer boundary by an amount equal to the kinetic energy produced. The kinetic energy is transferred at the speed of sound to other parts of the star, but there is a net outflow to balance the luminosity deficit.

From the equation of motion,

$$\frac{D}{Dt}\left(\frac{\dot{r}^2}{2} - \frac{GM_r}{r}\right) - P\frac{DV}{Dt} = -\frac{\partial}{\partial M_r}(4\pi r^2 \dot{r} P) \,. \qquad (9)$$

When this is integrated over the mass of the envelope and the boundary conditions $\dot{r}(M_c) = 0$, $P(M) = 0$ are applied the result is

$$\frac{d}{dt}(KE + PE) = \int_{M_c}^{M} \left(P \frac{DV}{Dt}\right) dM_r \quad . \tag{10}$$

During a periodic pulsation ΔKE and ΔPE are both zero over a period, but the integral over a period

$$I = \oint PdV \tag{11}$$

is not generally zero for any particular mass zone. For each mass zone this integral is positive if it is producing kinetic energy and negative if it is absorbing it. For a periodic pulsation the change in internal energy of any mass zone is zero over the period, so that

$$\oint PdV = \oint dQ \tag{12}$$

where dQ is the heat absorbed by the zone during time dt.

In Figure 4 the average of $\Delta M \oint PdV$ and $\Delta M \oint dQ$ is plotted for each mass zone. Zones where this quantity is positive are driving the pulsation. The model was approaching the limiting amplitude from above, and the dissipation exceeded the driving by 2.89×10^{42} ergs during the period. The peak kinetic energy was 3.42×10^{43} ergs. The region of partial ionization of hydrogen ($\Gamma_1 < 4/3$) is shown at its extreme positions in Figure 4. The outer boundary of the convection zone, defined as the point at which radiation carries half the flux, moves approximately in step with the outer edge of the hydrogen ionization zone.

Almost all of the driving comes from zones 19 to 23, over

which the boundaries of the ionization and convection zones move during a period. At maximum expansion the boundaries from 20 outward are radiative. During compression the opacity increases and blocks the flux until the convective flux can build up. By the time the convection zone has reached out to boundary 23 the compression has been reversed and the convection zone recedes again. As the zones become radiative again they release the ionization energy that was stored in them. The opacity that blocks the flux is mostly from H^- and neutral hydrogen; thus the driving does not depend on the uncertainties of the molecular opacity. The mean flux of kinetic energy from the driving region is small compared to the mean luminous flux through it.

The mass in zones 20 to 23 is 3.1×10^{31} gms and so the energy required to ionize them completely is roughly 4×10^{44} ergs, which is greater than the total luminosity integrated over a period. Thus these four zones are capable of storing all the luminous energy for an entire period. The total variation in internal energy of the envelope during a period is about 1.9×10^{45} ergs. The internal energy in zones 20 to 23 changes by almost 10^{44} ergs; most of this is ionization energy. At boundary 23, about $3\times10^{32}\,v_I$ ergs/sec are required to advance the ionization zone with velocity v_I if complete ionization is required. Thus even with the full luminosity this would give $v_I < 1$ km/sec. The full luminosity is not available but complete ionization is not required; in fact, the ionization zone advances by about 0.5 km/sec between boundaries 22 and 23.

The spatial smoothing of the convective flux (by the non-local treatment) provides an overshoot region which helps transfer energy

even outside the region of convective instability, but it also decreases the flux near the edge of the region of efficient convective transfer. Because of these two effects it is not absolutely certain that the smoothing works against the opacity mechanism, but it probably does.

There is weak dissipation in the middle of the ionization zone (see Fig. 4) but the dissipation is low at the bottom of the zone. There is slight driving in two zones. This suggests that the region of low Γ_1 can also contribute to the instability. The dissipation in the region of low Γ_1 is much less than in the region immediately below. The very strong driving at the outer edge of the ionization zone may cause overdriving of the ionization zone nearby; this could account for the dissipation which occurs near the middle of the ionization zone. There is no sign of the He II ionization zone which occurs around zones 7 and 8. In these zones Γ_1 never gets as low as 4/3. The data for zones 2 and 3 is spurious because of a small numerical instability in that region. The dissipation in the surface regions is much stronger than that in the Cepheid and RR Lyrae models of Christy. (See eg. Christy 1966). In the present model the surface region dissipates almost as much kinetic energy as the interior. In the outside few zones especially, much of the dissipation is caused by a strong shock. The region of dissociation of hydrogen molecules is always radiative, (although it is unstable to convection for part of the time), and is optically thin for much of the period. It is not clear whether the low Γ_1 in this region causes a reduction in the dissipation. In cooler models this region could become optically thick. Perhaps the hydrogen molecule dissociation region could contribute some driving in that situation.

Figure 5 is a plot of $\Delta M \oint d\Omega$ averaged over two periods during a time when the model was considerably more over-driven than during the period from which the data for Figure 4 was taken. The radius amplitude $2(R_{max} - R_{min})/(R_{max} + R_{min})$ is also plotted. The general features in Figure 5 are in agreement with those in Figure 4. The damping in the middle of the hydrogen zone, and at its bottom edge, is considerably stronger in Figure 5 than in Figure 4, but there is still a significant reduction in damping near the bottom edge compared to the region below it.

The strong driving near the surface is favorable for the excitation of overtone modes. In models hotter than the one being discussed here, there was not so much mass outside the ionization zone and the overtone mode did dominate. If the hydrogen molecule dissociation region could drive pulsation under some conditions, it might also excite the overtone modes. In the overtone models calculated, the node generally occurred near the middle of the hydrogen ionization zone, at the place where the dissipation shown in Figure 4 would occur.

Model 3 in Table 1 was tested for instability with the opacity fixed at its initial value in each zone. The perturbation decayed slowly and a very small amplitude pulsation could possibly have been sustained. Much of the ionization zone showed weak driving or very low dissipation. However, it is fairly certain that a large-amplitude oscillation could not be maintained in this model without the variation in opacity.

b) Velocity Curves

The velocity of the outer eight boundaries is plotted against time

in Figure 6 a. Outward velocities are positive. All the boundaries outside number 23 reach higher speeds on infall than during expansion. During infall, the acceleration may be 10% or 20% of the acceleration of gravity near the outer part of the convection zone, but at the outer two or three boundaries it may be as high as 80%. Near the time of velocity reversal, accelerations become comparable to the acceleration of gravity in outer zones. These accelerations have some influence on the convective flux, but in general the very large accelerations occur only in the radiative region near the surface. An asymmetry can be present in the dynamics because the inward acceleration never exceeds the acceleration of gravity, whereas the outward acceleration may.

The curves for boundaries inside number 22 are shown in Figure 6 b. Maximum inward velocity occurs earliest around boundaries 22 and 23. Above them, the phase shift to later times shows a compression wave propagating outward, becoming a shock by the time it reaches boundary 26 or 27. Inside boundary 22 the maximum inward velocity shifts to later times as a compression wave propagates inward. It reflects from the inner rigid sphere and returns about 3×10^6 seconds later at boundary 9. The sound speed inside boundary 1 is so high that the travel time from there to the centre and back is less than 10^6 seconds. The maximum outward velocity is reached first in the inner regions as the reflected wave returns. The curves are smooth out to boundary 22, but above there the wave arrives after the velocity has been reversed due to the compression wave originating around boundary 22. At boundaries 24-27 the first wave brings the velocity to zero and the second initiates the expansion. In this model the peak kinetic energy

was larger by a few per cent during infall than during expansion.

c) Behaviour of the Luminosity at Interior Boundaries

As expansion begins in the interior, the luminosity profile $L(M_r)$ has a hump in the middle of the ionization zone, but the luminosity at the surface is near its minimum value. The region where convection is effective (flux greater than 50%) reaches out to boundary 24. The hump in $L(M_r)$ is only about 30% above the mean luminosity; the luminosity amplitude in the interior of Christy's radiative models, (Christy 1966), is much larger than this. In the present model the non-local treatment of the convective luminosity reduced the amplitude and spread the peak out because of the close coupling to zones where the peak in local flux was not very high. The convective zone recedes as expansion occurs, and the divergence of the flux becomes positive and large in the transition region between convective and radiative energy transfer. This divergence results from a steep gradient in the radiative flux. The luminosity $L(M_r)$ is almost independent of M_r in the radiative region during the rise to maximum luminosity. After compression begins the convective zone spreads outward again. The initial increase in the convective flux outside the region of efficient convection is caused by overshoot. Convection contributes 10 or 15% of the luminosity at optical depth unity near the time of maximum luminosity, and essentially all of this is overshoot from deeper layers.

d) The Non-linearity of the Dynamics

The behaviour of the pressure and specific volume as functions

of time is shown in Figures 7a and 7b. Zone 21 is near the outside edge of the hydrogen ionization zone; zone 13 is near the inside edge of the ionization zone. The curves for zone 13 are more regular than those for zone 21, but even in zone 13 the non-linearity of the pulsation is quite evident. The phase relationship between P and V in zone 13 shows that it neither dissipates nor drives very strongly. The high-pressure spikes in zone 13 contribute significantly to the non-linearity in the instantaneous flux F' (see §III).

The specific volume in zone 21 has its main peak earlier than the peak in zone 13, but shows a secondary peak near the time of maximum in zone 13. The main peak in the specific volume in zone 21 is caused by the motion of the boundary between the radiative and convective regions during expansion. When boundary 22 becomes radiative, zone 22 begins to cool very rapidly. The pressure drop due to cooling causes a faster decrease in the outward velocity at boundary 22 than at boundary 21. Zone 22 is compressed and zone 21 expands; this causes the main peak in the specific volume. Eventually boundary 21 becomes radiative also, and soon its velocity drops below that of boundaries 20 and 22. Then zone 22 resumes expanding and compression begins in zone 21. The same process repeats at boundary 20, which is the last one to become radiative. A plot of pressure vs. specific volume for zone 21 is shown in Figure 8. The early peak in the specific volume does not make the difference between driving (positive area) and damping. Note that the specific volume varies by a factor of seven and the pressure varies by a factor of about sixteen.

The temperature for zone 21 is also shown in Figure 7a. The

rapid simultaneous increases in pressure and temperature terminate together as the compression almost stops and the specific heat begins to increase rapidly due to ionization of hydrogen. When expansion begins the pressure drops very rapidly. The temperature holds up longer, partly because of the high specific heat, and partly because for awhile the zone is absorbing heat from the flux. The rapid drop in temperature begins as boundary 21 becomes radiative and the expansion of zone 21 is terminated.

e) Miscellaneous Details

The mass of the hydrogen molecule dissociation region (defined by $\Gamma_1 < 4/3$) varies from 1.33×10^{31} gms to 2.9×10^{30} gms. For the hydrogen ionization zone the variation is from 2.53×10^{32} gms (12% of the mass of the star), to 1.56×10^{32} gms. The mass of the convection zone is about 10^{33} gms, and it changes by about 3×10^{31} gms during the pulsation. The turbulent kinetic energy calculated as $\Sigma \frac{1}{2} m v_c^2$ from the instantaneous convective velocity varied from 1.27×10^{43} to 2.64×10^{43} ergs. The largest turbulent energy density comes from just below the ionization zone around boundary 11. Probably the variation would be a little smaller if the actual convective velocity (see §III) were used. The variation in turbulent kinetic energy is comparable to the peak kinetic energy of the pulsation, which was about 3.4×10^{43} ergs. The energy required to increase the turbulent kinetic energy comes partly from the buoyant force and partly from the work done against the turbulent pressure. For a reliable calculation of the kinetic energy amplitude of the pulsation it will probably be necessary to include the

turbulent pressure in the equation of motion, and to write an additional differential equation for the time dependence of the turbulent kinetic energy. Neither of these were included in this work.

V. THE EXTERIOR REGIONS OF THE MODEL: COMPARISON WITH OBSERVATIONS

There are several uncertainties in the optically-thin part of the model. The diffusion equation with a Rosseland mean opacity has been used to calculate the radiative flux. The boundary condition relating the temperature and luminosity at the surface was written in the form

$$L = \mu (4\pi R^2 \sigma T^4) \quad , \tag{13}$$

where μ is a constant chosen as described in Appendix D. The optical depth was calculated from $\tau = \Sigma \kappa \rho \Delta r$, where Δr is the thickness of a mass zone. The number of zones in the region $\tau \leq 1$ varied from three to six; thus the grid of optical depth was very crude.

No attempt was made to fit the model to a particular star, but it is convenient for the purpose of discussion to compare it to Mira. The period of Mira is about 30 days longer than the period of the model, but the mass and luminosity of the model may be about right. The atmospheric temperature of the model is higher than the observed temperature of Mira.

a) The Bolometric Luminosity Curve

The bolometric luminosity curve for the model is shown in Figure 9. The range is about 1.64 magnitudes, which is larger than the observed one magnitude range of Mira, which seems to be typical (Pettit and Nicholson 1933). The general appearance of the light curve, with the rise to maximum occurring in less than half the period, is similar to that of Mira. The peculiar bumps on the curve repeat fairly regularly, but it is not certain that they are of physical significance; they could be caused by incomplete relaxation, or by the coarse zoning in the model.

For comparison the radius of boundary 27 is also plotted in Figure 9. The phase relation is qualitatively similar to that of Cepheids, in which maximum luminosity occurs near maximum outward velocity. The observations of Pettit and Nicholson (1933) first showed that the maximum bolometric luminosity followed the maximum visual luminosity by about 15% of the period. Their observations showed that the photospheric temperature was decreasing between these times, and so implied that the radius was increasing. They pointed out in their paper that the situation was qualitatively similar to that for a Cepheid. More recent observations, (eg. Eggen 1967), have confirmed the phase shift between the visual and infrared light curves.

b) Radius Curves

The radius variation for mass shells throughout the model is shown in Figure 10. The fractional amplitude of the $\tau = 1$ surface is about 0.45, compared to the value 0.365 determined by Pettit and

Nicholson (1933) for Mira. In the model the maximum radius at $\tau = 1$ occurs just after maximum bolometric luminosity. If a τ less than unity should be used to describe the photosphere, then maximum radius comes later, and the fractional amplitude is larger. If the region of $0.01 < \tau < 1$ is as extended as the model suggests during infall, then curvature effects will be important in the atmospheric structure.

The phase shift in times of maximum radius for the outer few boundaries is quite large, as shown in Figure 10. Observations of Mira by Joy (1926) show that the absorption lines have maximum inward velocity around the time of maximum visual light. If these lines are formed in a region of the star comparable to the outer zone of the model, and if maximum visual light does occur around minimum radius as stated by Pettit and Nicholson (1933), then it may be possible to understand the phase of the absorption line velocities.

Figure 11 shows the outward velocity plotted against optical depth for different times before velocity reversal. A positive slope indicates a velocity gradient corresponding to compression. By $t = 102.62$ there is a shock developing between $\tau = 0.1$ and 0.2. The actual thickness of the shock is not given by the calculation, since the method of artificial viscosity (Richtmyer 1957) smears it out over two or three zones; however, the speed of advance should be about right. By $t = 103.0$ the shock has moved to $\tau < 0.1$ and by $t = 103.28$ it has run through all the mass layers of the model. It is not possible to say from the model whether this shock would produce emission lines.

c) The Visual Luminosity and Effective Temperature

It is difficult to estimate the time at which the model reaches maximum visual luminosity. Pettit and Nicholson (1933) found that maximum visual luminosity occurred very nearly at the time of maximum temperature; this is consistent with the strong temperature sensitivity expected for the visual flux. Curves of the temperature vs. time for the outer layers of the model are shown in Figure 12. The maximum photospheric temperature would be expected to occur between $t = 103.30$ and 103.75; in terms of the radius, this is from near minimum to about the time-average, and in terms of the bolometric luminosity it is from near minimum to well above the time average. Although maximum compression occurs near $t = 103.31$, maximum temperature is delayed in the outer few zones because of a negative flux divergence in them during the initial states of expansion. The times of minimum temperature also show a shift corresponding to the times of maximum specific volume.

Maximum visual flux will occur when the temperature at the surface τ (visual) $\approx \frac{2}{3}$ is highest. This will not necessarily occur when the temperature is highest at the surface τ (Rosseland) $\approx \frac{2}{3}$, nor will it necessarily occur when the temperature defined by

$$4\pi R_e^2 \sigma T_e^4 = L \qquad (14)$$

is highest. (R_e is the radius at τ(Rosseland) = $\frac{2}{3}$). However, it is still useful to check the results of simple estimates of the temperature. The temperatures T' at τ(Rosseland) = $\frac{2}{3}$ and T_e defined in equation

(14) are given in Table 2 at various times during the period. The range of T' is 600°K, while that of T_e is only 380°K. Some of this difference is caused by a positive flux divergence near minimum luminosity. The maximum in T_e occurs at the time of maximum bolometric luminosity, whereas the maximum in T' occurs about 0.15 period earlier. If the radius is increasing at the time of maximum temperature, then the maximum visual luminosity may come after the maximum visual flux. If Smak's calibrations of bolometric correction vs. spectral type (Smak 1966) and temperature vs. spectral type (Smak 1964) are used with the temperature variation given by T', the maximum visual luminosity occurs only about 0.04 period before maximum bolometric luminosity. According to observations the interval should be about 0.15 period. The discrepancy may be in the model, or it may be in the method used to estimate the visual luminosity.

Pettit and Nicholson estimated radii from their temperature measurements using equation (14) and their measured bolometric luminosity curve. They found that the minimum radius occurred 0.15 period before maximum bolometric luminosity. In the model, the corresponding time interval is about $\frac{1}{3}$ of a period. If the Pettit and Nicholson radius curve can be compared with the radius curve for a mass shell in the model, at least near minimum radius, then there is a real discrepancy. An error in the time of maximum luminosity would not be surprising in view of the crude treatment of the atmosphere. In the model, the maximum luminosity occurs a little after maximum outward velocity; however, there is no reason to expect the model to behave exactly as a Cepheid.

VI. FIVE OTHER MODELS

a) Two Overtone Models

These models both had luminosity $L = 10^{37}$ ergs/sec and mass $M = 1.3\,M_{\odot}$. Model 1 had $\log T_e = 3.505$, and a core mass-fraction of 0.94. Model 2 had $\log T_e = 3.478$ and a core mass-fraction of 0.88. These models are identical to models 1.1 and 1.2 in Paper I.

The possibility of overtone pulsation in models of long-period variables may be important to the interpretation of the observations. In Figure 13 are shown the luminosity curve and the radius curves for two mass-shells in model 1. This model was perturbed in the fundamental mode but developed the overtone very clearly after only three fundamental periods. During the changeover the kinetic energy remained considerably below the level of the initial perturbation. The crosses in Figure 13 show the kinetic energy at times near the peak kinetic energy for each period. After the change to the overtone was well-established the kinetic energy grew rapidly. The mean luminosity was very clearly greater than the core luminosity of 10^{37} ergs/sec by the end of the time interval shown in Figure 13. This situation continued for many more periods, and the model was not followed to the final relaxed pulsation. The luminosity range was one magnitude, and the radius amplitude $\Delta R/R$ was about 0.1 at optical depth $\tau \approx 1$.

The probable reason for the overtone instability was discussed in §IV. The node occurred in the hydrogen ionization zone, probably at the position which minimized the dissipation in that region. Because the model was far from being relaxed, no detailed study of the driving was

possible. The pulsation mode was not a pure overtone even after 50 periods; the node still moved around over two or three boundaries during the period. A rough indication of the amplitude curve $\delta R/R$ is shown in Figure 14. In the region of strong driving it has a kink similar to the one in the amplitude curve for the fundamental mode. (See Figure 5.)

Both overtone models described in this section were calculated using a local treatment of convection. After the non-local method was developed and tested, model 1 was repeated from the beginning using the non-local equations. It was again excited in the fundamental mode, but with a smaller initial perturbation. The fundamental behaviour persisted for three or four periods but then the luminosity curve started to show extra bumps at the overtone frequency. The model was followed for about fifty more overtone periods. Compared to the same model with local convection it behaved very sluggishly. At the end of fifty periods there was no doubt that the overtone was the dominant mode, but the rate of increase of kinetic energy remained low. The luminosity amplitude $\Delta L/L$ was still only 20%, and the light curve was quite irregular compared to the clean pulses of the local-convection model. There can be no doubt that a realistic treatment of convection, including the non-local effects, will be necessary for investigation of short-period models.

The behaviour of model 2 was similar to that of model 1; it switched from the fundamental mode to the first overtone after five or six periods. A sample of its light curve and radius variation is shown in Figure 15a. Again, the excess luminosity was clear, since the core luminosity was 10^{37} ergs/sec. The dependence of the light curve on the

convective timescale τ (see §III) was tested by multiplying τ by 0.3 and continuing the calculation. The light-curve of the model after it had settled down again is shown in Figure 15b. Here again it is clear that the details of the treatment of convection are important. The luminosity excess was considerably reduced, but it was not eliminated. The minima were deeper but the amplitude $\Delta L/L$ was about the same.

It is interesting to note that the light curves in Figure 15 show broader maxima than minima, in contrast to the curve for a fundamental pulsator shown in Figure 9. Model 1 also showed this when the non-local calculation was used. Fundamental and overtone pulsators of the RR Lyrae type can be separated quite clearly by the difference in their light curves; fundamental pulsators show a sharp rise to maximum and a slow decline to a broad minimum, whereas overtone pulsators have a more symmetric light curve. The visual light-curves of long-period variables have been classed into similar forms. The fundamental-like curves are more numerous at the longest periods, while the more symmetric curves are more numerous at periods less than 200 days. (See Ledoux and Walraven [1958].) Between 200 and 340 days they are about equally common. The range of mean luminosities for long-period variables is probably considerably larger than the range for RR Lyrae stars; thus a sharp separation between fundamental and overtone at some particular period can't be expected. It is not certain how well the observed visual light curves can be compared with the bolometric curves of the models. However, model calculations in the future should be of considerable value in helping to separate the fundamental pulsators from the overtones. This will provide important information about the radii,

luminosities, and masses of long period variables.

b) A Mixed-Mode Model

The initial parameters of this model were $M = 1.3\ M_{\odot}$, $L = 2\times10^{37}$ ergs/sec, $\log T_e = 3.44$, and the core mass-fraction was 0.8 . This model was identical to model 2.3 in Paper I. The local calculation of convection was used.

The amplitude of the fundamental mode grew rapidly for five periods after the initial perturbation; the peak kinetic energy increased to about 80 times the initial perturbation of kinetic energy. During this time the model radiated 8×10^{44} ergs more than the energy it received from the core, and made a rapid readjustment of its internal structure. The fundamental mode died down again in about four periods more and the overtone became dominant. As this happened the luminosity drain was reversed and the envelope began to absorb energy from the luminosity and increase its mean radius. The overtone mode dominated the behaviour at the surface but the fundamental was still present in the interior, and it increased gradually in strength. After a total time of 1.4×10^{9} seconds the fundamental mode had become so strong that it dominated the behaviour even in the outer zones. After that it decreased in amplitude for another 6×10^{8} seconds, and was about equal in strength to the overtone component when the calculation was stopped.

Examples of radius and luminosity curves are shown for several stages of the calculation. Figure 16 a shows the behaviour at a time shortly after the initial change to the overtone, when the strength of the overtone relative to the fundamental was about maximum. Figure

16b shows the situation after the fundamental had grown back again, and Figure 16c shows the behaviour at the time the calculation was stopped. In all, the calculation covered about 120 overtone periods from the time the overtone first appeared.

There was no indication that either mode would ever become essentially pure. This model was restarted from the equilibrium model with an overtone velocity distribution, but it developed a strong modulation by the fundamental mode after five or six periods. The behaviour suggests that the model would always have a mixture. This causes a continuing irregularity in the light curve, and suggests a possible relation to the many semi-regular and irregular variable red giants.

The significance of the long-term changes in character, from fundamental to overtone and back, is not so clear; it may be related to the initial condition of the model. However, it was pointed out by Christy (1964) that this type of behaviour is known to occur in oscillating systems with non-linear coupling between modes. It is possible that this can arise in stellar pulsation, although it is not established by the behaviour of this particular model.

c) An Irregular Pulsator

The parameters of this model were $M = 1.3\,M_{\odot}$, $L = 2 \times 10^{37}$ ergs/sec, $\log T_e = 3.368$, and the core mass-fraction was 0.40. This model was identical to model 2.4 in Paper I. The local calculation of convection was used.

The luminosity curve, and the radius curve for a mass shell near the surface are shown in Figure 17. Although the model was initiated in

the fundamental mode, waves at a frequency reasonable for the first overtone built up quickly. In the fourth period the model expanded to a much larger radius than in the normal oscillation. The expansion was very smooth and slow; the velocity was only one or two km/sec through most of the interior. The amplitude was extraordinarily large even in the deep interior where the rigid boundary condition was applied. An appreciable fraction of the ionization energy of the envelope was converted to potential energy and luminosity. The peak kinetic energy of the subsequent infall was 9.7×10^{44} ergs, and by $t=55.0$, 2.39×10^{45} ergs had been lost in radiation since the beginning of the expansion. A very strong shock was produced when the infall was halted, and the outer three boundaries of the model, carrying about 0.7% of the total mass, reached escape velocity. It is not certain that the shock or the atmospheric structure was sufficiently well- represented for the mass estimate to be reliable. The peak kinetic energy during the bounce was 7.7×10^{44} ergs.

Because of the large loss of energy in radiation the model subsequently pulsated in a very erratic manner about a contracted configuration. The oscillation amplitude and mean radius increased gradually as some of the core luminosity was converted to potential energy.

This same calculation was repeated with a smaller initial perturbation, and the result was similar. However, the amplitude of the big expansion wasn't so large as in the previous case. The bounce was not so violent and the subsequent pulsations were fairly regular. The amplitude increased gradually and the computation became difficult because of strong shocks in the surface regions.

It was clear that the inner boundary condition was not good by the time the giant expansion had proceeded very far, and that it was expecially bad during the bounce. The possibility of unstable behaviour of this type is probably not in doubt, but the amplitude is very uncertain. This calculation was done with a relatively primitive version of the computational program, and the inner boundary condition could be applied deeper in the star if the latest version were used. It would be especially interesting to determine if the type of behaviour found in this model could occur many times, perhaps ejecting a small but non-negligible fraction of the mass each time.

d) A Model Close to Dynamic Instability

The parameters of this model were $M = 1.3\, M_{\odot}$, $L = 2 \times 10^{37}$ ergs /sec, $\log T_e = 3.347$, and the core mass-fraction was 0.20. This model was identical to model 2.5 in Paper I. The local calculation of convection was used.

This model was calculated to check the possibility that an extreme red giant could eject its envelope and form a planetary nebula. Abell and Goldreich (1966) presented arguments in favor of this hypothesis, and the problem was subsequently pursued by Paczynski (1968), by Paczynski and Ziolkowski (1968a,b), and by the author. The internal energy per gram can exceed the gravitational energy per gram in an extreme giant envelope when the radius is so large that the ionization energy of hydrogen per gram is comparable to the potential energy per gram. Thus the ejection of the envelope seems possible from energy considerations. However, there are several sources of uncertainty.

The energy criterion is based on an adiabatic expansion, but it is possible that most of the energy would escape in the form of radiation, and leave the mass behind. Also, it must be demonstrated that real stars actually reach the evolutionary state where the proposed ejection becomes possible; in other words, the initial condition of the time-dependent model must be justified.

This model was the closest to dynamical instability of any that was calculated. The core mass is undoubtedly too small to be consistent with stellar evolution considerations. An equally-unstable model with larger core mass could probably have been obtained at higher luminosity, but there were computational difficulties with high-luminosity models. Since the main interest at this point was to investigate the behaviour of the envelope, the present model was considered adequate.

Two initial models were tested, differing only in the depth at which the inner boundary condition was applied. The results of four different calculations are given in Table 3. The kinetic energy as a function of time is shown in Figure 18. Cases 3 and 5 used the initial model with the deep integration; cases 1 and 2 were calculated on an early version of the program using an explicit system of difference equations. Case 2 differed from case 1 only in that the initial velocity perturbation was directed inward instead of outward. Cases 3 and 5 differed only in the magnitude of the initial perturbation.

In case 1, after an initial small decrease in the kinetic energy the expansion occurred without any preliminary oscillations. The expansion proceeded very smoothly, as in the model discussed in §VIc, and the velocities never much exceeded 10 km/sec. Escape velocity was

never reached, even when the outer layers reached a radius of about 2×10^{14} cms. The model was optically thin to about 1.5×10^{14} cms at this time. As the envelope expanded the boundary of the surface radiative region moved in through the mass, always remaining a little outside of the hydrogen ionization zone. The hydrogen ionization zone and the hydrogen molecule dissociation region both showed unstable behaviour by their outward accelerations. The expansion finally stopped when most of the mass had passed through these regions.

The 10^{46} ergs lost in luminosity (see Table 3) was a dominant factor in the behaviour. The energy required to disperse the entire envelope to infinity in cases 3 and 5 was only 1.13×10^{46} ergs. Even if only 25% of the envelope had escaped, that would have been sufficient for comparison with a planetary nebula. It is clear that the non-adiabatic behaviour of the envelope is of extreme importance. If solid particles could form and keep the opacity high, the energy loss could be delayed. It is also possible that a more luminous model, with a greater fraction of envelope mass in the hydrogen ionization zone, would have gone farther.

Some comments on the behaviour of case 2 are of interest since it was the only one of the four in which the initial perturbation was a compression. The hydrogen ionization zone showed a tendency toward an infall instability such as occurs during pre-main-sequence contraction. The modest inward motion of the perturbation was not reversed until the outside radius of the star had dropped to about 65% of its initial value. The temperature and pressure in the zone adjacent to the rigid inner boundary went from $T = 6.2\times10^{4}$ to 8.2×10^{4} °K, and $P = 1.01\times$

10^6 to 6.37×10^6 dynes/cm^2 by the time the infall was halted. The subsequent expansion shown in Figure 18 was extreme, but eventually the envelope began to fall back.

In cases 3 and 5 there was more mass below the hydrogen ionization zone, which could contribute to the push once it started to recombine. However, the results showed clearly that the additional mass tended to damp the instability. The small initial perturbation of case 3 produced little indication of the severe instability observed in cases 1 and 2. The larger perturbation in case 5 produced a better response but it still fell far short of cases 1 and 2. It would have been interesting to follow the pulsation in cases 3 and 5; it is quite possible that these cases would have worked up to a giant expansion after several oscillations.

An obvious serious problem with these calculations is the interior boundary condition. Even for cases 3 and 5 the data in Table 3 show that the boundary condition was completely unrealistic by the time the expansion had proceeded very far. Unfortunately, the structure of the static models makes it difficult to integrate much deeper without adding a considerable number of zones.

Paczynski (1969) also calculated a model of this type, in which he integrated a little deeper than in case 3. He found essentially the same behaviour. The envelope expanded slowly and never reached the escape velocity. There was a large energy loss in luminosity, and a complete breakdown in the inner boundary condition.

It will be useful to pursue calculations of this type when a satisfactory procedure (other than brute force - i.e. many more zones) is

devised for treating the inner boundary condition. Experience with other calculations suggests that a more sophisticated treatment of convection should be included. Also, in view of the importance of radiative energy losses, a better treatment of the surface radiative regions may be necessary.

VII. DISCUSSION

a) The Structural Changes

It is clear from the discussion in §III that the treatment of convection is responsible, at least in part, for the difference between the equilibrium luminosity and the time-average luminosity of a high-amplitude model pulsating about the equilibrium configuration. The

uncertainty in the reality of an effect of the magnitude found here is the principal deficiency in the work. Because of this, relaxed models were not used in the discussion of the periods of models in Paper I. (See Appendix E.) However, this uncertainty does not influence the general conclusions on the dynamical behaviour of the models investigated.

b) The Non-Linearity

The non-linearity of high-amplitude pulsations can have important consequences. The simple one-zone adiabatic model discussed by Usher and Whitney (1968) showed that the time-average radius can be much greater than the equilibrium radius during a high-amplitude pulsation. This same behaviour was evident in Figure 2; the time-average radius and luminosity decreased markedly as the pulsation was damped out. Even if there were no non-linear effects in the energy transfer itself, the change in mean radius would change the luminosity.

There is no reason why the time-average properties of a non-linear oscillator should be identical to the properties it would have when at rest in the equilibrium position. The model never passes through the equilibrium configuration during the course of the pulsation because of the phase shifts in the motions and in the energy transfer. Thus some shift in the mean luminosity should be expected. Determining the magnitude of the change, and the time-scale over which it occurs, is the important problem.

Because of the extreme behaviour of some of the models it is possible to identify interesting properties which could have gone unnoticed except if a very well-relaxed model were studied for a very

long time. An example is the behaviour of the model in § VI b, which pulsated with a mixture of fundamental and overtone. The quasi-periodic change in relative strength of the two modes is accompanied by a change in the mean radius, which in turn would cause a change in the period. Periodic variations in period have been noted for several stars; it was shown by Campbell and Sterne (1937) that this behaviour is reasonably certain for R Cnc, S Ser, and U Boo.

c) The Instability Region in the HR Diagram

Although no attempt was made to locate the boundaries of the region where convective stars are unstable to pulsation, it is possible to make some qualitative statements about them. In the luminosity range investigated, the low-temperature boundary is determined by the boundary of the Hayashi forbidden region. The high-temperature boundary is more interesting. It has been suspected that the onset of effective convection is responsible for the low-temperature boundary of the Cepheid instability region; however, the existence of variable stars at much lower temperature showed that convective stars could be unstable. The hottest model studied in any detail was the overtone model described in § VI a, with $\log T_e = 3.505$. It was quite unstable when the local calculation of convection was used, but much less unstable when the non-local treatment was used. In high-temperature models, the region of driving by the opacity mechanism is thin and close to the surface. The flux carried by overshoot from the convection zone may be a sufficiently large fraction of the total that the opacity mechanism becomes ineffective at high temperature. The Γ-mechanism alone was

unable to drive a large amplitude oscillation in the fundamental model discussed in §IV a. Overtone models calculated using local convection have a high narrow peak in $L(M_r)$ near the node at the time of maximum compression. The non-local method of calculation gives a much wider but lower peak. The extra width may interfere with the operation of the overtone mode.

The opacity mechanism may be capable of exciting only the overtone mode below a certain luminosity, because the fraction of the envelope mass which is in or above the hydrogen ionization zone generally decreases with decreasing luminosity. Any low-level excitation by the Γ-mechanism would eventually be choked off for the same reason. If the low-temperature boundary continues to slope toward higher effective temperature at lower luminosity, it might eventually intersect the high-temperature boundary and provide a low-luminosity cut-off of the instability region.

I wish to thank W. D. Arnett for his help in the initial development of the computer program, and for his continuing interest in this work. I am grateful to R. F. Christy and Peter Goldreich for guidance and encouragement throughout the course of the work. I thank Dr. B. Paczynski for an interesting conversation, and for communicating his result on the planetary nebula problem. I gratefully acknowledge the financial assistance of the California Institute of Technology, the National Research Council of Canada, and the Woodrow Wilson Foundation.

APPENDIX A

LINEAR STABILITY ANALYSIS

The linear stability analysis which has proved so useful in the discussion of radiative stars has not been applied very effectively to convective stars. However, it can be used to obtain a simple result which may be of importance. For simplicity, the convective luminosity is treated as if it can react immediately to changes in conditions in the star, and non-local effects are neglected.

a) Method 1

This discussion follows the method of Baker (1966) for the one-zone model. The luminosity variation is written in the form

$$\frac{\delta L}{L} = \epsilon \frac{\delta r}{r} + \eta \frac{\delta P}{P} + \xi \frac{\delta T}{T} \tag{A1}$$

where ϵ, η, ξ are unspecified coefficients. The time-dependence e^{st} is substituted into the linearized system of equations; a cubic equation of the form

$$s^3 + AK\sigma s^2 + B\sigma^2 s + K\sigma^3 D = 0 \tag{A2}$$

gives the possible values for s.

$$A = (\delta\eta + \alpha\xi)(\Gamma_3 - 1) \tag{A3}$$

$$B = (3\Gamma_1 - 4) \tag{A4}$$

$$D = (\Gamma - 1)\left[\delta(\epsilon - 4\eta) - (4\alpha - 3)\xi\right] \tag{A5}$$

where

$$\Gamma_3 - 1 \equiv (\partial \ell n T / \partial \ell n \rho)_s , \quad \Gamma_1 \equiv (\partial \ell n P / \partial \ell n \rho)_s$$

$$\delta \equiv -(\partial \ell n \rho / \partial \ell n T)_P \geq 1, \quad \alpha \equiv (\partial \ell n \rho / \partial \ell n P)_T \geq 1 ,$$

$\sigma^2 = R^3/GM$, and K is a measure of the departure from adiabacy. $K = 0$ is the adiabatic case. Nuclear energy generation has not been included in the equations.

The cubic equation has a real root with sign opposite to the sign of D. If $D < 0$ there is a positive root s_0, and an initial perturbation will grow exponentially with timescale $1/s_0$ until non-linear effects become important. For a radiative star, $\epsilon = 4$, $\eta = -(\partial \ell n \kappa / \partial \ell n P)_T$, $\xi = -\left[(\partial \ell n \kappa / \partial \ell n T)_P - 4\right]$. With Kramers opacity $\eta = -1$ and $\xi = 17/2$. Then

$$D = (\Gamma_3 - 1)\left[8\delta - \frac{17}{2}(4\alpha - 3)\right] \tag{A6}$$

In an ionization zone both α and δ are > 1. If they are set to unity for simplicity the result is

$$D = -\tfrac{1}{2}(\Gamma_3 - 1) , \tag{A7}$$

and the condition for instability is satisfied. The convective luminosity is of the form

$$L \propto r^2 C_P \rho T (\nabla - \nabla_A)^{3/2} . \tag{A8}$$

A very simple linearization of this is

$$\frac{\delta L}{L} = 2\frac{\delta r}{r} + \frac{\delta P}{P} . \tag{A9}$$

The terms left out are not really negligible, but they will be ignored for now. With this linearization, $\epsilon = 2$, $\eta = 1$, $\xi = 0$ and

$$D = -2(\Gamma_3 - 1) \quad . \tag{A10}$$

This also satisfies the condition for instability, and the growth rate is four times larger than for the radiative case.

b) Method 2

This discussion is based on a criterion for secular stability derived by Jeans (1928) and discussed by Ledoux (1965). The condition for secular stability against a homologous contraction is

$$n - 3m < 3\mu + \nu \quad , \tag{A11}$$

where μ and ν are the exponents of ρ and T in the nuclear energy-generation formula, and m and n are the exponents of ρ and $1/T$ in the opacity formula. For Kramers opacity the inequality (A11) becomes $\frac{1}{2} < 3\mu + \nu$. The opacity exponents enter through the linearized expression for the radiative luminosity. The result of repeating the calculation using equation (A9) is $2 < 3\mu + \nu$.

The point of concern with the models is that only the envelope is studied; in effect, $3\mu + \nu = 0$. In the absence of nuclear energy generation a star contracts on a Kelvin time-scale to supply the energy lost in luminosity. The situation with envelope models is different because energy is supplied at a constant rate appropriate to the static model. However, this cannot prevent the instability from developing if the conditions for it are satisfied.

c) Conclusions

The very crude arguments above suggest that the problem may be

more serious for convective than for radiative envelopes. From equation (A6) it is clear that $\epsilon < 0$, $\eta > 0$, $\xi > 0$ contribute toward a negative D. The coefficient ϵ is positive for both the radiative and convective luminosity. The discussion in §III showed that the instantaneous convective luminosity increases strongly during compression; at boundary 13 the flux increases by a factor of eight, whereas $\delta P/P = 2.96$ and $\delta T/T = 1.29$. This suggests that in a low amplitude situation where the linear analysis would be valid, the adopted linearization in equation (A9) may under-estimate the destabilizing effect of the temperature and pressure dependence.

No published work on Cepheid or R R Lyrae pulsation has suggested that a secular instability exists for those models. Perhaps the surface region of the star where $(\partial\kappa/\partial T)_\rho > 0$, (which favors pulsational instability), can stabilize the models against secular contraction. To first order in K, the real root of equation (A2) is

$$s_0 = -K\sigma D/B \quad . \tag{A12}$$

In the convective stars with large ionization zones, the ratio $(\Gamma_3 - 1) / (3\Gamma_1 - 4)$ which appears in D/B can become large. The growth rate of a pulsation is proportional to $K\sigma$ also; thus the high growth rate observed in the present models suggests that they are more non-adiabatic than R R Lyrae models, and so K is larger. Both of these results favor a rapid growth rate for the secular instability if it really exists.

Since the analysis is very crude, the results are far from being established. Non-linear calculations will eventually confirm or deny

that this instability is of importance in understanding the behaviour of the models. It is clear from the second method, and could have been shown by the first, that any of the usual nuclear reactions would be able to stabilize the star, even if the envelope alone were unstable.

APPENDIX B

I. THE INITIAL MODELS

The dynamical equations are written in Lagrangian form, with M_r as the spacial independent variable. The grid-points for the difference equations are at specified values of M_r, and are labelled from 1 to N starting from the inner boundary. The variables r and L are also defined on this grid. The N-1 zones between the grid points are numbered from 3/2 to N-$\frac{1}{2}$; the thermodynamic variables are defined on the mass zones.

The difference equations used to integrate the static models follow directly from the Lagrangian form of the hydrostatic equation and the equation of continuity. The hydrostatic equation is used to advance the pressure, and the condition of luminosity-constancy is used to determine the temperature by iteration. Then the equation of continuity is used to advance the radius. Initial values for the inward integration are obtained from a model integrated with the differential equations. (See Paper I.)

The difference form used for the convective luminosity is given in Appendix C. The local expression is used, since otherwise a step-by step integration would be impossible. The expression used for the radiative luminosity is

$$L_{rad} = \frac{8\sigma}{3} \frac{(4\pi R_k^2)^2}{K_k} \frac{T^4_{k-\frac{1}{2}} - T^4_{k+\frac{1}{2}}}{(m_{k-\frac{1}{2}} + m_{k+\frac{1}{2}})} , \qquad (B1)$$

where $m_{k-\frac{1}{2}}$ is the mass of the zone between boundaries k-1 and k. The opacity κ_k is a mean of $\kappa_{k-\frac{1}{2}}$ and $\kappa_{k+\frac{1}{2}}$, of the form used by Christy (1964).

II. INITIAL EQUILIBRIUM OF STATIC MODELS

The most obvious possible explanation of the difference between model 1 and model 2 in Table 1 is that the solution of the equations in the static model program does not satisfy very well the dynamical equations with time-derivatives set equal to zero. This possibility was checked by having the dynamical program print out the initial acceleration and luminosity at each grid-point. The luminosity was independent of depth to one part in 10^5, and the accelerations were less than 5×10^{-5}, of the local acceleration of gravity. The luminosity was less than the core luminosity more often than it was higher. There was no systematic trend in the accelerations. The initial equilibrium of one other model was checked and found satisfactory also. It was not determined whether all the models would make an adjustment analogous to the difference between model 1 and model 2 in Table 1. If the problem really is one of incompatibility of the two sets of equations, then the model structure must be very sensitive to small deviations from equilibrium.

APPENDIX C

I. LOCAL EQUATIONS

The equations for the convective flux are quite similar to those used by Mihalas (1965). In difference form they are written:

$$F'_k = \tfrac{1}{2}\left(\frac{\ell}{H}\right)_k \langle C_p \rho T\rangle_k \, v_k \, (\nabla - \nabla_E)_k \tag{C1}$$

$$v_k = \tfrac{1}{2}\left(\frac{\ell}{H}\right)_k \left[\left\langle \frac{PVQ}{2}\right\rangle_k (\nabla - \nabla_E)_k\right]^{1/2} \tag{C2}$$

$$\nabla_k = \frac{\ell n(T_{k-1/2}/T_{k+1/2})}{\ell n(P_{k-1/2}/P_{k+1/2})} \tag{C3}$$

$$\frac{\nabla_E - \langle \nabla_A\rangle_k}{\nabla_k - \nabla_E} = \frac{16\sigma\langle T^4\rangle_k}{(\ell/H)_k \langle C_p\rho T\rangle_k} \frac{1}{v_k} \frac{\langle\kappa\rho\rangle_k \ell_k}{1+\langle\kappa\rho\rangle_k^2 \ell_k^2} \tag{C4}$$

$$\ell_k = \langle PV\rangle_k / g_k \tag{C5}$$

$$(\ell/H)_k = (P_{k-1/2} - P_{k+1/2})\, A_k/(m_k g_k)\ , \tag{C6}$$

where

$$\langle X\rangle_k \equiv (X_{k-1/2} + X_{k+1/2}) \,/\, 2 \quad ,$$

and

$$m_k \equiv (m_{k+1/2} + m_{k-1/2}) \,/\, 2 \quad .$$

A_k and g_k are, respectively, the area and the acceleration of gravity at boundary k. The ratio of mixing-length to pressure scale-height

(ℓ/H) is unity in a hydrostatic model. If the equations are used in a non-static situation, they must be written in a form which causes the convection to die out in freely-falling material, and to increase when the effective gravity $-\nabla P/\rho$ is larger than the acceleration of gravity. This is taken into account by the definition of (ℓ/H) in equation (C6).

The equation used to advance the convective flux by one timestep Δt is

$$F(t + \Delta t) = \frac{\Delta t}{\tau} F' + (1 - \frac{\Delta t}{\tau}) F(t) \qquad \text{(C7)}$$

for $\Delta t/\tau < 1$, and

$$F(t + \Delta t) = F' \qquad \text{(C8)}$$

for $\Delta t/\tau \geq 1$. F' is the instantaneous flux calculated from equation (C1). This equation was used by Cox, Brownlee, and Eilers (1966). The equation is used even if F' drops to zero; then, if $\Delta t/\tau \ll 1$ the flux decays approximately exponentially. The expression used for the time-scale τ is

$$\tau = \ell/v \, . \qquad \text{(C9)}$$

The definitions of ℓ and v were discussed in §III.

II. NON-LOCAL EQUATIONS

The convective luminosity at time $t+\Delta t$ is written in a form

$$L_k = \beta L_k^* + (1-\beta)\left[\alpha \langle L_{k-1} \rangle + (1-\alpha) \langle L_{k+1} \rangle\right] , \tag{C10}$$

where

$$L_k^* = \frac{\Delta t}{\tau} L_k' + (1 - \frac{\Delta t}{\tau}) L_k(t) \tag{C11}$$

is similar to equation (C6) except that it is written with the luminosity instead of the flux.

$$\beta = \text{Min}\left[(r_{k+1}-r_{k-1})/2\ell_k, 1\right] . \tag{C12}$$

The factor β determines the coupling between boundary k and the two adjacent boundaries.

$$\alpha = (r_{k+1}-r_k) / (r_{k+1}-r_{k-1}) \tag{C13}$$

is the weighting function for the contributions from boundaries $k-1$ and $k+1$.

$$\langle L_{k+1} \rangle = \gamma L_{k+1} + (1-\gamma) L_{k+1}(t) , \tag{C14}$$

where

$$\gamma = \text{Min}\left[v_k \Delta t/(r_{k+1}-r_k) , 1\right] . \tag{C15}$$

Note that in all the above equations, L_j written without an argument refers to time $t+\Delta t$. For each value of k, equation (C10) contains $L(t+\Delta t)$ at three consecutive boundaries. This coupled system of linear equations is easily solved when boundary conditions are specified at the end-points of the grid. At the outer boundary it is assumed that $F' = 0$ and

$$L_N(t+\Delta t) = \left[1 - (r_N - r_{N-1}) / \ell_{N-1}\right] \langle L_{N-1} \rangle \ . \qquad \text{(C16)}$$

Normally, L_{N-1} is very small. At the inner boundary the convective luminosity is fixed at the value given by the static model.

APPENDIX D

THE DYNAMICAL CALCULATIONS

The two equations which describe the radial pulsation of a spherically-symmetric star are the equation of motion,

$$\ddot{r} = -4\pi r^2 \frac{\partial P}{\partial M_r} - \frac{GM_r}{r^2} \quad , \tag{D1}$$

and the first law of thermodynamics,

$$-\frac{\nabla \cdot \vec{F}}{\rho} = \frac{DE}{Dt} + P\frac{DV}{Dt} \quad . \tag{D2}$$

The pressure P includes the artificial viscosity term used in the automatic treatment of shock waves (Richtmyer 1957). E is the internal energy per gram and D/Dt is the derivative following the motion.

The dynamical program was changed many times during the course of this work. By the time the calculations described in this work were completed, the finite difference analogues of equations (D1) and (D2) were being written in the form used by Fraley (1968), and so they will not be repeated here. The advantage of the form used by Fraley for the equation of motion is that the <u>difference</u> equations conserve energy exactly, independent of changes in size of the timestep. The accuracy of the energy conservation during the integration forward in time is determined by the accuracy of the iterated solution of the equations. The disadvantage of Fraley's form is that the system of equations is only marginally stable. Numerical difficulties arising from this can be overcome by the method suggested by Fraley.

The equations are solved by the Newton-Raphson iteration method. Several terms, including the convective flux, were omitted from the linearization of the first law of thermodynamics, but none were neglected in the linearization of the equation of motion. The equation of state and the subroutine which calculated the convective flux were used during each iteration.

A rigid sphere with a constant luminosity was used for the inner boundary condition. The pressure in the zone outside the surface boundary was put equal to zero. A constant μ was defined from the original static model by

$$L_N = \mu(4\pi R_{N-1} R_N \sigma T^4_{N-\frac{1}{2}}) \quad , \tag{D3}$$

where N refers to the boundary at the surface, and $N-\frac{1}{2}$ refers to the zone just inside it. The value of μ was always between 1.5 and 2.0. Equation (D3) was then used with that value of μ, as a boundary condition for the dynamical model. This condition is very similar to the one used by Christy (1964).

A term of the form $-\lambda\dot{r}$ was included in the equation of motion. The kinetic energy is damped on a timescale $1/\lambda$.

The basic method used in the HS mode was described by Cox, Brownlee, and Eilers (1966), except that the solution was iterated in the present program.

APPENDIX E

THE MODELS IN PAPER I

Because of the changes in structure which always occurred before the models reached a relaxed pulsation, the periods of the relaxed models were different from those of the initial static models. The periods given in Paper I were estimated from the pulsating models before a significant structural change had occurred; they are presumably similar to the periods which would have been obtained from a linear non-adiabatic analysis of the static model.

TABLE 1

RADII OF MASS SHELLS

Boundary Number	Radius (10^{12} cms) Model 1	Model 2	Model 3	Model 4
1	1.58	1.58	1.58	1.58
2	1.96	1.92	1.90	1.79
3	2.38	2.29	2.26	2.01
4	2.87	2.73	2.68	2.29
5	3.42	3.24	3.16	2.63
6	4.08	3.84	3.74	3.04
7	4.86	4.56	4.43	3.54
8	5.82	5.45	5.28	4.16
9	6.97	6.52	6.33	4.95
10	8.36	7.83	7.60	5.87
11	10.04	9.40	9.12	7.20
12	11.44	10.70	10.38	8.21
13	12.66	11.83	11.48	9.10
14	13.76	12.85	12.46	9.89
15	14.75	13.77	13.34	10.61
16	15.63	14.60	14.15	11.28
17	16.42	15.34	14.87	11.90
18	17.10	15.99	15.50	12.48
19	17.68	16.56	16.05	13.00
20	18.13	17.02	16.41	13.47
21	18.42	17.33	16.69	13.87
22	18.68	17.59	16.94	14.15
23	18.96	17.86	17.19	14.37
24	19.20	18.10	17.43	14.56
25	19.39	18.31	17.63	14.73
26	19.54	18.48	17.81	14.88
27	19.67	18.62	17.96	15.00
28	19.81	18.75	18.09	15.11
29	19.95	18.88	18.23	15.20

TABLE 2

TEMPERATURE ESTIMATES

Time (10^7 sec)	R_e (10^{13} cms)	L (10^{37} ergs/sec)	T_e (°K)	T' (°K)
103.06	1.16	0.409	2550	2364
103.31	1.21	0.518	2650	2623
103.56	1.44	0.946	2830	2818
103.75	1.65	1.356	2890	2896
104.03	1.84	1.753	2920	2863
104.13	1.89	1.860	2930	2835
104.27	1.95	1.646	2790	2670
104.40	1.95	1.493	2720	2584
104.72	1.79	1.130	2660	2437
105.00	1.51	0.767	2620	2335
105.31	1.22	0.551	2680	2299
105.54	1.16	0.432	2590	2379
105.77	1.16	0.461	2630	2474

TABLE 3

DATA FOR MODEL NEAR DYNAMICAL INSTABILITY

	Case 1	Case 2	Case 3	Case 5
R_1^* (10^{13}cm)	0.147	0.147	0.0252	0.0252
R_1/R_s †	0.0416	0.0416	0.0071	0.0071
R_2 at t = 0 (10^{13}cm)	0.354	0.354	0.0478	0.0478
R_2 at peak KE	1.96	2.04	0.141	0.455
T_2 at t = 0 (10^4 °K)	6.21	6.21	24.30	24.30
T_2 at peak KE	1.89	1.80	9.86	3.65
P_2 at t = 0 (10^6 dyn/cm^2)	1.01	1.01	24.50	24.50
P_2 at peak KE	0.0019	0.0016	0.448	0.0068
Initial KE (10^{43} ergs)	1.53	1.53	1.33	4.89
Peak KE	63.8	80.9	5.30	24.6
Peak L (10^{37} ergs/sec)	22.0	23.6	10.0	15.9
Time t_L of peak L (10^7 sec)	12.93	23.37	13.86	11.54
$\int (L-L_c)dt$ at time t_L (10^{43}ergs)	926.	881.	588.	804.
$R_s(t_L)$ (10^{13} cm)	11.1	11.3	8.68	11.4

*Subscripts refer to boundaries or zones, numbered outward from the inner boundary. Zone 2 is between boundaries 1 and 2.

†The surface radius $R_s = 3.89 \times 10^{13}$ cm at t = 0.

FIGURE CAPTIONS

Fig. 1. The light-curve of a $1M_\odot$ model with core luminosity 10^{37} ergs/sec. The unit of time is 10^7 sec.

Fig. 2. The surface luminosity (L) and radius of mass-shell 27(R). The pulsation energy was being dissipated by an artificial frictional term in the equation of motion. The two pairs of curves show the results of damping on a short or long time-scale. At $t=122.5$ the mechanism for producing kinetic energy in the model was almost making up the losses in the damping term, and so the damping timescale was decreased again to speed the decay. ΔL and ΔR show the full luminosity and radius amplitude for the undamped model.

Fig. 3. The non-local flux F and the non-local luminosity L are shown at a mass-shell near the inner edge of the hydrogen ionization zone. Also shown are the instantaneous flux F' and the radius R of the mass-shell.

Fig. 4. Kinetic energy production and dissipation. The average of $\Delta M \oint dQ$ and $\Delta M \oint PdV$ is plotted for each mass zone. The peak kinetic energy is 3.42×10^{43} ergs.

Fig. 5. Kinetic energy production and dissipation. The radius amplitude $\delta R/R$ is also shown. This is the same model as in Figure 4, but the pulsation amplitude is higher.

Fig. 6 a. Velocity vs. time for the outer mass-shells. Zero velocity for each shell is indicated by the horizontal line near the shell number. Outward velocity is positive.

Fig. 6 b. Velocity vs. time for interior mass-shells.

Fig. 7 a,b. The specific volume, pressure, and temperature for zone 21, near the outside of the ionization zone, and for zone 13, near the inside.

Fig. 8. Pressure vs. specific volume for zone 21. Kinetic energy is produced in this zone.

Fig. 9. L is the bolometric luminosity at the surface; R is the radius of mass-shell 27.

Fig. 10. Radius vs. time for the mass-shells indicated.

Fig. 11. Velocity vs. optical depth, showing the development of a shock as the inward velocity is reversed. Negative velocity is inward.

Figure Captions, (Cont'd.)

Fig. 12. Temperature vs. time for the outer mass zones.

Fig. 13. Luminosity L, radius R, and kinetic energy for overtone model 1. The radius curves are for boundaries 20 and 10.

Fig. 14. Fractional amplitude $\delta R/R$ for overtone model 1.

Fig. 15a. Radius and luminosity curves for overtone model 2. Core luminosity is 10^{37} ergs/sec.

Fig. 15b. The radius and luminosity curves in model 2 when the convective timescale has been multiplied by a factor 0.3.

Fig. 16a. Luminosity and radius curves for the mixed-mode model just after the fundamental mode has decayed to its lowest level.

Fig. 16b. Curves for the same model after the fundamental mode has grown back and is again dominant.

Fig. 16c. The fundamental mode has decayed again.

Fig. 17. Surface luminosity, and radius of mass-shell 21.

Fig. 18. Kinetic energy curves for four calculations of a model near dynamical instability.

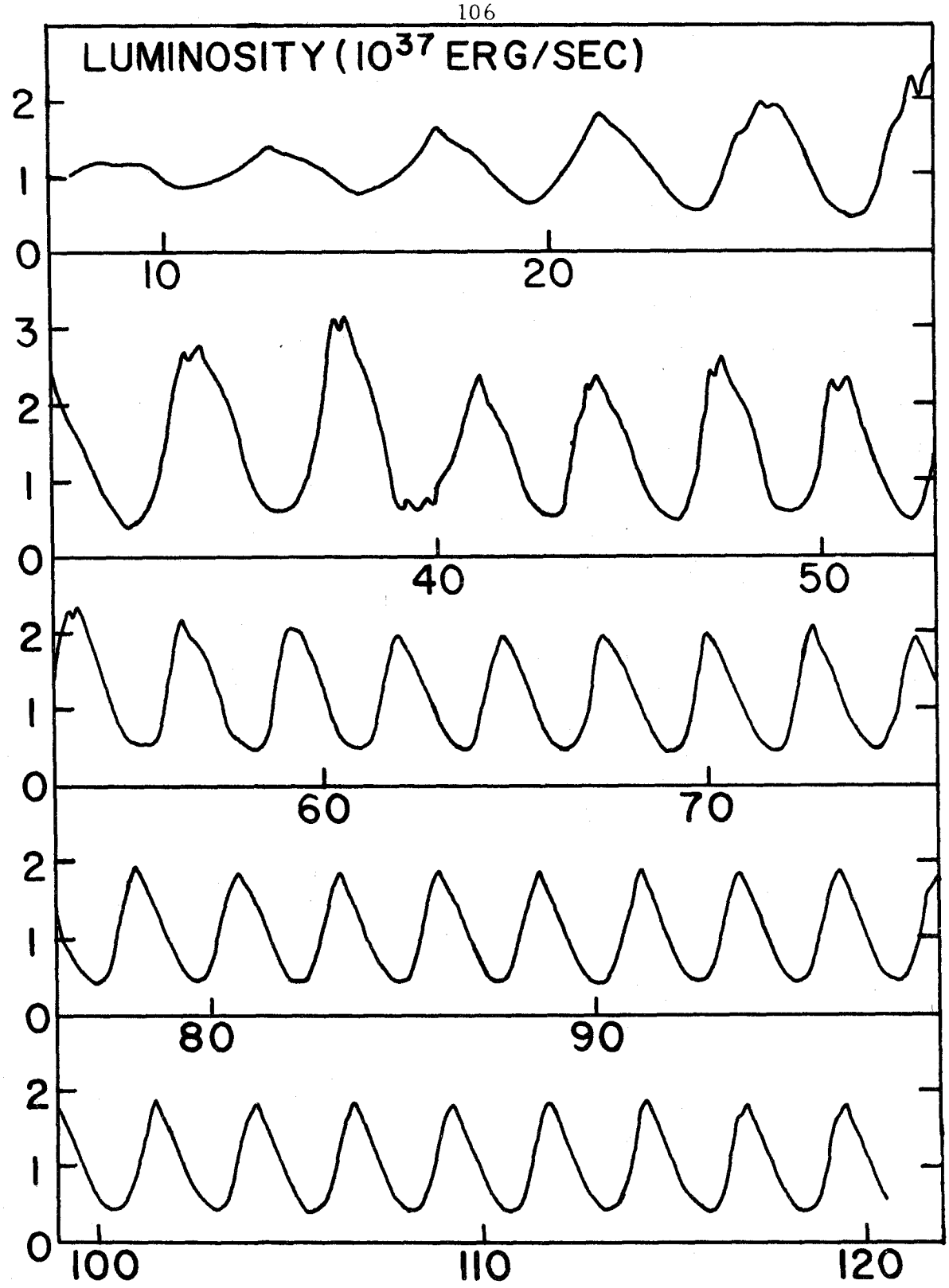
LUMINOSITY (10^37 ERG/SEC)
2
1
0
10
20
3
2
1
0
40
50
2
1
0
60
70
2
1
0
80
90
2
1
0
100
110
120
TIME (10^7 SEC)

Figure 1

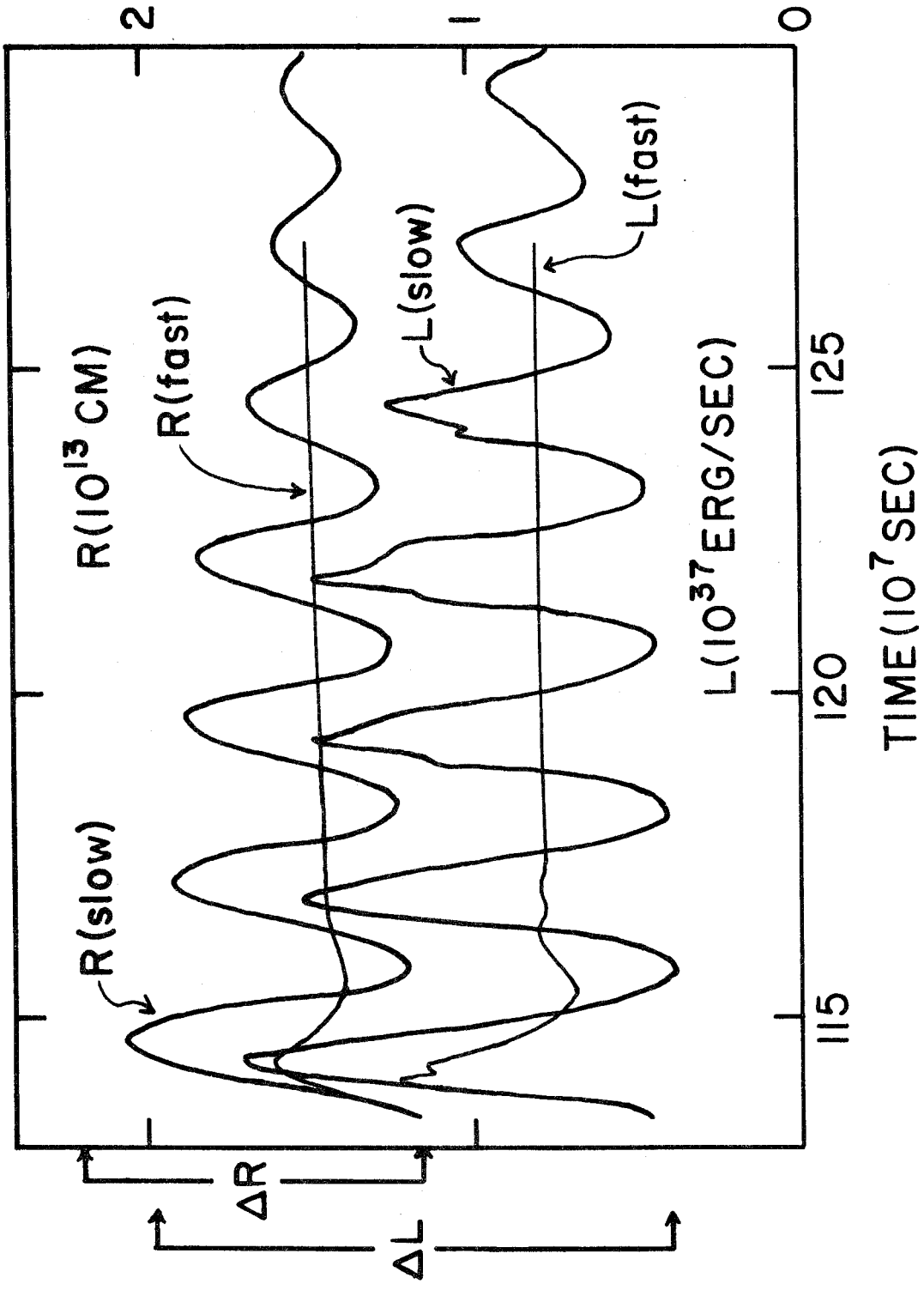
2
1
0
R(10^13 CM)
R(fast)
R(slow)
L(slow)
L(fast)
L(10^37 ERG/SEC)
115
120
125
TIME(10^7 SEC)
ΔR
ΔL

Figure 2

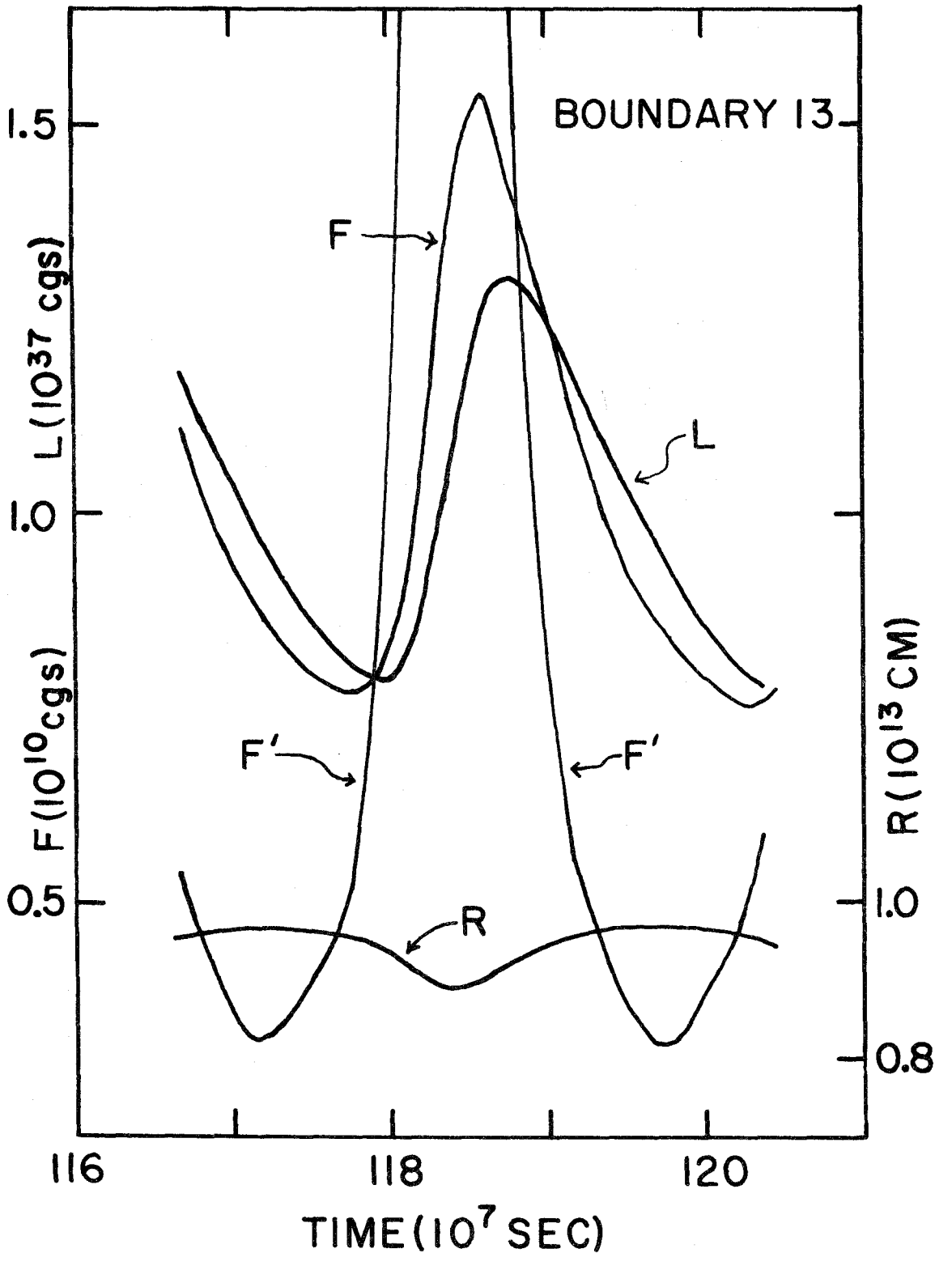
BOUNDARY 13
F
L
F'
F'
R
1.5
1.0
0.5
L(10^37 cgs)
F(10^10 cgs)
1.0
0.8
R(10^13 CM)
116
118
120
TIME(10^7 SEC)

Figure 3

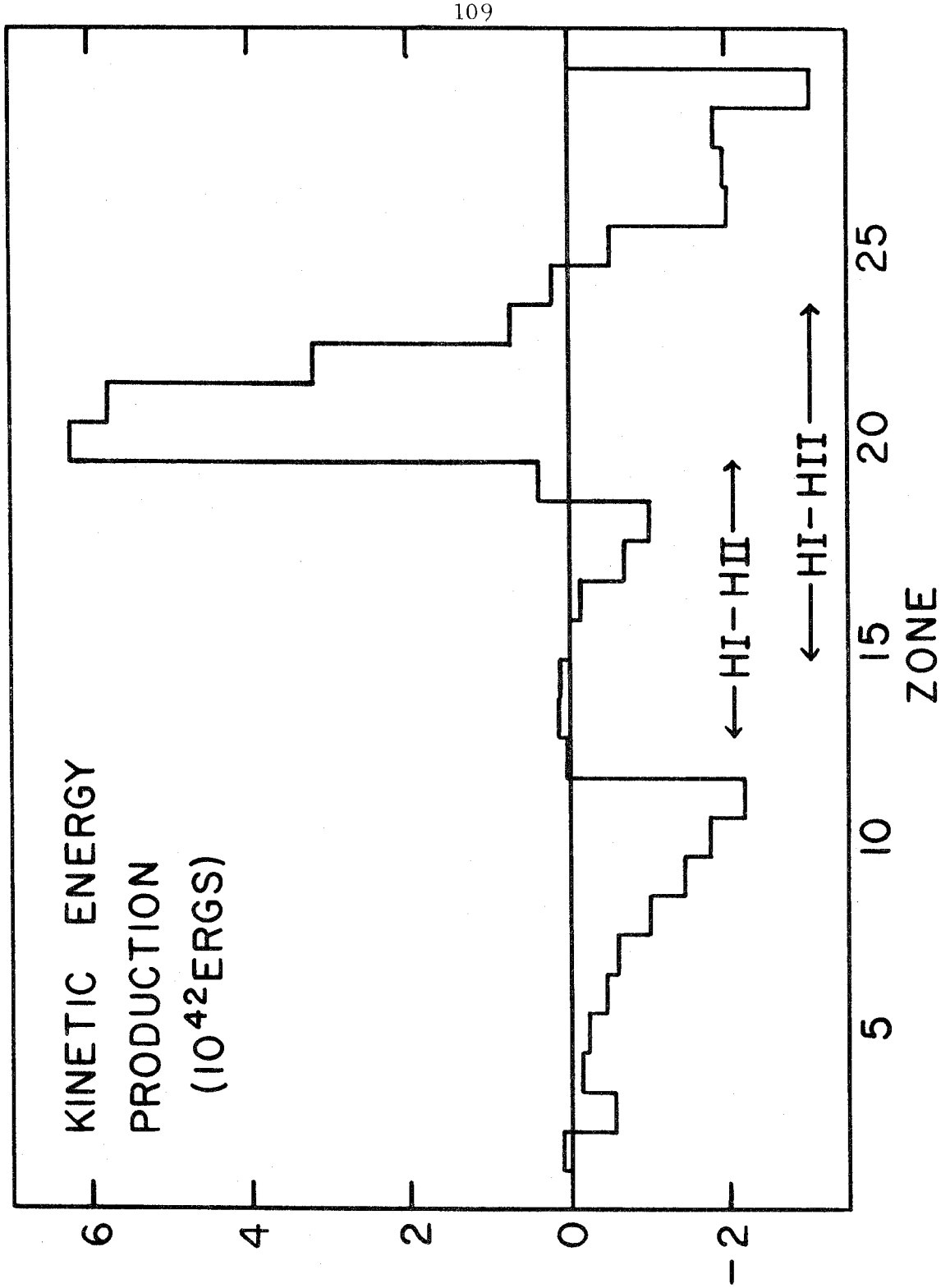
KINETIC ENERGY
PRODUCTION
(10^42ERGS)
6
4
2
0
-2
5
10
15
20
25
ZONE
HI-HII
HI-HII

Figure 4

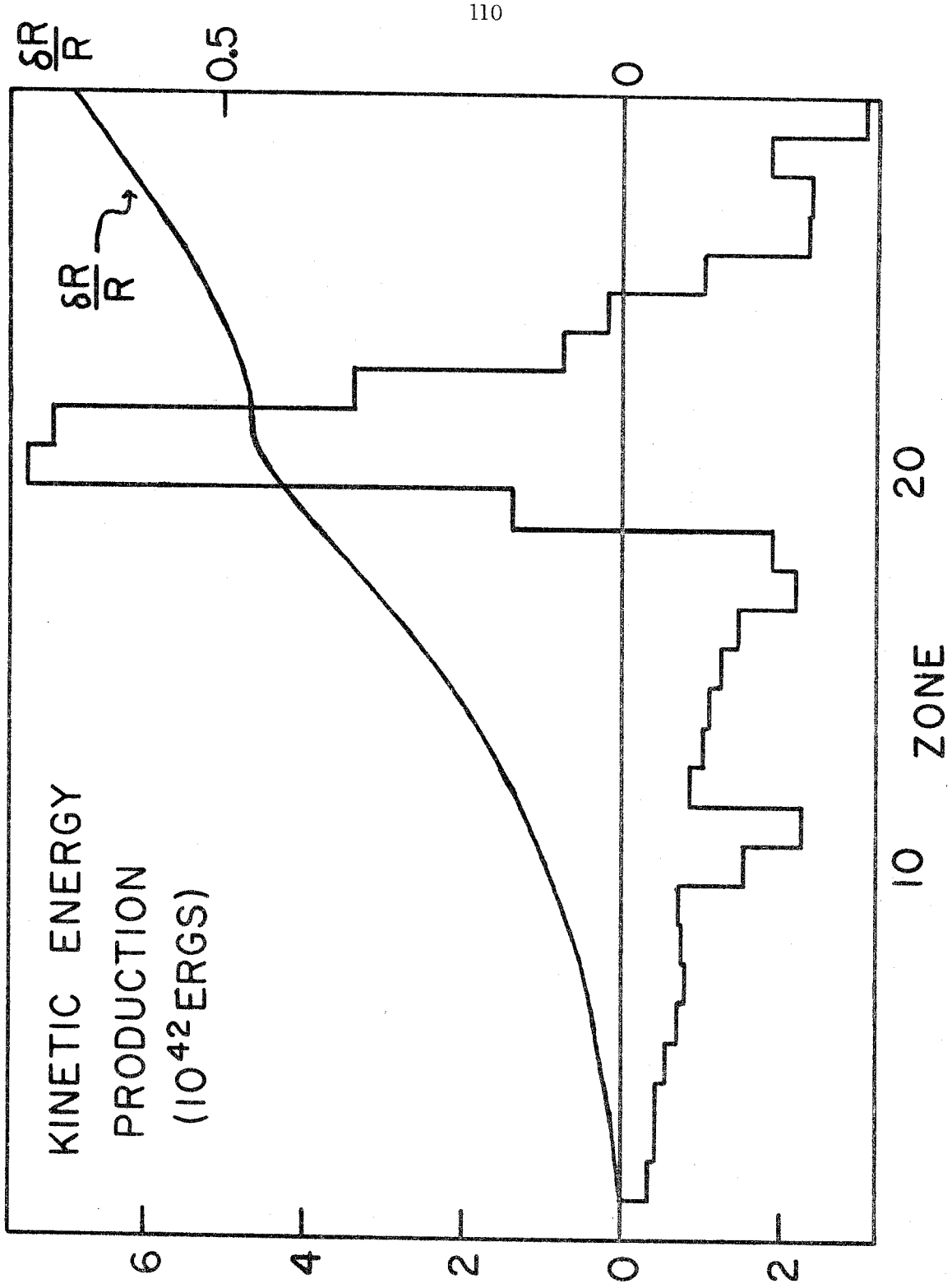
δR/R
0.5
0
δR/R
KINETIC ENERGY PRODUCTION (10^42 ERGS)
6
4
2
0
2
10
20
ZONE

Figure 5

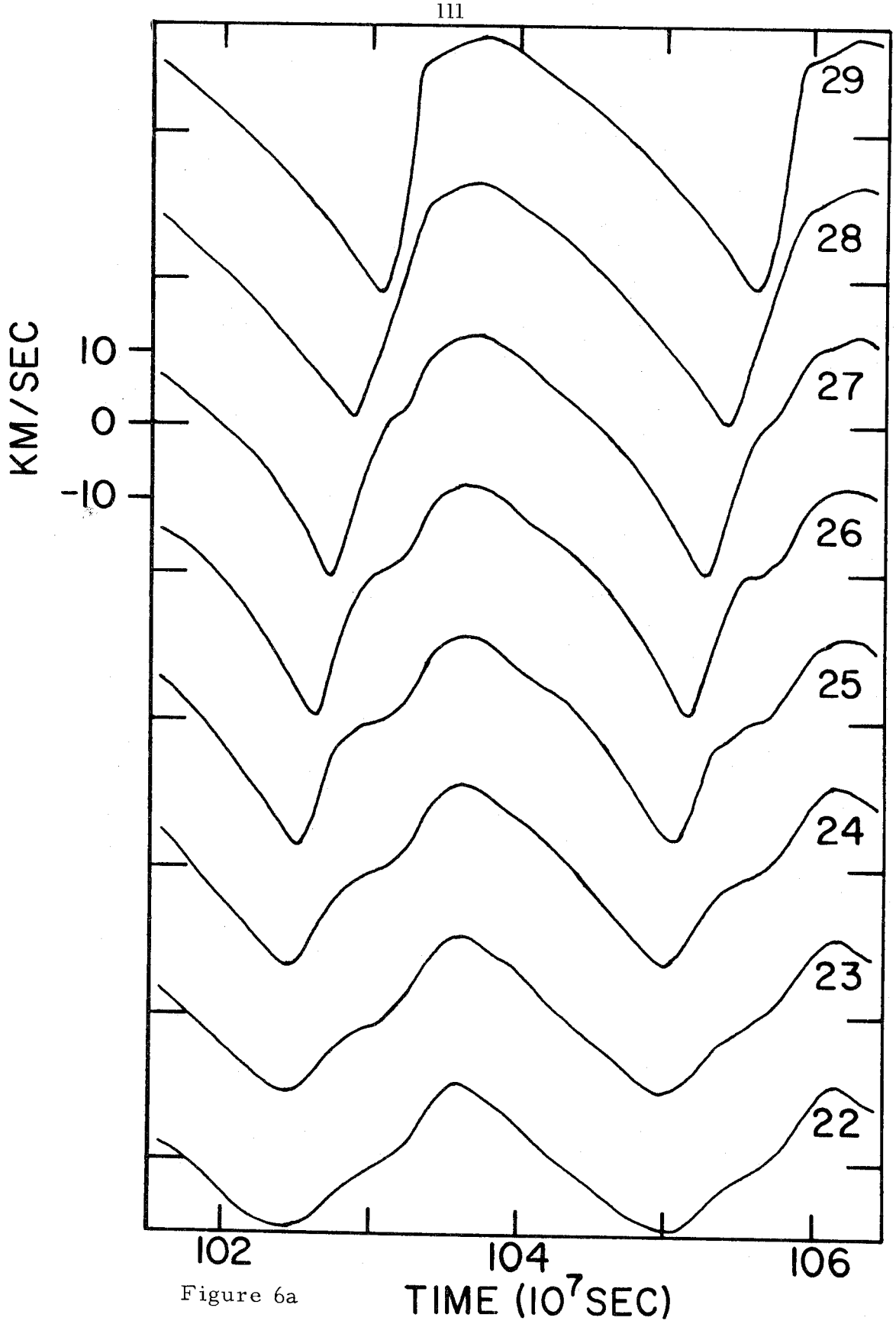

Figure 6a

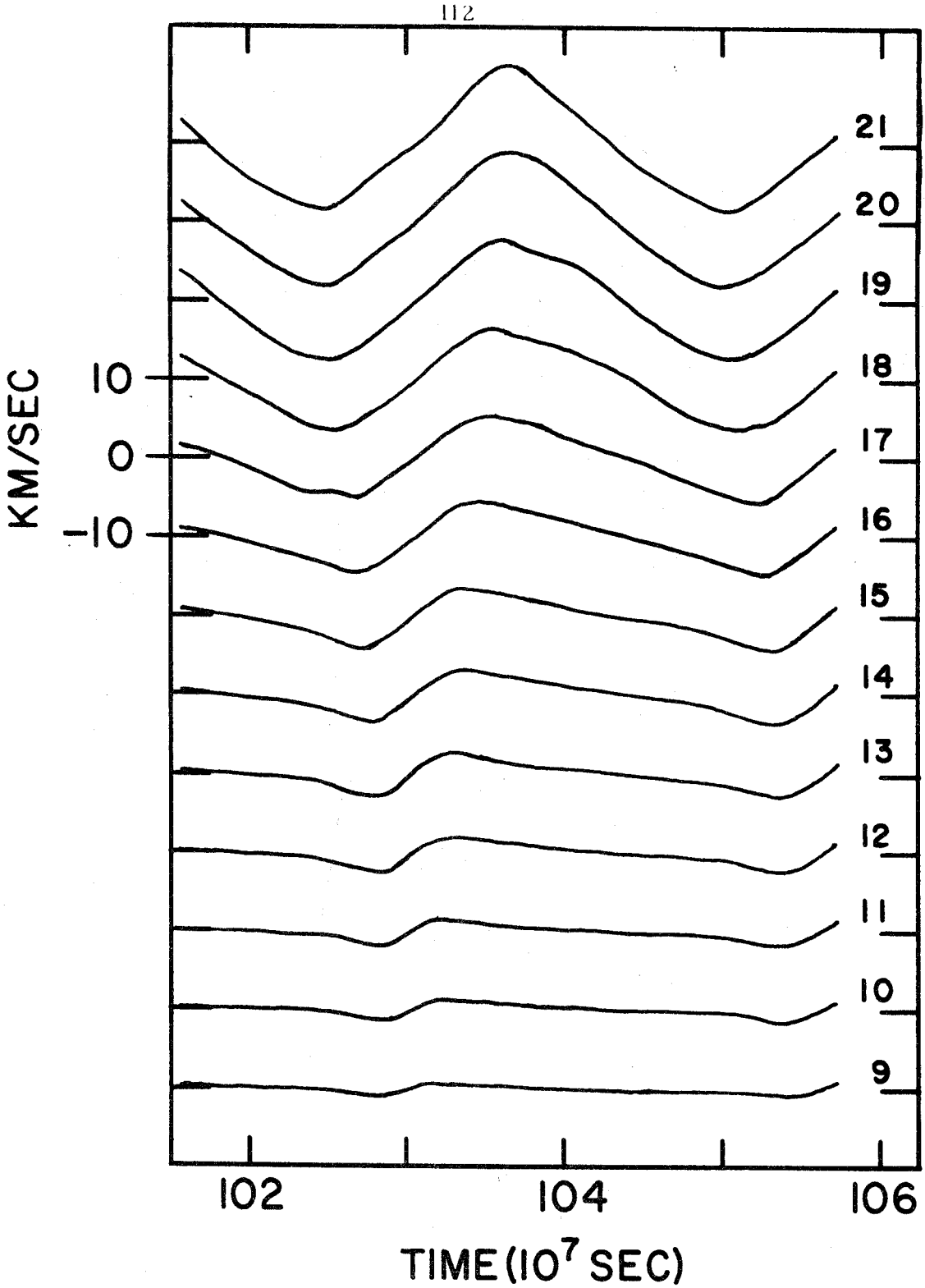
KM/SEC
10
0
-10
21
20
19
18
17
16
15
14
13
12
11
10
9
102
104
106
TIME(10^7 SEC)

Figure 6b

Figure 7a

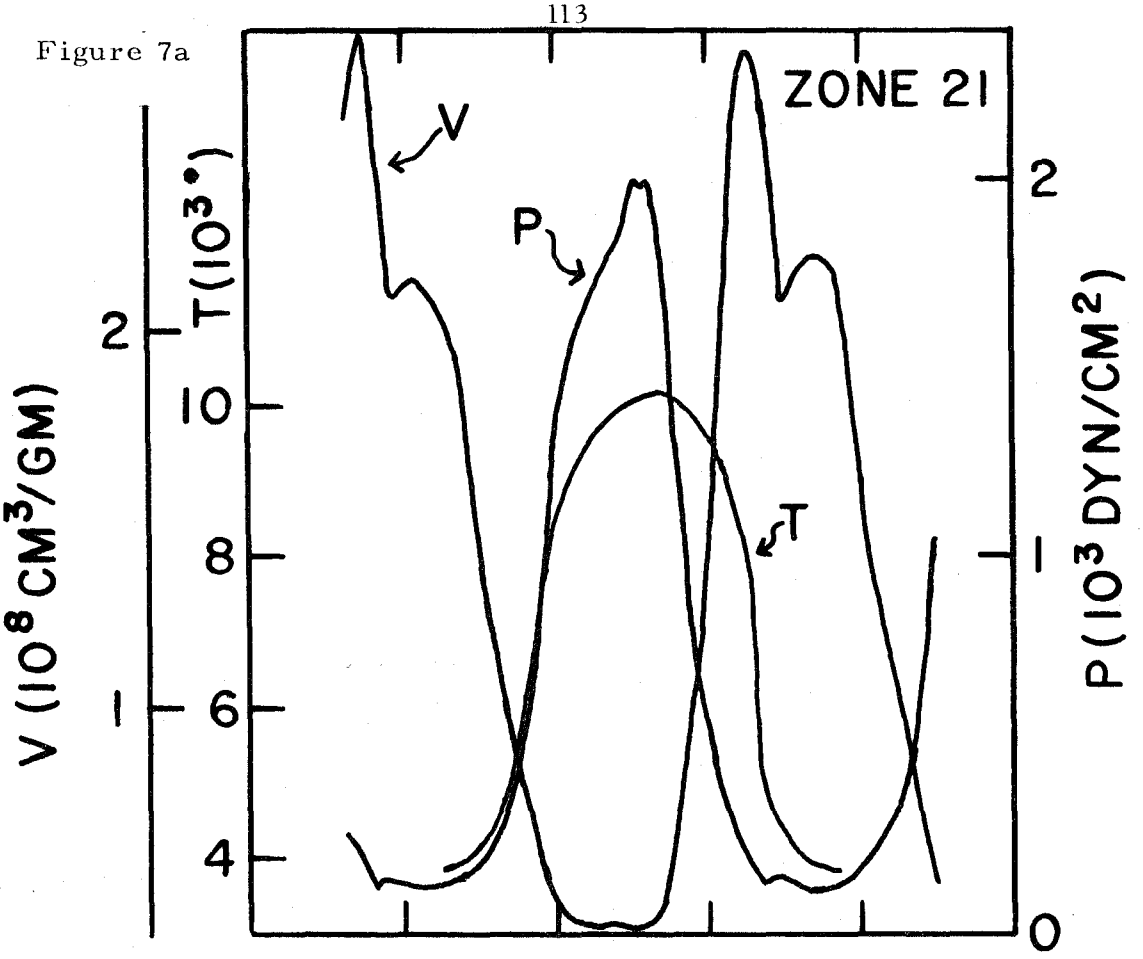

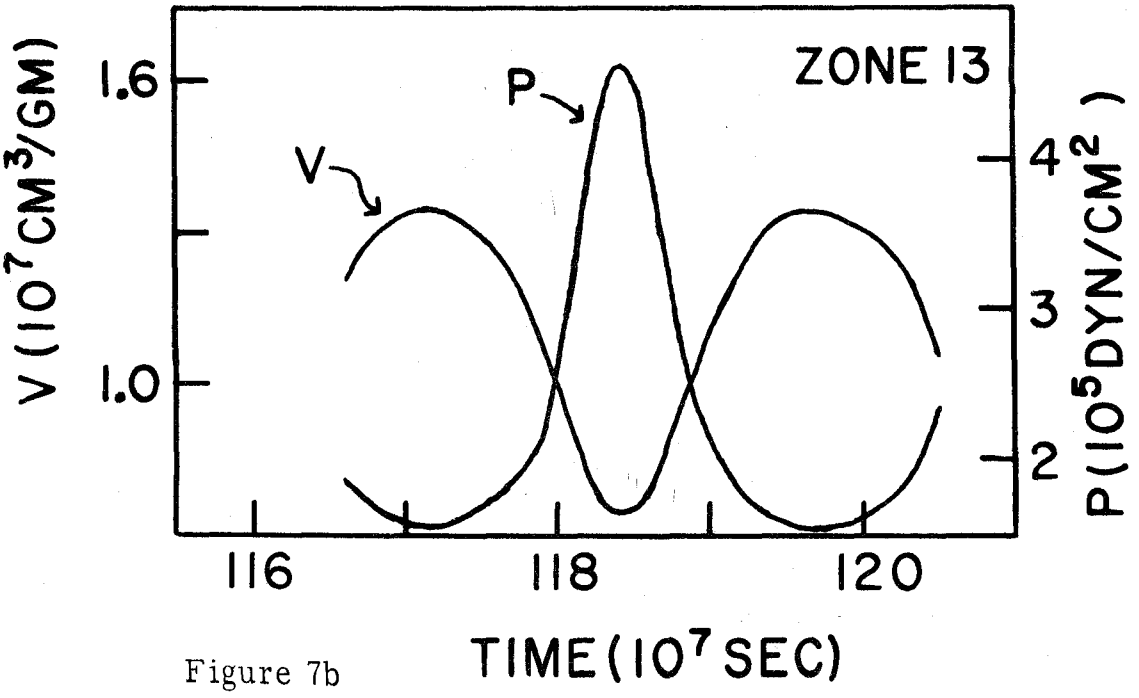

Figure 7b

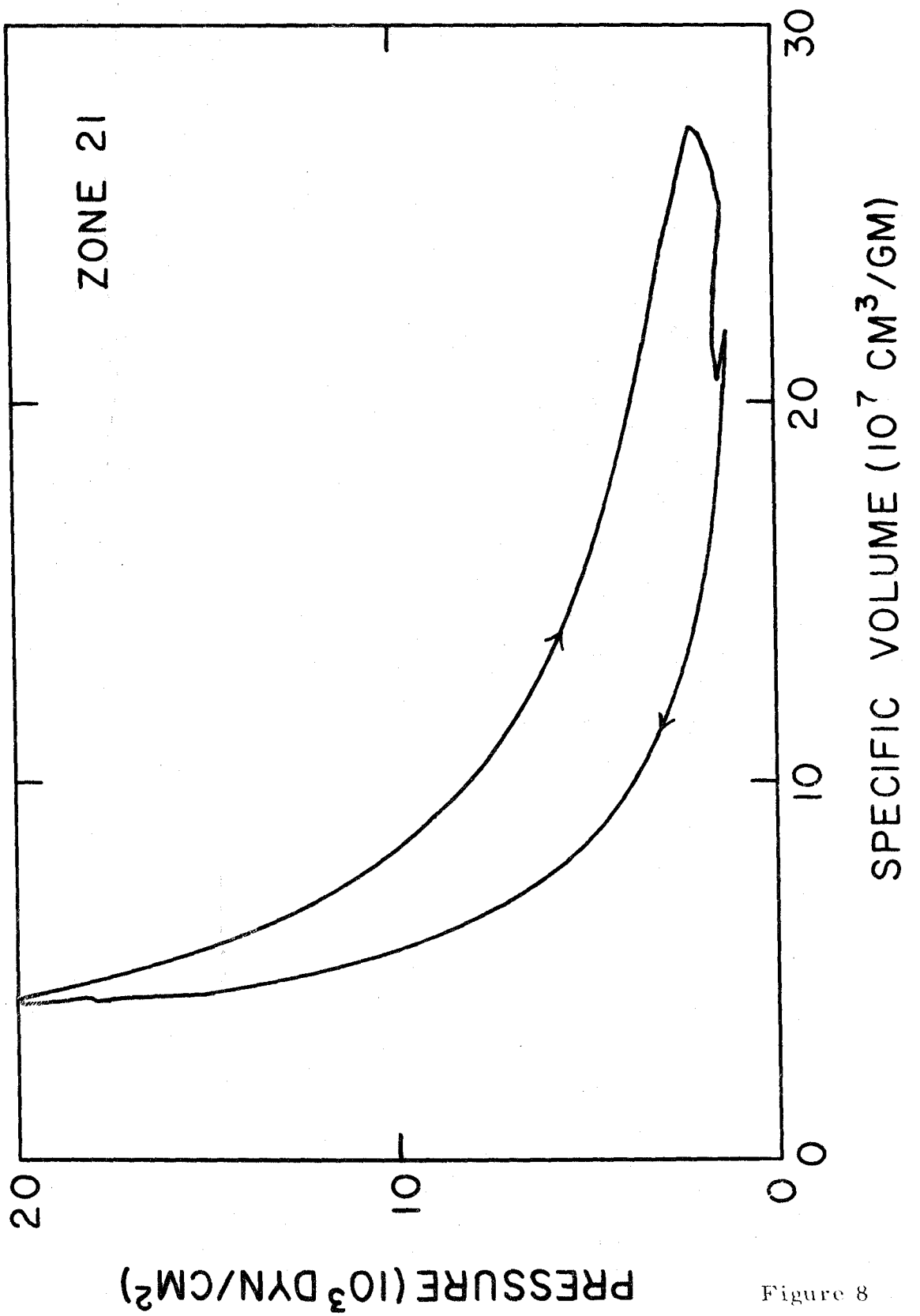
ZONE 21
0
10
20
30
SPECIFIC VOLUME (10^7 CM^3/GM)
0
10
20
PRESSURE (10^3 DYN/CM^2)

Figure 8

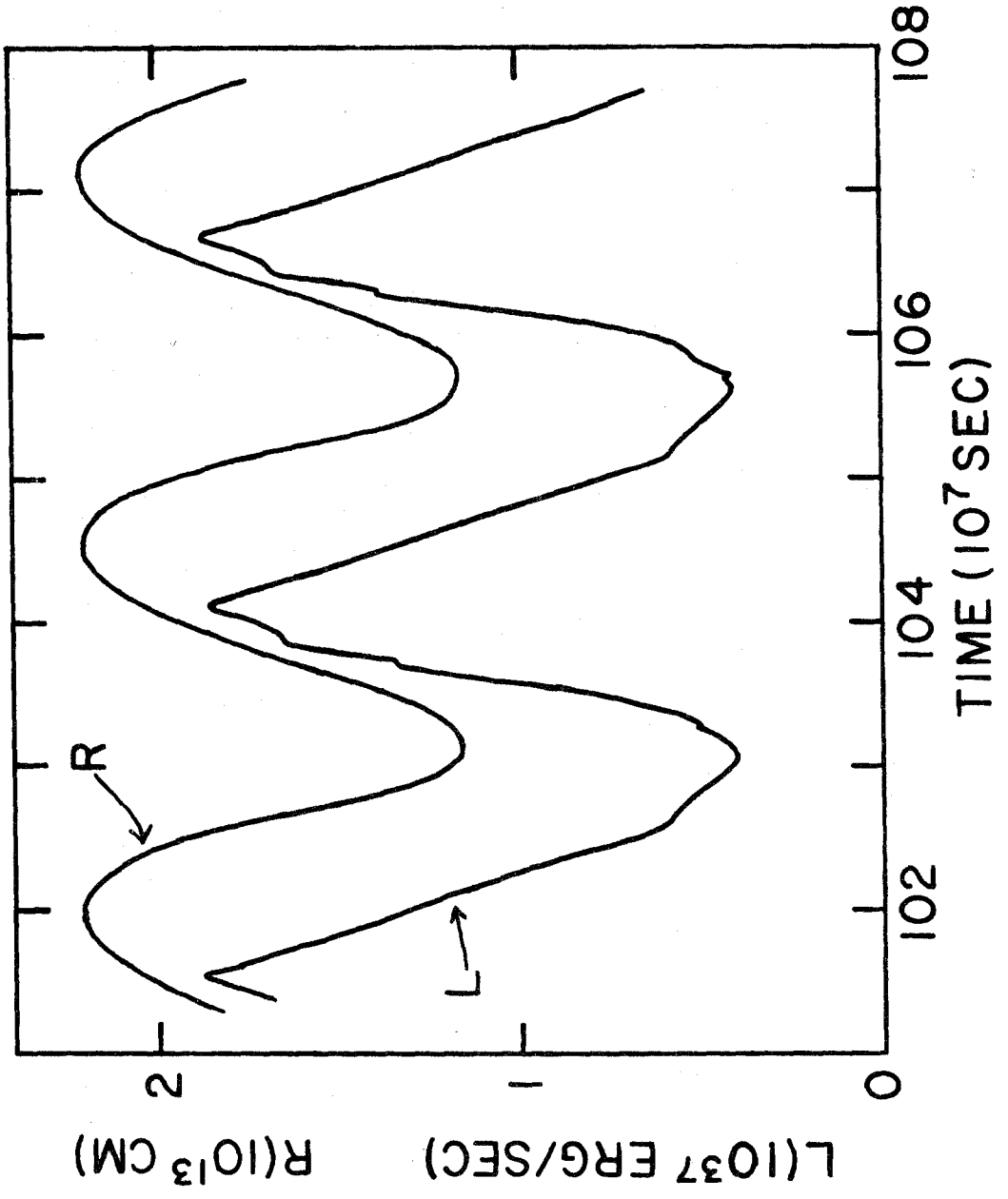

Figure 9

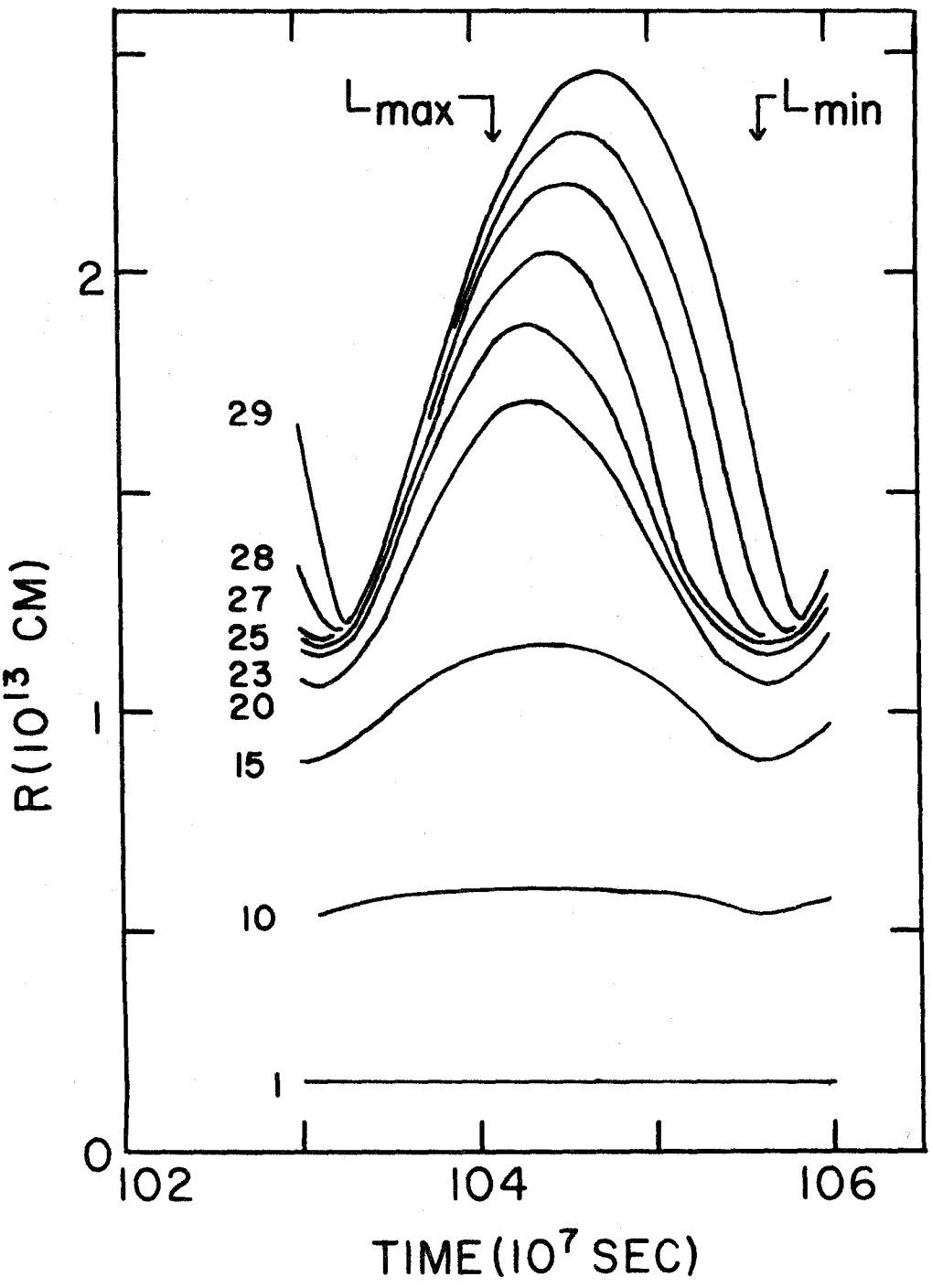
Lmax
Lmin
29
28
27
25
23
20
15
10
1
2
1
0
R(10^13 CM)
102
104
106
TIME(10^7 SEC)

Figure 10

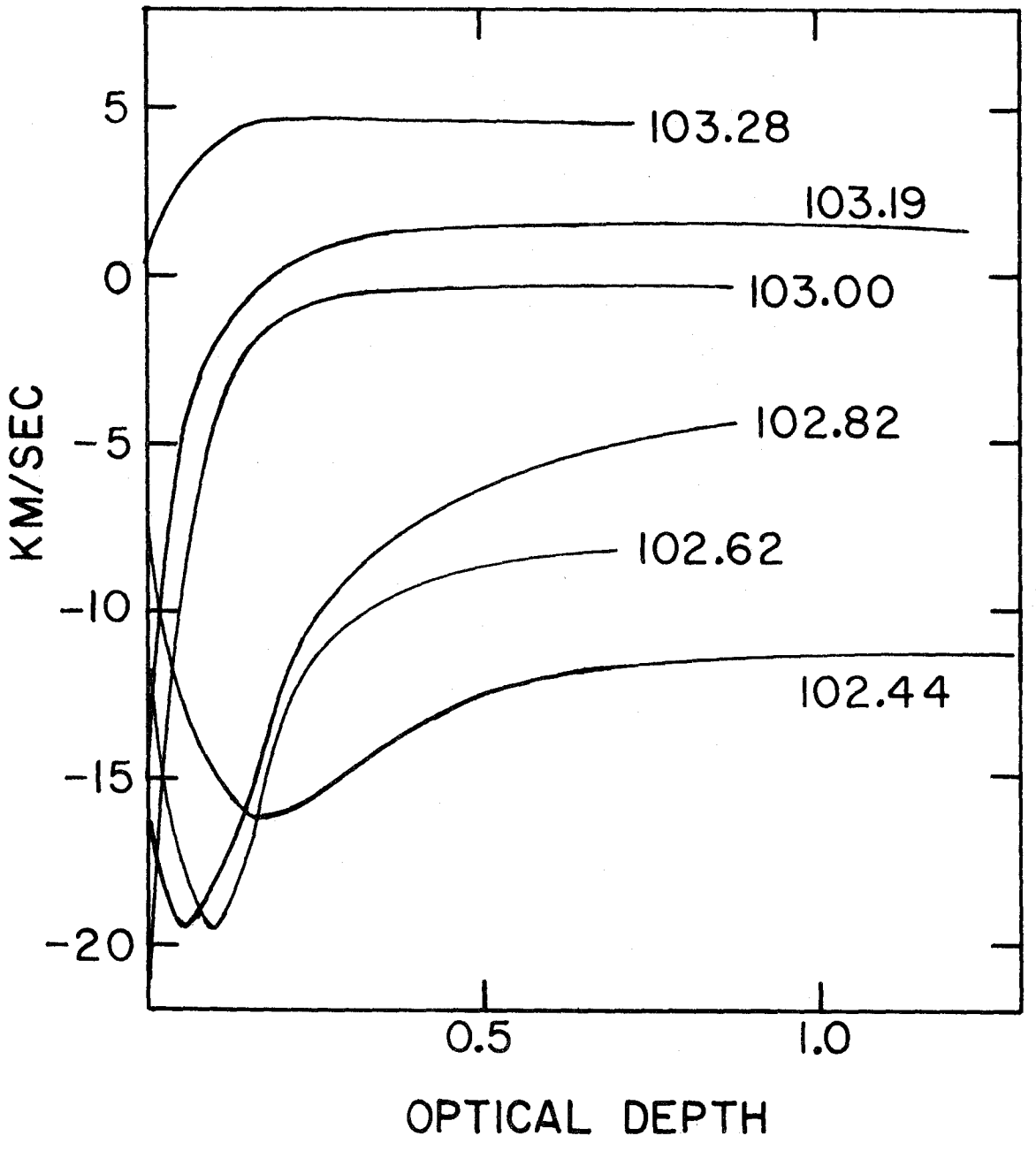
5
0
-5
-10
-15
-20
KM/SEC
103.28
103.19
103.00
102.82
102.62
102.44
0.5
1.0
OPTICAL DEPTH

Figure 11

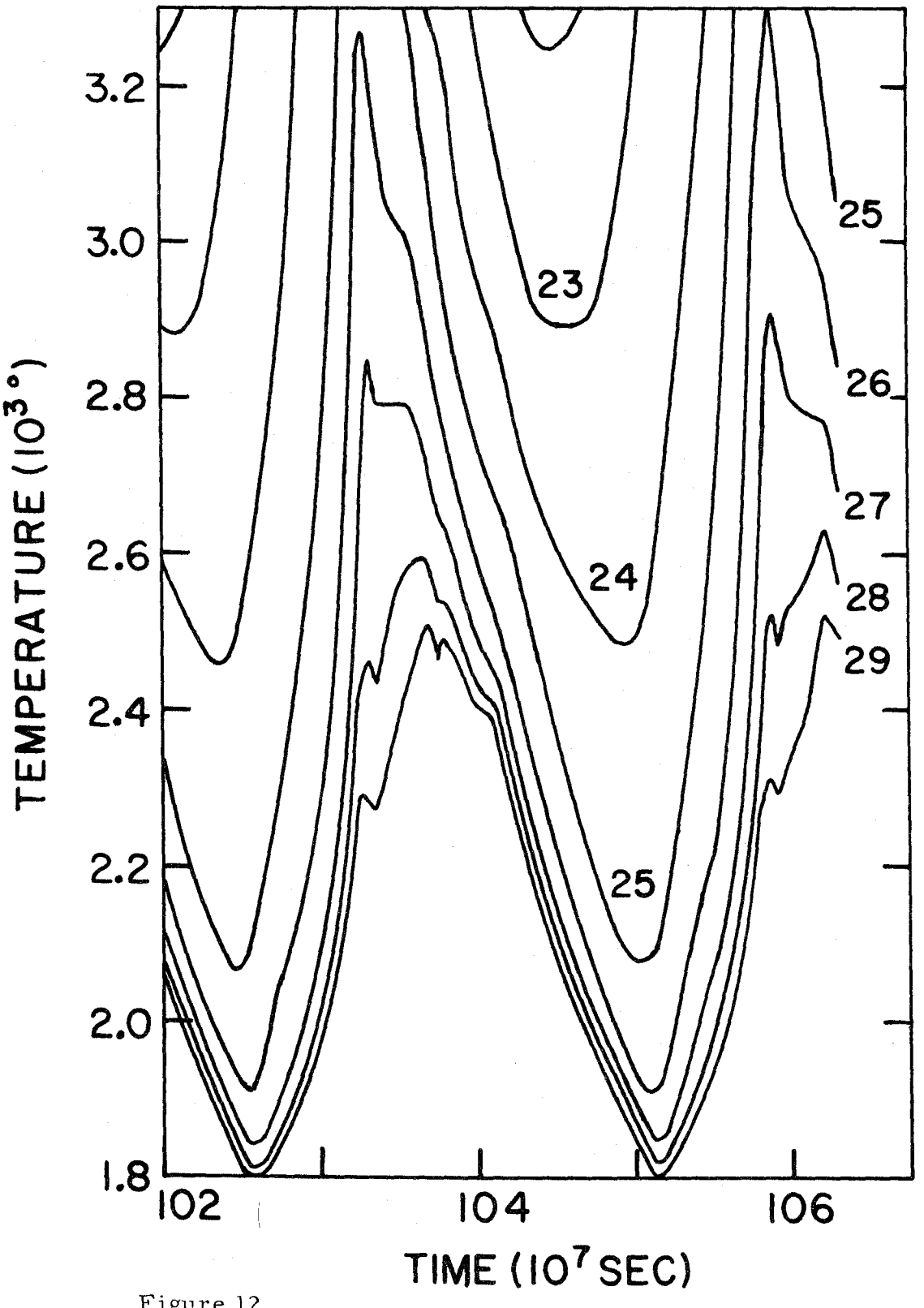
TEMPERATURE (10^3°)
3.2
3.0
2.8
2.6
2.4
2.2
2.0
1.8
102
104
106
TIME (10^7 SEC)
23
24
25
25
26
27
28
29

Figure 12

Figure 13

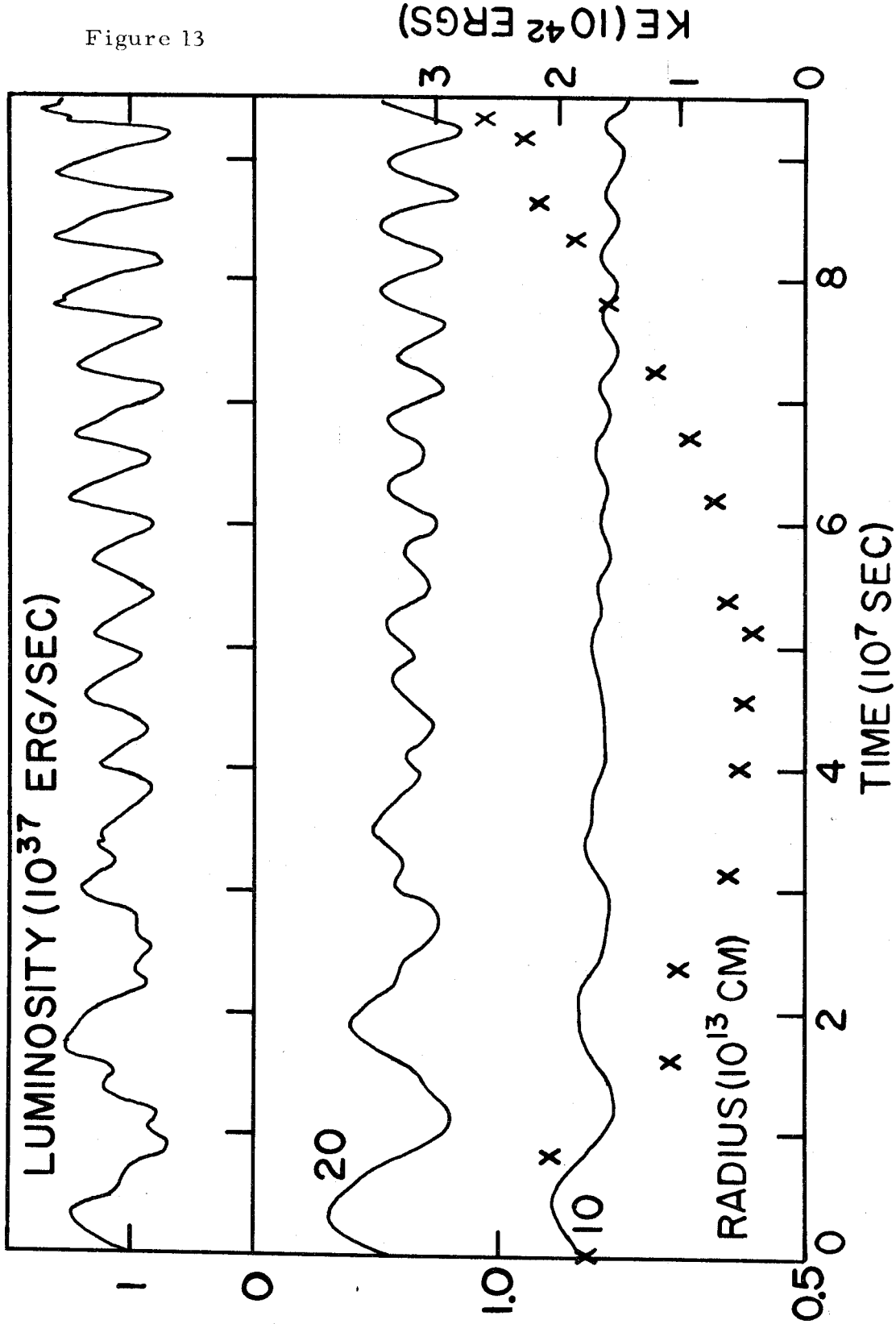
KE (10^42 ERGS)
LUMINOSITY (10^37 ERG/SEC)
RADIUS (10^13 CM)
TIME (10^7 SEC)

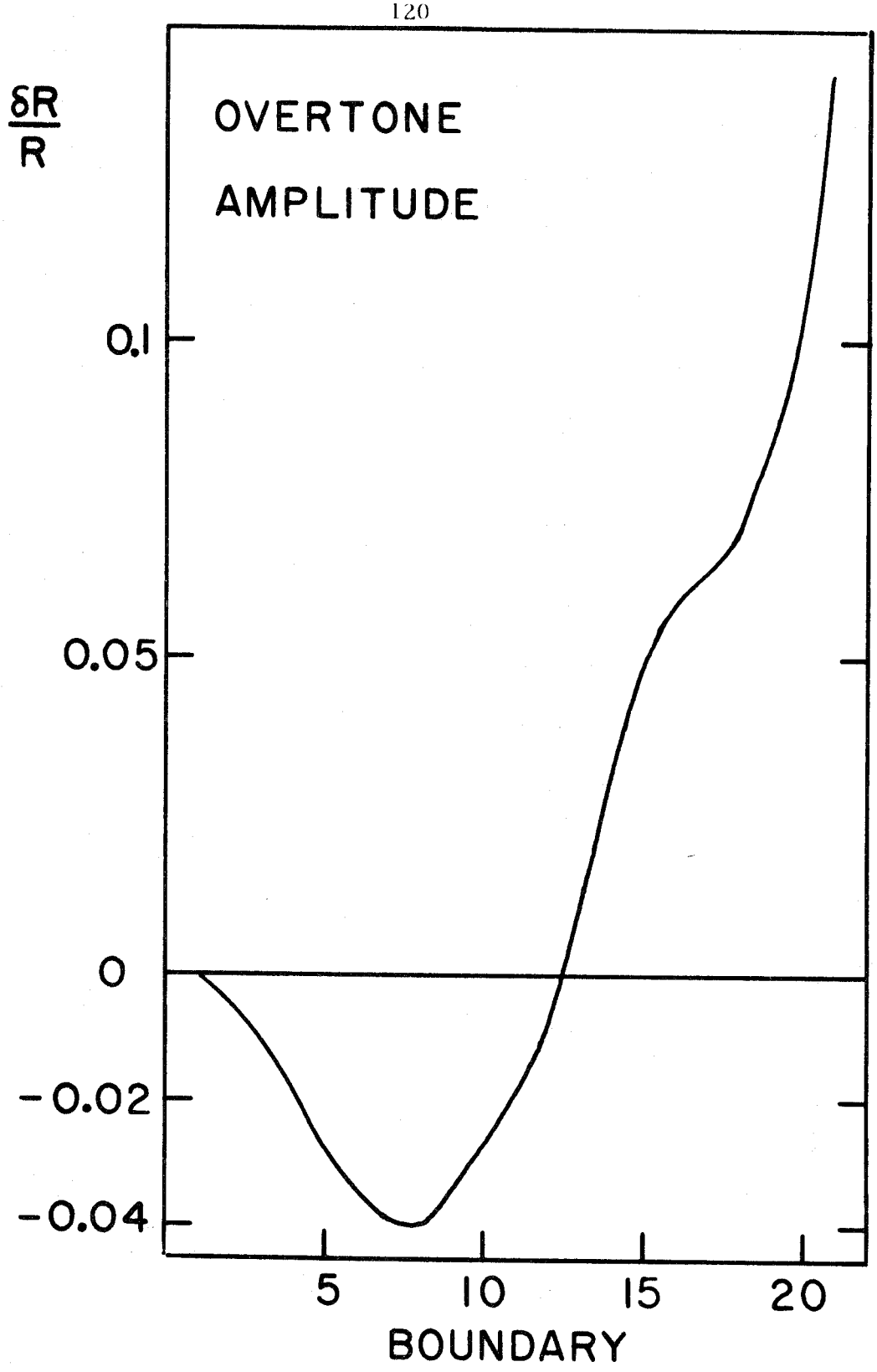

Figure 14

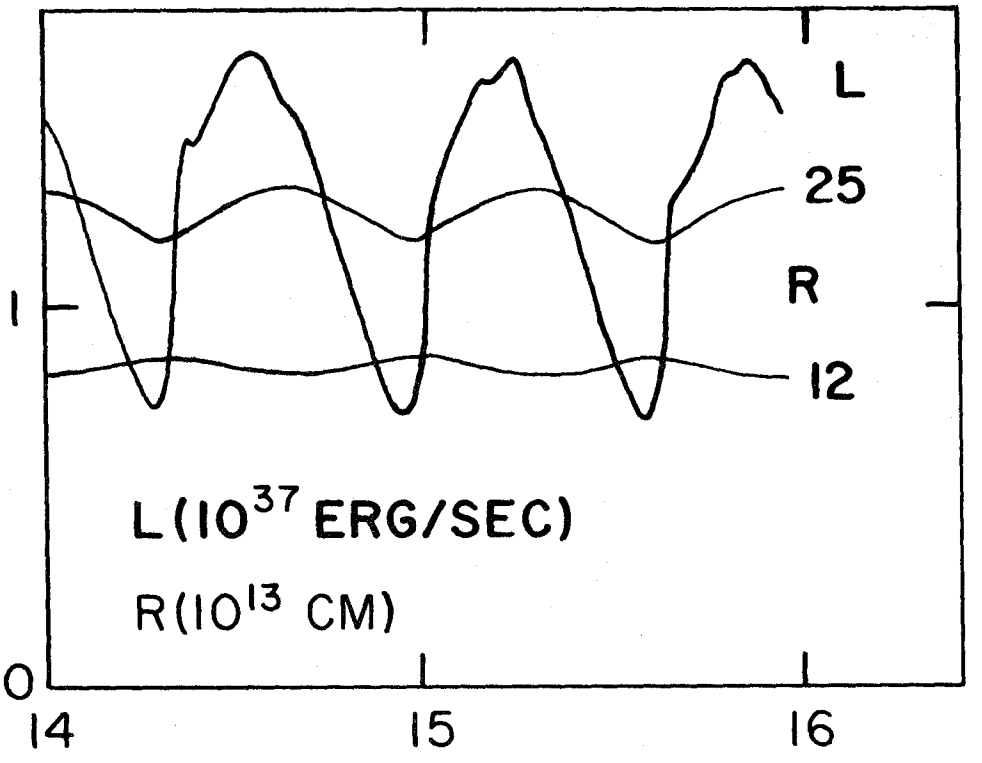

Figure 15a

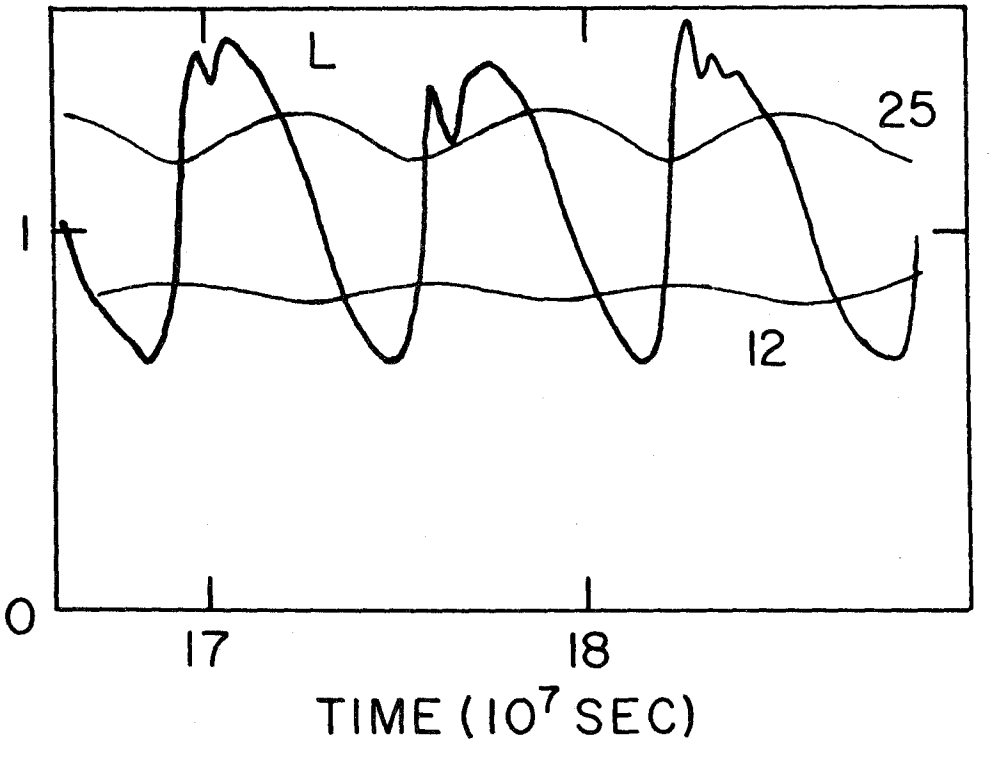

Figure 15b

Figure 16a

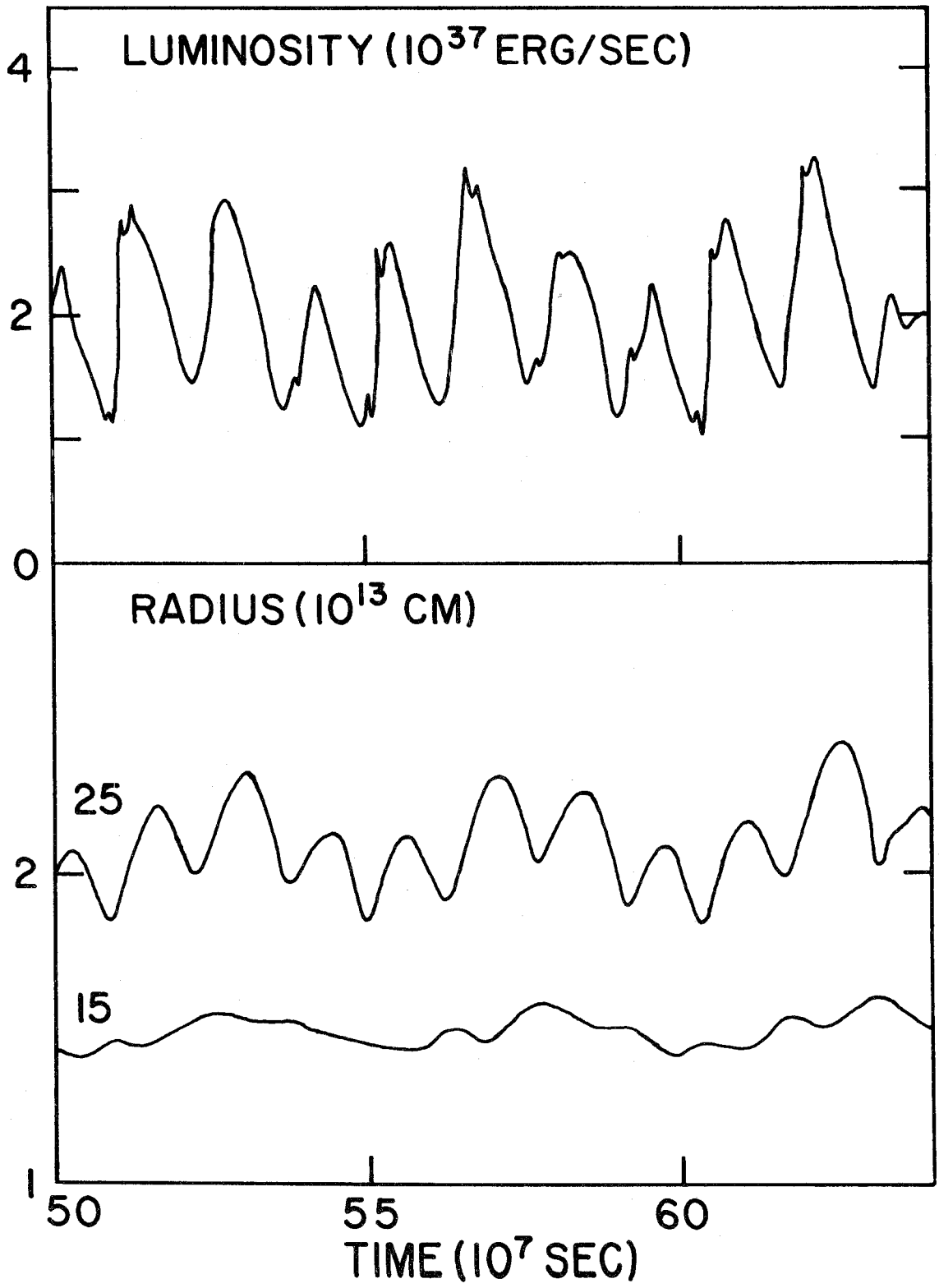
LUMINOSITY (10^37 ERG/SEC)
4
2
0
RADIUS (10^13 CM)
25
15
2
1
50
55
60
TIME (10^7 SEC)

Figure 16b

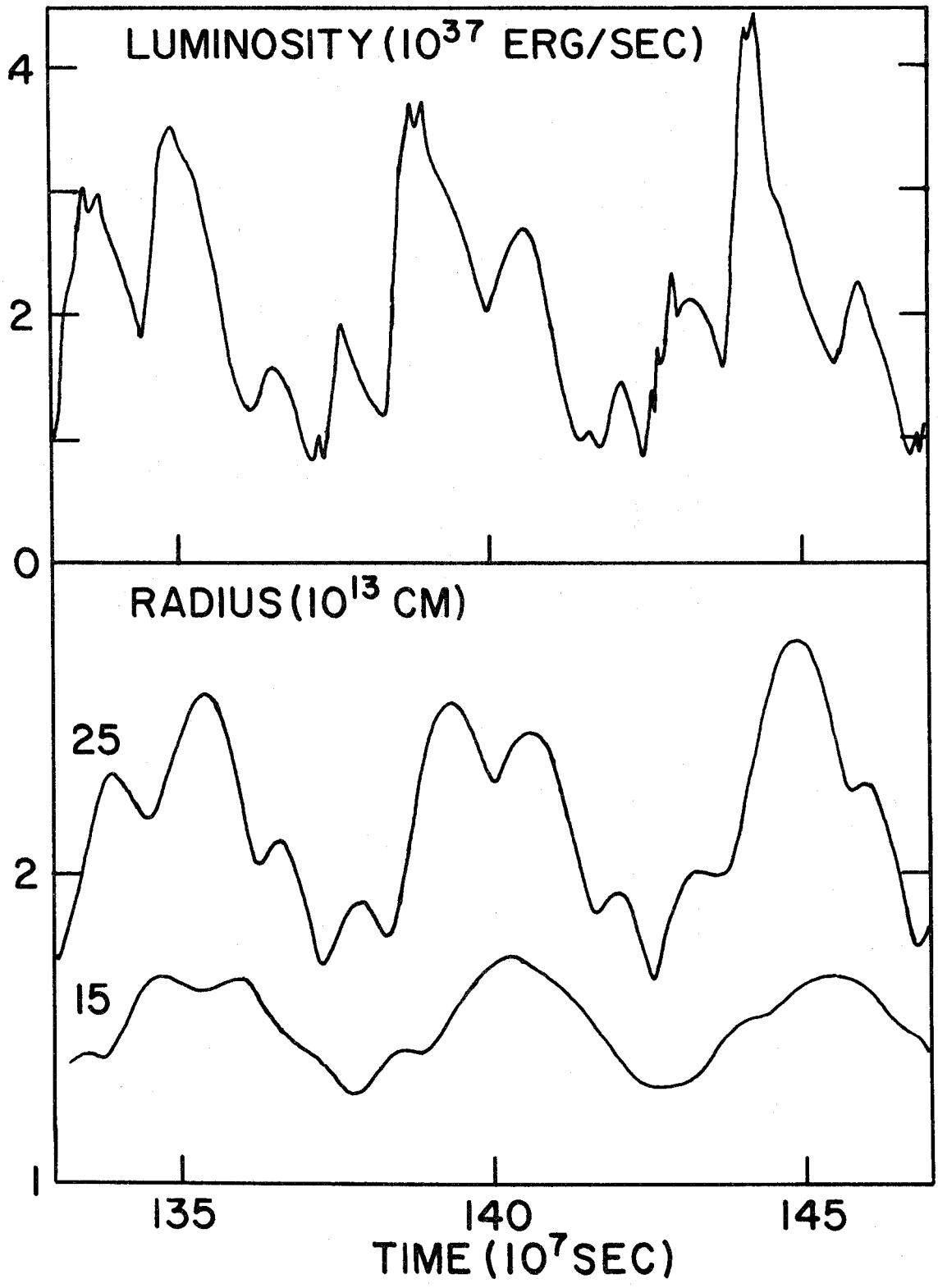
LUMINOSITY (10^37 ERG/SEC)
4
2
0
RADIUS (10^13 CM)
25
15
2
1
135
140
145
TIME (10^7 SEC)

Figure 16c

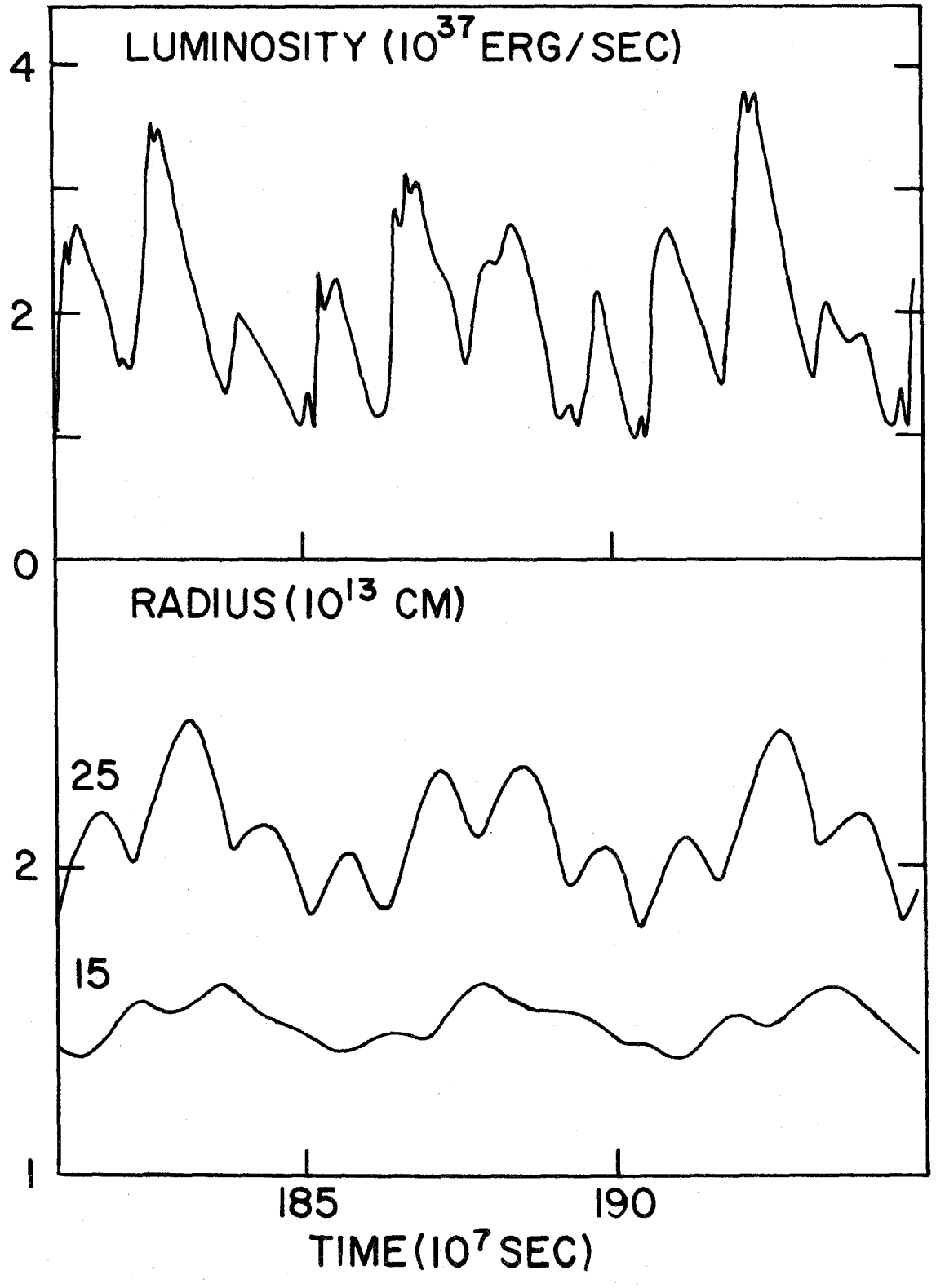
LUMINOSITY (10^37 ERG/SEC)
4
2
0
RADIUS (10^13 CM)
25
15
2
1
185
190
TIME (10^7 SEC)

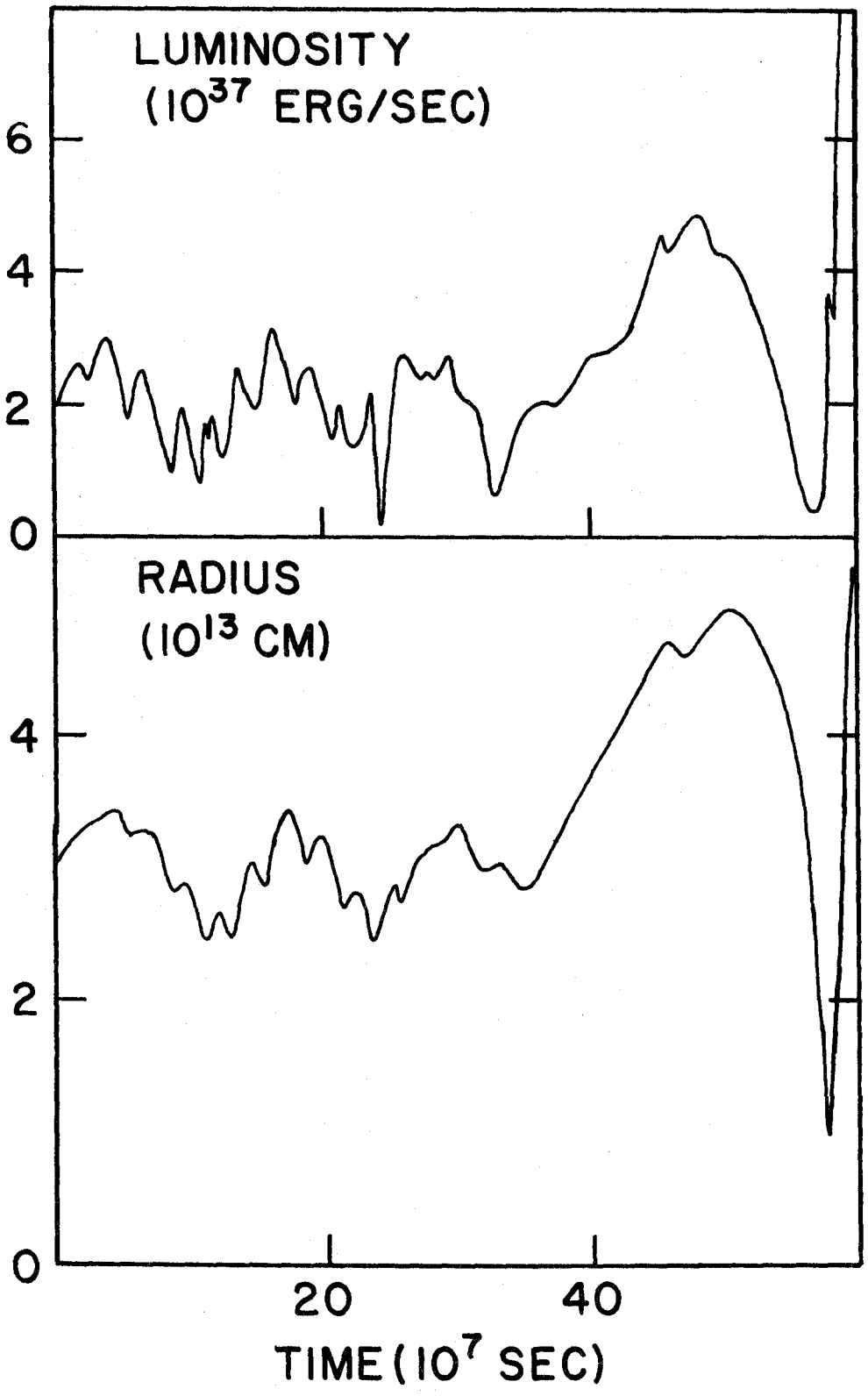
LUMINOSITY
(10^37 ERG/SEC)
6
4
2
0
RADIUS
(10^13 CM)
4
2
0
20
40
TIME (10^7 SEC)

Figure 17

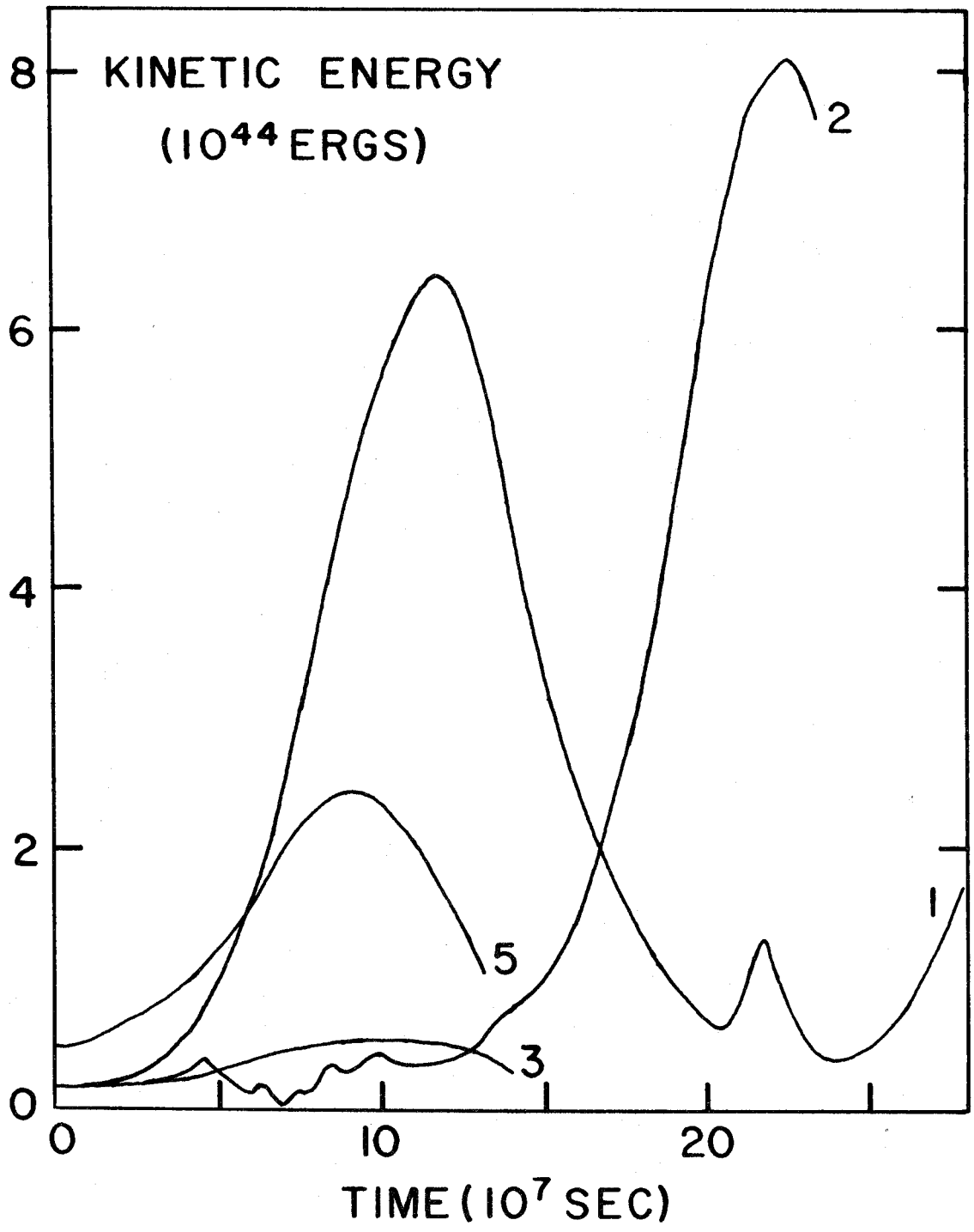

Figure 18

REFERENCES

Abell, G. O., and Goldreich, P. 1966, Pub. A.S.P., 78, 232.

Baker, N. 1966, Stellar Evolution, ed. R. F. Stein and A.G.W. Cameron (New York: Plenum Press).

Batchelor, G. K. 1953, Theory of Homogeneous Turbulence (Cambridge: Cambridge University Press).

Campbell, L., and Sterne, T.E. 1937, Harvard Ann., 105, 459.

Castor, John I. 1968, (private communication).

Christy, R. F. 1964, Rev. Mod. Phys., 36, 555.

Christy, R. F. 1966, Ap. J., 144, 108.

Cox, A. N., Brownlee, R.R., and Eilers, D.D. 1966, Ap.J., 144, 1024.

Eggen, O.J. 1967, Ap.J. Suppl., 14, 307.

Fraley, G. S. 1968, Astrophys. and Space Sci., 2, 96.

Jeans, J. 1928, Astronomy and Cosmogony (Cambridge: Cambridge University Press).

Joy, A. H. 1926, Ap.J., 63, 281.

Keeley, D. 1969, (submitted to Ap.J.).

Ledoux, P. 1965, Stellar Structure, ed. L. H. Aller and D.B. McLaughlin (Chicago: University of Chicago Press), chap.X.

Ledoux, P., and Walraven, Th. 1958, Hdb. d. Phys., 51, 353.

Mihalas, D. 1965, Ap.J., 141, 564.

Nicholson, S. B., and Pettit, E. 1933, Ap.J., 78, 320.

Paczynski, B. 1968, Acta Astron., 18, 511.

Paczynski, B. 1969, (private communication).

Paczynski, B., and Ziolkowski, J. 1968a, I.A.U. Symposium No. 34; Planetary Nebulae.

References - (cont'd.)

Paczynski, B., and Ziolkowski, J. 1968b, Acta Astron., 18, 255.

Richtmyer, R. D. 1957, Difference Methods for Initial Value Problems (New York: Interscience Publishers).

Smak, J. 1964, Ap. J. Suppl., 9, 141.

Smak, J. 1966, Ann. Rev. Astr. and Ap., 4, 19.

Usher, P. D., and Whitney. C. A. 1968, Ap. J., 154, 203.

PART 3

SUPPLEMENTARY MATERIAL

I. IMPROVEMENTS REQUIRED IN THE CALCULATIONS

a) Convection

It was clear from the discussion of the approach to relaxed pulsation, (Part 2, §II, III), that the results obtained were caused by the non-linearity of the equations for the convective flux. It was not clear how sensitive was the result to the particular treatment of convection used in this work. The importance of the structural change, if it is real, has already been pointed out. For this reason, a treatment of convection is required which was developed from the beginning for use in a time-dependent situation.

The change in turbulent kinetic energy during a period was found to be comparable with the peak pulsation energy. Thus the differential equation describing the growth and decay of turbulent kinetic energy should certainly be included in future calculations. This could have an effect on the pulsation amplitude and on the shape of the bolometric luminosity curve. The improvement suggested here would be a step in the direction of identifying overtone pulsators by their light curves.

Energy transfer by overshoot from the convection zone may be important in de-activating the opacity mechanism at the high-temperature side of the instability region in the HR diagram. Thus a more quantitative treatment of the overshoot region is required.

b) The Atmosphere

For a static model,using the diffusion equation in the atmosphere

is roughly equivalent to using the plane-parallel gray atmosphere temperature distribution. The plane-parallel approximation is being pushed to its limit, but is probably not too bad in most cases. For a time-dependent model the diffusion equation has the additional fault of predicting too rapid relaxation to radiative equilibrium in optically thin regions (eg. Castor 1966). Also, the time-dependent model may deviate far more from plane-parallel geometry than the original static model. (See eg. Part 2, §V.) Both the diffusion equation and the boundary condition relating the surface luminosity to the temperature and radius are not very good in that case. An improvement in the treatment of the atmosphere would result in a better bolometric luminosity curve, and may give some information on the velocity curves of absorption and emission lines.

Vast amounts of data in the form of visual light curves have been accumulated for long-period variables; it will be a long time before a comparable amount of data has been collected for the infra-red region where these stars radiate most of their energy. The infra-red data which is now becoming available will help to check the physics of the models. However, if the models are to be used for analysis of past observations, they must be able to predict a reasonable visual light curve. Alternatively, they must demonstrate that gross characteristics such as the shapes (but not the amplitudes) of the light curve in the visual and infra-red are not too different. It is not certain that this will be the case.

c) The Interior Boundary Conditions

If the present calculations are to be extended to include violent large-amplitude pulsation, or dynamical instability, it is clear from the discussion in Part 2, §VIc and d that a better treatment of the inner boundary condition is required.

II. FURTHER USEFUL INVESTIGATIONS

It is clear that many refinements must be made in the models before they can be used for detailed analysis of the observations. However, there are several problems which may be studied profitably with only some, or none, of the improvements which may ultimately be made. It would be useful to compare the dynamical periods with the prediction of a linear adiabatic analysis to determine if the latter is reasonably reliable for the type of models considered in this work. A calculation of some relaxed overtone models might give more insight into the reasons for the high-temperature boundary of the instability region. Some type of non-local treatment of convection should be used, but the method used in the present work might be adequate for an initial investigation. It would also be interesting to see if the overtone is the only high-amplitude mode at somewhat lower luminosity than in the present models. There are many giants with luminosity lower than the Mira stars which have low-amplitude irregular variability. It might also be possible to learn something about these objects.

III. STATIC MODEL CALCULATIONS WITH DIFFERENCE EQUATIONS

The equations used for the static model integration are:

$$P_{k-\frac{1}{2}} = P_{k+\frac{1}{2}} + \frac{GM_k m_k}{4\pi R_k^4} \tag{1}$$

$$R_{k-1}^3 = R_k^3 - \frac{3}{4\pi} \frac{V_{k-\frac{1}{2}}}{m_{k-\frac{1}{2}}} \tag{2}$$

$$L_k = L_{core} \tag{3}$$

where

$m_{k-\frac{1}{2}} = M_k - M_{k-1}$ is the mass of a zone,

$m_k = \frac{1}{2}(m_{k-\frac{1}{2}} + m_{k+\frac{1}{2}})$

$V_{k-\frac{1}{2}}$ is the specific volume

The expression for the radiative luminosity was given previously (Part 2, Appendix D) and will not be repeated. The expression for the convective luminosity was given in Part 2, Appendix C.

Many of the problems associated with the mass division have been discussed by Christy (1964). Since the models are to be used as initial conditions for time-dependent calculations the number of grid points must be kept to a minimum. However, the grid should be fine

enough that all the important features of the structure can be represented sufficiently accurately.

Two conditions are required if derivatives are to be represented accurately by finite differences:

1) Since P, T^4, and R^3 are not approximately linear in M_r, the point-to-point changes in them should not be too large.

2) Masses of adjacent zones must be equal or the hydrostatic and diffusion equations will not be correctly centred for second order accuracy.

The second condition can't be followed strictly because of the structure of the star. Small zone masses are required near the surface and near the core because of the strong dependence of pressure on M_r in those regions. (See Figure 1). In the intermediate region, the zones are chosen as large as possible, consistent with the condition

$$0.75 < m_{k+\frac{1}{2}} / m_{k-\frac{1}{2}} < 1.4 \quad . \qquad (4)$$

Christy (1964) found that a factor as large as 1.5 did not result in serious error.

Log T changes rapidly with M_r near the outside boundary of the hydrogen ionization zone, but it is best not to put many grid points in this region. In a time-dependent calculation the position of the steep rise in temperature moves around in the mass grid, so a high density of points would be required over a much larger range of mass than is obvious from the static structure. Because of the requirement (equation [4]) on the gradient of zone masses, a concentration of

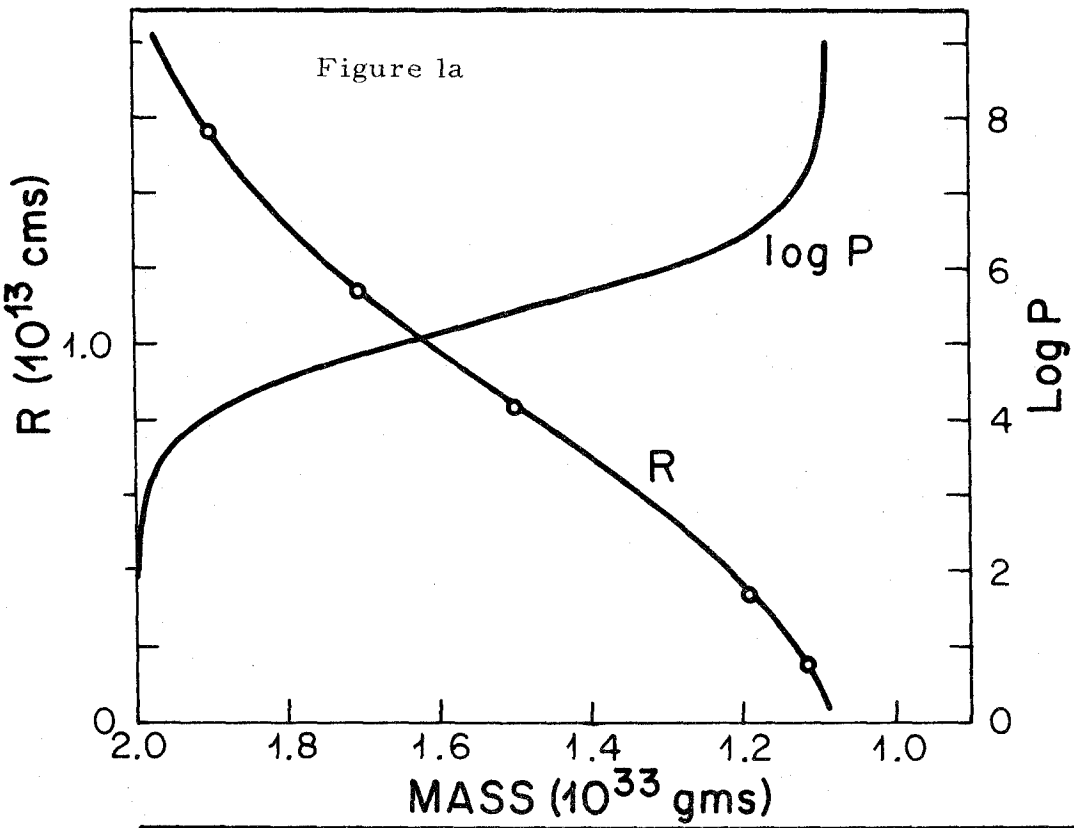

Figure 1a

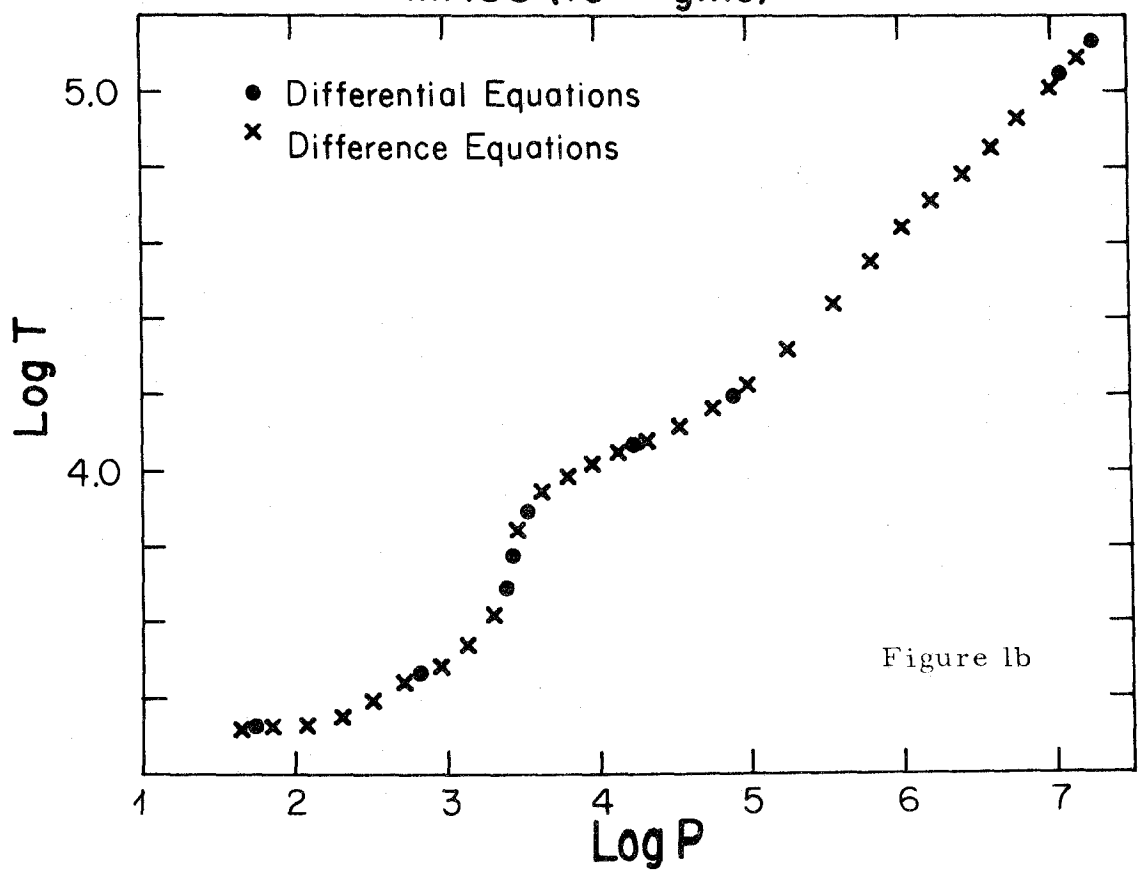

Figure 1b

Fig. 1a. The solid lines show the solution of the differential equations. The crosses on the radius curve indicate points on the solution of the difference equations.

Fig. 1b. The crosses show all the zones from the difference-equation solution. The circles show some points from the differential equations.

points in the critical region would make necessary a higher density of points throughout the interior. Christy (1964) showed that for many purposes the region of steep temperature gradient could be represented satisfactorily with only a few grid points if the mean opacity at a grid point was defined appropriately. This is discussed in more detail below.

If the mass grid was fine enough, the difference equations gave the same results as accurate integration of the differential equations by standard numerical methods; however, a coarse grid was required for models used in extensive time-dependent calculations because of the cost of computation. Models with a coarse grid are not independent of the position of the grid points, or of the expression used for the opacity mean. The greatest sensitivity to both of these occurs in the region of high temperature gradient. Small differences between the solutions of differential and difference equations in this region may grow into large differences when M_r gets close to the core mass. Red giant envelopes have structures which correspond to solutions of the differential equations which are not regular at $r = 0$, and for small r such solutions are sensitive to small changes in the outer part of the envelope.

The difference equations have solutions which are qualitatively similar to those of the differential equations, even when a coarse grid is used. However, models which connect onto the same physical core would be different at the surface. For some purposes it was useful to have strictly similar results from the difference and differential equations. It was found that the sensitivity to the opacity mean could be used to compensate for the sensitivity of the position of the grid points. The expression used for the opacity at a boundary k was

$$\frac{1}{\kappa_k} = \frac{\alpha\, T^4_{k-1/2}/\kappa_{k-1/2} + (1-\alpha)\, T^4_{k+1/2}/\kappa_{k+1/2}}{\alpha\, T^4_{k-1/2} + (1-\alpha)\, T^4_{k+1/2}} \qquad (5)$$

where α is a free parameter. With $\alpha = 0.5$ this mean is identical to that of Christy (1964). The situation in the present models is somewhat different from that in Christy's models. In Christy's models the sharp rise in temperature ends when the hydrogen opacity reaches its peak, whereas in the present models it ends when convection becomes effective; however, the models are quite similar at the low-temperature side of the steep rise. In the present work α was chosen to make the solution of the difference equations agree with the solution of the differential equations at the inner mass-point. Usually α was in the range $0.4 < \alpha < 0.55$. Models showing excessive sensitivity to α were rezoned. In Figure 1 the solution of the differential equations is compared with the solution of the difference equations. Figure 1a shows r as a function of M_r. The solid line is from the differential equations, and the crosses are grid-points from the difference equations. Figure 1b shows log T as a function of log P, since both of these are defined on zones. The crosses indicate the solution of the difference equations, and the points outline the results from the differential equations.

IV. DETAILED DISCUSSION OF THE DYNAMICAL PROGRAM

a) Difference Equations

The general conditions under which the solution of a difference

equation will approximate the solution of a differential equation are discussed by Richtmyer (1957). However, for complicated non-linear systems, previous experience is an important guide to constructing suitable difference equations.

The integration forward in time can be done by an explicit or implicit method. An explicit scheme was used by Christy (1964). Its main advantage is that only one non-linear system of algebraic equations must be solved during a time-step; this system comes from the difference representation of the first law of thermodynamics. The main disadvantage is that for mathematical stability of the difference equations, the time-step must be less than the sound travel-time across any mass zone. The implicit system does not have this limitation, but it has the disadvantage of yielding two coupled systems of non-linear equations which must be solved simultaneously for changes in the temperature and radius. For the present models the zones in the far interior typically have sound-travel times of the order of 2×10^4 seconds, while the pulsation periods are often greater than 10^7 seconds. With the implicit method, time-steps between 10^5 and 10^6 seconds can be used.

The method of solution of the two systems of equations is illustrated by the following simple example.

Problem: Find r and T such that $f(r,T) = 0$ and $g(r,T) = 0$. Let T_0, r_0 be trial values. Then correction terms are given by

$$(\partial f/\partial T)\,\delta T + (\partial f/\partial r)\,\delta r = -f(r_0, T_0)$$

$$(\partial g/\partial T)\,\delta T + (\partial g/\partial r)\,\delta r = -g(r_0, T_0)\ , \tag{6}$$

where the derivatives are evaluated at (r_0, T_0). The process is iterated until it converges. Reasonably good trial values may be required.

In the actual model calculations there is an equation

$$f_{k+1/2}\left(T_{k+3/2},\ T_{k+1/2},\ T_{k-1/2},\ r_{k+1},\ r_k\right) = 0 \qquad (7)$$

for each zone; this comes from the first law of thermodynamics. For each boundary the equation of motion has the form

$$g_k\left(r_{k+1},\ r_k,\ r_{k-1},\ T_{k+1/2},\ T_{k-1/2}\right) = 0 \quad . \qquad (8)$$

Equations (7) and (8) must be solved simultaneously for all values of k.

b) The Heat Equation

The difference representation for the first law of thermodynamics is

$$\Delta E_{k+1/2}^{m+1/2} + (P+q)_{k+1/2}^{m+1/2}\ \Delta V_{k+1/2}^{m+1/2} - \Delta t\left(L_k^{n+1/2} - L_{k+1}^{n+1/2}\right) / m_{k+1/2} = 0, \quad (9)$$

where q is the artificial viscosity term. The points on the time grid are denoted by superscripts. $\Delta E^{n+1/2} \equiv E^{n+1} - E^n$; $P^{n+1/2}$ means an average value of P^n and P^{n+1}. A similar convention holds for subscripts, but for them, integer subscripts refer to averages for quantities defined on zones, whereas half-integer subscripts refer to averages if the quantity to which they refer is defined on a boundary.

Let $X^{(m)}$ be the approximate value of a quantity X after m iterations; $X(\text{exact}) = X^{(m)} + \delta X$. Equation (9) is linearized and written

in the form

$$2\delta E + \left(P^{(m)} + P^{n} + q^{(m)} + q^{n}\right)\delta V + \left(\delta P + \delta q\right)\Delta V^{(m)} - \Delta t\left(\delta L_{k} - \delta L_{k+1}\right)/m_{k+\frac{1}{2}} = CON, \tag{10}$$

where

$$CON = -2\Delta E^{(m)} - \left(P^{(m)} + P^{n} + q^{(m)} + q^{(n)}\right)\Delta V^{(m)}$$

$$+ \Delta t\left[\left(L_{k}^{(m)} - L_{k+1}^{(m)}\right) + \left(L_{k}^{n} - L_{k+1}^{n}\right)\right]/m_{k+\frac{1}{2}}. \tag{11}$$

Subscripts $k+\frac{1}{2}$ have been suppressed in obvious places. Equation (10) must now be expressed entirely in terms of δR and δT. The mean values of the pressure and luminosity have been written as arithmetic means. In equation (10), $\delta E = E_{T}^{(m)}\delta T + E_{V}^{(m)}\delta V$ and $\delta P = P_{T}^{(m)}\delta T + P_{V}^{(m)}\delta V$, with $E_{T} \equiv (\partial E/\partial T)_{V}$, etc.

The artificial viscosity term is defined by

$$q_{k+\frac{1}{2}} = \begin{cases} C(U_{k+1} - U_{k})^{2}/V_{k+\frac{1}{2}} & \text{for } U_{k+1} - U_{k} < 0 \\ 0 & \text{for } U_{k+1} - U_{k} \geq 0\,, \end{cases} \tag{12}$$

where the constant C was equal to 2 in this work. Then

$$\delta q = -q^{(m)}\left[\delta V/V^{(m)} + 2\delta\left(U_{k+1} - U_{k}\right)/\left(U_{k+1} - U_{k}\right)\right]. \tag{13}$$

If $\Delta R^{n+\frac{1}{2}} = \Delta t\left(U^{n+1} + U^{n}\right)/2$, then

$$\Delta R^{(m)} + \delta R = \Delta t\left(U^{(m)} + U^{n} + \delta U\right) / 2 . \tag{14}$$

At each step in the iteration, $\Delta R^{(m)}$ is determined. Then

$$U^{(m)} = 2\Delta R^{(m)} / \Delta t - U^{n} \tag{15}$$

and $\delta U = 2\delta R/\Delta t$. The change in specific volume is

$$\delta V = \left(A_{k+1}\delta r_{k+1} - A_{k}\delta r_{k}\right) / m_{k+1/2} . \tag{16}$$

The variation in luminosity $\delta L = A\delta F + 2L\,\delta R/R$. The expression resulting from the linearization of the variations in convective flux is very complex and has not been used. Calculations of numerical derivatives of the convective flux would also be time-consuming. Also, $\delta F_{k} - \delta F_{k+1}$ for the convective flux would contain terms in δR at four consecutive boundaries, whereas all the terms considered so far include δR at only two different boundaries. Including four terms would complicate the matrix inversion procedure used in solving for the δR's and δT's. It is usually possible to obtain reasonably good convergence of the iterations even when δF (convective) is left out; therefore it was omitted from the linearization.

For the radiative flux

$$\delta F = 2F^{(m)}\delta R/R + \left(\partial F/\partial T_{k-1/2}\right)\delta T_{k-1/2} + \left(\partial F/\partial T_{k+1/2}\right)\delta T_{k+1/2} + \kappa_{k} F\,\delta(1/\kappa_{k}). \tag{17}$$

In the expression for $\delta(1/\kappa_{k})$ the terms depending on specific volume

also have been omitted because they depend on four different δR's. This does not usually cause serious convergence problems. The final form for equation (10) is

$$-CM\,\delta T_{k-1/2}+CO\,\delta T_{k+1/2}-CP\,\delta T_{k+3/2}-CRM\,\delta R_k+CRP\,\delta R_{k+1}=CON \qquad (18)$$

where subscripts $k+1/2$ are implied on all the coefficients.

c) The Equation of Motion

The basic form for the equation of motion is

$$\frac{\Delta U_k^{n+1/2}}{\Delta t} = -\frac{A_k^{n+1/2}}{m_k}\left(\Delta P_k^{n+1/2}+\Delta q_k^{n+1/2}\right)-\frac{GM_k}{(R_k^2)^{n+1/2}} \qquad (19)$$

The means in this equation were taken in two different ways. In case 1, the first term was written as $\langle A_k(\Delta P_k+\Delta q_k)\rangle/m_k$ and the second was written as $GM_k\langle 1/R_k^2\rangle$, where $\langle A\rangle$ denotes an arithmetic mean. In case 2, used by Fraley (1968),

$$A^{n+1/2} = 4\pi\left[(R^n)^2+R^nR^{n+1}+(R^{n+1})^2\right]/3\,, \qquad (20)$$

and $1/(R^2)^{n+1/2} = 1/(R^nR^{n+1})$, and arithmetic means were used for $P^{n+1/2}$ and $q^{n+1/2}$.

$$\Delta U^{n+1/2} = U^{n+1}-U^n = \left(2\Delta R^{n+1/2}/\Delta t - U^n\right) \qquad (21)$$

Equation (19) is linearized (no terms are neglected) and put in the form

$$DP\,\delta R_{k+1} + DO\,\delta R_k + DM\,\delta R_{k-1} - TP\,\delta T_{k+\frac{1}{2}} + TM\,\delta T_{k-\frac{1}{2}} = DON\,, \qquad (22)$$

where subscript k is implied for all the coefficients.

Boundary conditions are required before equations (14) and (22) can be solved. At the inner boundary (k=1), L_1 and r_1 are fixed constants. When these conditions are applied, equation (18) can be put in the form

$$\delta T_{3/2} = CC\,\delta T_{5/2} + DD + EE\,\delta R_2 \qquad (23)$$

for k=2. When the boundary conditions and equation (23) are used in equation (17) for k = 2 the result can be put in the form

$$\delta R_2 = RR\,\delta T_{5/2} + SS + RT\,\delta R_3 \qquad (24)$$

for k = 2. Equations (22) and (23) are then substituted into equations (18) and (21) and the whole set of equations for all k can be reduced to the form of (22) and (23). When the surface boundary conditions $P_{n+\frac{1}{2}}=0$ and $L_N = 4\pi R_N R_{N-1}\sigma T^4_{N-\frac{1}{2}}$ are used, δR_N and $\delta T_{N-\frac{1}{2}}$ can be calculated. Then all the δR's and δT's can be calculated sequentially by substituting known values into the analogues of equations (23) and (24).

d) Energy Conservation

The equation of motion and the heat equation can be combined in the form

$$\frac{D}{Dt}\left(\frac{\dot{r}^2}{2} - \frac{GM_r}{r} + E\right) = -\frac{\partial}{\partial M_r}\left[L_r + 4\pi r^2 \dot{r}(P+q)\right]. \tag{25}$$

An integration over the envelope gives

$$\frac{\partial}{\partial t}\int_{M_c}^{M}\left(\frac{\dot{r}^2}{2} - \frac{GM_r}{r} + E\right) dM_r = L(M_c) - L(M) \tag{26}$$

if $\dot{r}(M_c) = 0$ and $P + q = 0$ at $M_r = M$. An integration of equation (26) gives

$$\text{(energy of envelope at time } t_2) = \int_{t_1}^{t_2}\left[L(M_c) - L(M)\right]dt$$

$$+ \text{ (energy of envelope at time } t_1) \tag{27}$$

The difference equations should satisfy an equation of this form for the entire time $t_2 - t_1$ of the calculation. Whether or not a difference-equation analogue of (27) holds depends on the form of the equations as well as on the accuracy of the iteration procedure by which they are solved. Fraley's form of the equation of motion (19) conserves energy exactly if the equations are solved exactly. This is demonstrated as follows. Equation (19) is multiplied by $(U^{n+1}+U^n)/2 \equiv \Delta R^{n+1/2}/\Delta t$ and rearranged to give

$$m\frac{\left[(U^{n+1})^2 - (U^n)^2\right]}{2} + \frac{GMm\Delta R^{n+1/2}}{(R^2)^{n+1/2}} = -\Delta R^{n+1/2}(A\Delta P)^{n+1/2}. \tag{28}$$

The potential energy term reduces to $-GMm/R^{n+1} + GMm/R^n$ if $(R^2)^{n+1/2} \equiv R^n R^{n+1}$. In the heat equation (9),

$$\Delta V_{k+1/2}^{n+1/2} = \frac{4\pi}{3}\left[\frac{(R_{k+1}^{n+1})^3-(R_k^{n+1})^3}{m_{k+1/2}}\right]-\frac{4\pi}{3}\left[\frac{(R_{k+1}^{n})^3-(R_k^{n})^3}{m_{k+1/2}}\right]. \tag{29}$$

This has the form

$$\Delta V_{k+1/2}^{n+1/2} = \left(\Delta R_{k+1}^{n+1/2}\, A_{k+1}^{n+1/2} - \Delta R_k^{n+1/2}\, A_k^{n+1/2}\right) / m_{k+1/2} \tag{30}$$

where $A^{n+1/2}$ was defined in equation (20). When the term $P^{n+1/2} m \Delta V^{n+1/2}$ in equation (9) is summed over all zones, the result can be written in the form

$$\sum_{k=2}^{N}\left(P_{k-1/2}-P_{k+1/2}\right)^{n+1/2}\Delta R_k^{n+1/2}\, A_k^{n+1/2}\,. \tag{31}$$

This will cancel all the pressure terms in equation (28) when it is summed over all boundaries, if $A^{n+1/2}$ in equation (28) is defined as in equation (20), and if the mean pressure $P^{n+1/2}$ is chosen the same way in equations (9) and (19). Thus the final result is

$$\sum_{k=2}^{N} m_k\left[\left(\frac{U^{n+1}}{2}\right)^2-\frac{GM_k}{R_k^{n+1}}\right]+\sum m_{k-1/2}\, E_{k-1/2}^{n+1} = \Delta t\left(L_1^{n+1/2}-L_N^{n+1/2}\right)$$
$$+\sum_{k=2}^{N} m_k\left[\left(\frac{U^{n}}{2}\right)^2-\frac{GM_k}{R_k^{n}}\right]+\sum m_{k-1/2}\, E_{k-1/2}^{n}\,, \tag{32}$$

which when summed over all the timesteps between t_1 and t_2 gives exactly the form of equation (27). If the alternative method of averaging is used in the equation of motion, equation (32) will not be satisfied exactly. If the model performs a periodic oscillation, then the deviations from energy conservation will also be periodic; if the magnitude of the

maximum deviation is not too large, there is no problem in the interpretation of the behaviour of the model.

The kinetic energy of the turbulence changes as the convection zone grows or shrinks, but this energy has not been included in the discussion of conservation. A partial differential equation must be written for the mean square turbulent velocity, and it then is included in the sum over all boundaries. The turbulent pressure term must be included in the equation of motion, and the heat equation must also be modified to account for the energy which is dissipated by the turbulence and the work done by buoyant forces to increase the turbulent energy. All this has been discussed by Fraley (1968), and by Castor (1968).

REFERENCES

Abell, G. O., and Goldreich, P. 1966, Pub. A. S. P., 78, 232.

Castor, John I. 1966, unpublished Ph. D. thesis, California Institute of Technology.

Castor, John I. 1968, (private communication).

Christy, R. F. 1964, Rev. Mod. Phys, 36, 555.

Fraley, G. S. 1968, Astrophys. and Space Sci., 2, 96.

Richtmyer, R. D. 1957, Difference Methods for Initial Value Problems, (New York: Interscience Publishers).